

ND-A190 606

DENSE-SPRAY STRUCTURE AND PHENOMENA PART 1  
TURBULENCE/DISPERSED-PHASE INT (U) MICHIGAN UNIV ANN  
ARBOR GAS DYNAMICS LABS R N PARTHASARTHY ET AL

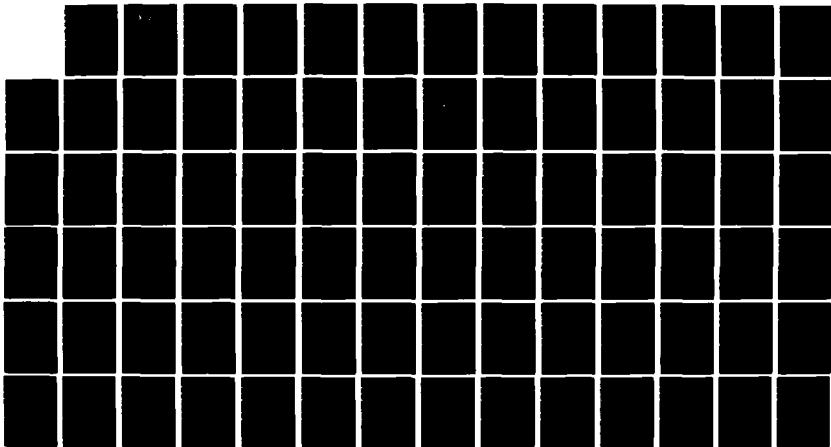
171

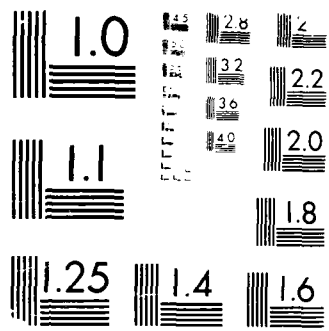
UNCLASSIFIED

15 AUG 87 AFOSR-TR-87-1758-PT-1

F/G 20/4

NL





MICROCOPY RESOLUTION TEST CHART  
ANSI #2 - 1983

2

Unclassified  
SECURITY CLASS.

AD-A190 606

IQN PAGE Form Approved OMB No. 0704-0188

|  |   |
|--|---|
| 1a. REPORT SECL<br>Un  | 1b. RESTRICTIVE MARKINGS<br><b>ONE FILE COPY</b>  |
| 2a. SECURITY CLASSIFICATION AUTHORITY<br><b>SELECTED</b>       | 3. DISTRIBUTION/AVAILABILITY OF REPORT<br>Approved for public release; distribution is unlimited. |
| 2b. DECLASSIFICATION/DOWNGRADING SCHEDULE<br><b>JAN 9 1988</b> | 5. MONITORING ORGANIZATION REPORT NUMBER(S)<br><b>AFOSR-TR- 87- 1758</b>                          |
| 4. PERFORMING ORGANIZATION REPORT NUMBER(S)<br><b>D</b>        |   |

|   |                                      |  |
|---|--------------------------------------|--|
| 6a. NAME OF PERFORMING ORGANIZATION<br>Dept. of Aerospace Engr.<br>The University of Michigan | 6b. OFFICE SYMBOL<br>(if applicable) | 7a. NAME OF MONITORING ORGANIZATION<br><b>AFOSR/NA</b> |
|---|--------------------------------------|--|

|   |   |
|---|---|
| 6c. ADDRESS (City, State, and ZIP Code)<br>217 Aerospace Engineering Building<br>Ann Arbor, MI 48109-2140 | 7b. ADDRESS (City, State, and ZIP Code)<br>Building 410, Bolling AFB DC<br>20332-6448 |
|---|---|

|  |                                      |   |
|--|--------------------------------------|---|
| 8a. NAME OF FUNDING/SPONSORING ORGANIZATION<br><b>AFOSR/NA</b> | 8b. OFFICE SYMBOL<br>(if applicable) | 9. PROCUREMENT INSTRUMENT IDENTIFICATION NUMBER<br><b>AFOSR-85-0244</b> |
|--|--------------------------------------|---|

| 8c. ADDRESS (City, State, and ZIP Code)<br>Building 410, Bolling AFB DC<br>20332-6448 | 10. SOURCE OF FUNDING NUMBERS  |                     |                         |          |                         |        |      |    |  |
|---|--|---------------------|-------------------------|----------|-------------------------|--------|------|----|--|
|   | <table border="1"> <tr> <th>PROGRAM ELEMENT NO.</th> <th>PROJECT NO.</th> <th>TASK NO.</th> <th>WORK UNIT ACCESSION NO.</th> </tr> <tr> <td>61102F</td> <td>2308</td> <td>A2</td> <td></td> </tr> </table> | PROGRAM ELEMENT NO. | PROJECT NO.             | TASK NO. | WORK UNIT ACCESSION NO. | 61102F | 2308 | A2 |  |
| PROGRAM ELEMENT NO.   | PROJECT NO.  | TASK NO.            | WORK UNIT ACCESSION NO. |          |                         |        |      |    |  |
| 61102F  | 2308   | A2                  |                         |          |                         |        |      |    |  |

11. TITLE (Include Security Classification)  
(U) Dense-Spray Structure and Phenomena: Part I - Turbulence/Dispersed-Phase Interactions

12. PERSONAL AUTHOR(S)  
R. N. Parthasarathy and G. M. Faeth

|                               |  |   |                         |
|-------------------------------|--|---|-------------------------|
| 13a. TYPE OF REPORT<br>Annual | 13b. TIME COVERED<br>FROM 7/15/86 TO 7/14/87 | 14. DATE OF REPORT (Year, Month, Day)<br>15 August 1987 | 15. PAGE COUNT<br>70 pp |
|-------------------------------|--|---|-------------------------|

16. SUPPLEMENTARY NOTATION

|                  |   |       |           |
|------------------|---|-------|-----------|
| 17. COSATI CODES | 18. SUBJECT TERMS (Continue on reverse if necessary and identify by block number)<br>turbulent dispersion<br>multiphase flow<br>particle-laden jets |       |           |
| FIELD            |   | GROUP | SUB-GROUP |
| 21               |   | 01    |           |
| 21               | 02  |       |           |

19. ABSTRACT (Continue on reverse if necessary and identify by block number)

This report describes one aspect of an investigation of dense-spray processes: namely turbulence dispersed-phase interactions. The work was divided into two phases: (1) measurements of particle-laden jets injected into a still liquid; and homogeneous particle flows, consisting of particles falling in a still (in the mean) liquid bath.

The structure of turbulent, dilute, particle-laden water jets, submerged in still water, was studied both experimentally and theoretically. Nonintrusive measurements were made of mean and fluctuating phase velocities and particle number fluxes. Analysis was used to help interpret the measurements, considering three limiting cases, as follows: (1) locally-homogeneous flow, where relative velocities between the phases are ignored; (2) deterministic separated flow, where relative velocities are considered, but particle/turbulence interactions are ignored; and (3) stochastic separated flow, where both phenomena are considered using random-walk methods. The locally-homogeneous flow approximation was more effective than for past work involving larger density ratios between the phases; neverthe-

|   |   |
|---|---|
| 20. DISTRIBUTION/AVAILABILITY OF ABSTRACT<br><input checked="" type="checkbox"/> UNCLASSIFIED/UNLIMITED <input checked="" type="checkbox"/> SAME AS RPT <input type="checkbox"/> DTIC USERS | 21. ABSTRACT SECURITY CLASSIFICATION<br><b>Unclassified</b> |
| 22a. NAME OF RESPONSIBLE INDIVIDUAL<br><b>Julian M Tishkoff</b>   | 22b. TELEPHONE (Include Area Code)<br><b>(202) 767-4935</b> |
|   | 22c. OFFICE SYMBOL<br><b>AFOSR/NA</b>                       |

less, stochastic analysis yielded best agreement with measurements. Effects of enhanced drag (due to high relative turbulent intensities of particle motion) and effects of particles on liquid turbulence properties (turbulence modulation), were observed. Several recent proposals for treating these phenomena were examined; however, none appears to be adequate for reliable general use. Work on this aspect of the investigation was completed.

Effects of turbulence modulation were pursued, by considering particles falling in a water bath, where turbulence/particle interactions are the main mechanism influencing the turbulence properties of the continuous phase. The test arrangement and instrumentation was assembled, including the development of a two-point phase-discriminating laser Doppler anemometer capable of providing spatial and temporal correlations of continuous-phase turbulence properties. Measurements show the progressive strengthening of the turbulence field in the continuous phase with increased particle loading, leading to particle-induced turbulent particle dispersion. Power spectra of streamwise continuous-phase velocity fluctuations show that the particles create a very respectable turbulence field, involving: an energy-containing range, an inertial range, and a high frequency cut-off.



## Table of Contents

|  | <u>Page</u> |
|--|-------------|
| Abstract.....                                      | ii          |
| List of Tables.....                                | vi          |
| List of Figures.....                               | vii         |
| Nomenclature.....                                  | ix          |
| Acknowledgements.....                              | xi          |
| 1. Introduction.....                               | 1           |
| 2. Particle-Laden Jets.....                        | 2           |
| 2.1 Introduction.....                              | 2           |
| 2.2 Experimental Methods.....                      | 3           |
| 2.2.1 Apparatus.....                               | 3           |
| 2.2.2 Instrumentation.....                         | 5           |
| 2.2.3 Test Conditions.....                         | 10          |
| 2.3 Theoretical Methods.....                       | 12          |
| 2.3.1 General Description.....                     | 12          |
| 2.3.2 Continuous Phase (SSF Formulation).....      | 12          |
| 2.3.3 Dispersed Phase (SSF Formulation).....       | 14          |
| 2.3.4 Particle Source Terms (SSF Formulation)..... | 16          |
| 2.3.5 Numerical Solution.....                      | 17          |
| 2.3.6 Simplified Analysis.....                     | 17          |
| 2.4 Results and Discussion.....                    | 17          |
| 2.4.1 Drag Calibrations.....                       | 17          |
| 2.4.2 Near-Injector Properties.....                | 18          |
| 2.4.3 Properties Along Axis.....                   | 21          |
| 2.4.4 Liquid Properties.....                       | 26          |
| 2.4.5 Particle Properties.....                     | 31          |
| 2.4.6 Particle Number Fluxes.....                  | 38          |
| 2.4.7 Sensitivity Study.....                       | 45          |
| 2.5 Conclusions.....                               | 48          |
| 3. Homogeneous Particle Flow.....                  | 49          |
| 3.1 Introduction.....                              | 49          |
| 3.2 Experimental Methods.....                      | 50          |

|                                 |    |
|---------------------------------|----|
| 3.2.1 Apparatus.....            | 50 |
| 3.2.2 Instrumentation.....      | 53 |
| 3.2.3 Test Conditions.....      | 55 |
| 3.3 Results and Discussion..... | 57 |
| 3.3.1 Number Fluxes.....        | 57 |
| 3.3.2 Flow Visualization.....   | 57 |
| 3.3.3 Phase Velocities.....     | 61 |
| 3.4 Summary.....                | 65 |
| 4 Summary of Investigation..... | 66 |
| 4.1 Articles and Papers.....    | 66 |
| 4.2 Participants.....           | 66 |
| 4.3 Oral Presentations.....     | 67 |
| References.....                 | 67 |

## LIST OF TABLES

| <u>Table</u> | <u>Title</u>  | <u>Page</u> |
|--------------|---|-------------|
| 1            | Summary of Particle-Laden Jet Test Conditions.....        | 10          |
| 2            | Source Terms and Empirical Constants.....                 | 13          |
| 3            | Sensitivity Study of SSF Analysis.....                    | 48          |
| 4            | Summary of Homogeneous Particle Flow Test Conditions..... | 56          |

## LIST OF FIGURES

| <u>Figure</u> | <u>Caption</u>   | <u>Page</u> |
|---------------|--|-------------|
| 1             | Sketch of the particle-laden jet apparatus.....                            | 4           |
| 2             | Sketch of the single-channel phase-discriminating LDA.....                 | 6           |
| 3             | Sketch of the LDA measuring volume.....                                    | 8           |
| 4             | Sketch of the particle-flux measuring system.....                          | 9           |
| 5             | Particle-size distribution.....  | 11          |
| 6             | Mean and turbulent liquid properties at $x/d = 8$ .....                    | 19          |
| 7             | Mean and fluctuating particle velocities at $x/d = 8$ .....                | 20          |
| 8             | Mean particle number fluxes at $x/d = 8$ .....                             | 22          |
| 9             | Mean liquid velocities along axis.....                                     | 24          |
| 10            | Mean particle velocities along axis.....                                   | 25          |
| 11            | Mean particle number fluxes along axis.....                                | 27          |
| 12            | Mean and turbulent properties for the single-phase jet ( $x/d = 16$ )..... | 28          |
| 13            | Mean and turbulent properties for the single-phase jet ( $x/d = 24$ )..... | 29          |
| 14            | Mean and turbulent properties for the single-phase jet ( $x/d = 40$ )..... | 30          |
| 15            | Mean and turbulent liquid properties (case I, $x/d = 16$ ).....            | 32          |
| 16            | Mean and turbulent liquid properties (case I, $x/d = 24$ ).....            | 33          |
| 17            | Mean and turbulent liquid properties (case I, $x/d = 40$ ).....            | 34          |
| 18            | Mean and turbulent liquid properties (case II, $x/d = 16$ ).....           | 35          |
| 19            | Mean and turbulent liquid properties (case II, $x/d = 24$ ).....           | 36          |

|   | <u>Page</u> |
|---|-------------|
| 20 Mean and turbulent liquid properties (case II, $x/d = 40$ ).....     | 37          |
| 21 Mean and fluctuating particle velocities (case I, $x/d = 16$ ).....  | 39          |
| 22 Mean and fluctuating particle velocities (case I, $x/d = 24$ ).....  | 40          |
| 23 Mean and fluctuating particle velocities (case I, $x/d = 40$ ).....  | 41          |
| 24 Mean and fluctuating particle velocities (case II, $x/d = 16$ )..... | 42          |
| 25 Mean and fluctuating particle velocities (case II, $x/d = 24$ )..... | 43          |
| 26 Mean and fluctuating particle velocities (case II, $x/d = 40$ )..... | 44          |
| 27 Mean particle number flux distributions (case I).....                | 46          |
| 28 Mean particle number flux distributions (case II).....               | 47          |
| 29 Sketch of the homogeneous particle flow apparatus.....               | 51          |
| 30 Sketch of the two-point phase-discriminating LDA.....                | 54          |
| 31 Particle number flux measurements.....                               | 58          |
| 32 Particle tracks for the three particle loadings.....                 | 60          |
| 33 Power spectrum of streamwise velocities (low condition).....         | 62          |
| 34 Power spectrum of streamwise velocities (medium condition).....      | 63          |
| 35 Power spectrum of streamwise velocities (high condition).....        | 64          |

## NOMENCLATURE

| <u>Symbol</u> | <u>Description</u>                             |
|---------------|--|
| $a$           | acceleration of gravity                        |
| $C_D$         | drag coefficient                               |
| $C_i$         | empirical constants                            |
| $d$           | injector exit diameter                         |
| $d_p$         | particle diameter                              |
| $E(f)$        | power spectrum of velocity fluctuations        |
| $f$           | frequency                                      |
| $f_f$         | fluid passing frequency                        |
| $f_k$         | Kolmogorov frequency                           |
| $f_p$         | particle passing frequency                     |
| $f_{pk}$      | characteristic highest frequency               |
| $I_r$         | relative turbulence intensity                  |
| $k$           | turbulence kinetic energy                      |
| $l_k$         | Kolmogorov length scale                        |
| $L_e$         | dissipation length scale of eddy               |
| $\dot{m}_o$   | injector mass flow rate                        |
| $m_p$         | particle mass                                  |
| $M_A$         | acceleration modulus                           |
| $\dot{M}_o$   | injector thrust                                |
| $\dot{n}_i$   | number of particles in group $i$ per unit time |
| $\dot{n}''$   | particle number flux                           |
| $r$           | radial distance                                |
| $Re$          | Reynolds number                                |
| $S_o$         | source term                                    |
| $S_{po}$      | source term due to particles                   |
| $t$           | time   |
| $t_e$         | eddy lifetime                                  |
| $t_k$         | Kolmogorov time scale                          |
| $u$           | axial velocity                                 |
| $u_k$         | Kolmogorov velocity scale                      |

|               |  |
|---------------|--|
| $u_r$         | difference between dispersed and continuous phase velocities |
| $v$           | radial velocity  |
| $V_j$         | volume of computational cell $j$                             |
| $w$           | tangential velocity  |
| $x$           | streamwise distance  |
| $\delta_{ij}$ | Kronecker delta function                                     |
| $\Delta t_p$  | residence time of a particle in a computational cell         |
| $\Delta_A$    | correction of virtual mass force                             |
| $\Delta_H$    | correction of Basset history force                           |
| $\epsilon$    | rate of dissipation of turbulence kinetic energy             |
| $\mu$         | viscosity  |
| $\mu_t$       | turbulent viscosity  |
| $\nu$         | kinematic viscosity  |
| $\rho$        | density  |
| $\sigma_i$    | turbulent Prandtl/Schmidt number                             |
| $\phi$        | generic property   |
| $\zeta$       | integration variable, equation (6)                           |

#### Subscripts

|          |  |
|----------|--|
| $c$      | centerline value                             |
| $in$     | start of particle path in computational cell |
| $out$    | end of particle path in computational cell   |
| $p$      | particle property                            |
| $r$      | relative value                               |
| $o$      | initial condition                            |
| $\infty$ | ambient condition                            |

#### Superscripts

|           |   |
|-----------|---|
| $(-)$     | time-averaged quantity  |
| $(\sim)$  | particle (Favre)-averaged quantity                              |
| $(-)'$    | time averaged root-mean-square fluctuating quantity             |
| $(\sim)'$ | particle (Favre)-averaged root-mean-square fluctuating quantity |

## ACKNOWLEDGEMENTS

The authors wish to acknowledge the assistance of T.-Y. Sun and J. P. Gore during the initial phases of the investigation. We also wish to acknowledge the contributions of the staff of the Gas Dynamics Laboratories at The University of Michigan: C. Iott, for help with apparatus development and flow visualization; W. Eaton, T. Griffin and G. Gould, for assisting apparatus development; and S. Bauerle for helping to prepare this report.

This research was supported by the Air Force Office of Scientific Research, Grant No. AFOSR-85-0244, under the Technical Management of J. Tishkoff.

## 1. INTRODUCTION

The potential value of rational design procedures for liquid-fueled combustors has motivated numerous efforts to develop methods for analyzing spray evaporation and combustion processes. The goal is to reduce the time and cost of cut-and-try combustor development. This investigation seeks to contribute to the development of this methodology, by studying several fundamental phenomena associated with sprays – particularly the dense-spray region near the exit of the fuel injector passage. The research has application to airbreathing propulsion systems, e.g., liquid-fueled primary combustors and afterburners. The results of the research are also relevant to other spray combustion processes, e.g., liquid-fueled rocket engines, fuel-injected internal-combustion engines, diesel engines, furnaces, etc. Finally, the research involves examination of turbulence/dispersed-phase interactions which are present for a wider class of dispersed turbulent flows, including processes relevant to solid rocket motors and particle-laden exhaust plumes.

The overall investigation is divided into two main tasks, as follows: (1) direct consideration of the near-injector, dense-spray region of pressure-atomized sprays; and (2) turbulence/dispersed-phase interactions in particle-laden liquid flows, which are related to dense-spray processes, but provide a much simpler system for fundamental study. Findings for the two tasks are reported separately, with this report limited to turbulence/dispersed-phase interactions. Descriptions of the pressure-atomized spray study can be found in Parthasarathy et al. (1986), Ruff & Faeth (1987) and Ruff et al. (1987, 1987a).

The investigation is planned for a three-year period, with this report covering the second year of the study. Two experimental configurations were considered to study turbulence/dispersed-phase interactions, namely: particle-laden liquid jets, consisting of glass beads in water, injected into a still water bath; and homogeneous particle flows, consisting of glass beads falling through a stagnant (in the mean) tank of water. The particle-laden jet experiment highlights the dynamics found in spray processes at high pressure, typical of combustion in modern propulsion systems, where the densities of the continuous and dispersed phases are comparable. The homogeneous particle flow provides conditions where effects of turbulence modulation (the direct modification of continuous-phase turbulence properties by the dispersed phase) can be studied without the complications of more conventional turbulence processes.

The particle-laden jet and homogeneous particle flow studies are considered in the next two sections of the report. The report concludes with a summary of articles, participants, and papers associated with the turbulence/dispersed-phase task of this investigation.

## 2. PARTICLE-LADEN JETS

### 2.1 Introduction

Particle-laden turbulent jets in liquids are encountered in industrial and natural processes. Furthermore, these flows provide a useful simulation of sprays in high-pressure environments, since they have comparable phase-density ratios. The present study considers particle-laden turbulent water jets in still water, motivated by these applications. The work involved both measurements of flow structure and analysis to help interpret the measurements and to initiate development of predictive methods for these flows. The study was limited to nearly monodisperse particles and dilute particle concentrations (particle volume fractions less than 5%).

A complete discussion of earlier studies of particle-laden jets will not be undertaken since reviews of these flows have recently appeared (Faeth, 1983, 1987). The present study extends earlier work on multiphase jets in this laboratory, which included: particles in gases (Shuen et al. 1983, 1983a, 1985), drops and sprays in gases (Solomon et al. 1985, 1985a; Shuen et al. 1986), and bubbles in liquids (Sun & Faeth, 1986; Sun et al. 1986). The earlier flows involved either very large or very small phase-density ratios, yielding different response of the dispersed phase to the motion of the continuous phase. However, conditions where phase densities are comparable were not considered; therefore, the present study was designed to help fill this gap in the literature. Comparable phase densities are of particular interest, since all effects of interphase momentum transfer are important – particle inertia, virtual mass, drag, and the Basset history force. Furthermore, these flows also exhibit high relative turbulence intensities for particle motion, which influences particle drag properties (Clift et al. 1978). Thus, they represent a good test of methods used to predict particle motion in turbulent environments.

The present experiments involved solid glass spheres (roughly 0.5 mm in diameter) in water, yielding a phase-density ratio of 2.45:1. Mean and fluctuating phase velocities were measured using a phase-discriminating laser-Doppler anemometer (LDA). Particle number fluxes were measured by detecting Mie scattering from particles within a laser light sheet. As a baseline, measurements of flow properties in a pure water jet were completed, using the same injector. Particle drag properties were calibrated, using separate single-particle experiments, in order to reduce uncertainties in separated-flow analysis.

Analysis of flow properties was similar to recent work in this laboratory (Shuen et al. 1983, 1983a, 1985; Solomon et al. 1985, 1985a; Sun & Faeth 1986; Sun et al. 1986). Three limiting approximations were considered, as follows: (1) locally-homogeneous flow (LHF) where interphase transport rates are assumed to be infinitely fast so that the relative velocities of the phases can be ignored; (2) deterministic separated flow (DSF), where the relative velocities between the phases are considered, but particle/turbulence interactions are ignored; and (3) stochastic separated flow (SSF), where effects of both relative velocities and particle/turbulence

interactions are considered using random sampling for turbulence properties, in conjunction with random-walk computations for particle motion. Exact numerical simulation of multiphase turbulent jets is not feasible for Reynolds numbers encountered in practice, due to the large range of length scales in the flow. Thus, continuous-phase turbulence properties were analyzed using widely-adopted methods of  $k-\epsilon$  turbulence models, while averaging over phenomena on the scale of particle size, similar to past treatments of multiphase jets in this laboratory. All empirical aspects of the turbulence model, however, were established by early work with constant density single-phase shear flows (Lockwood & Naguib 1975) and subsequently verified by comparison with measurements in constant- and variable-density single-phase round jets (Jeng et al. 1984). Two extensions of analysis were also undertaken, as follows: (1) consideration of effects of anisotropy of continuous-phase turbulence on the anisotropy of fluctuating particle motion, since Shuen et al. (1985) suggested that this phenomenon was important; and (2) consideration of effects of particles on the turbulence structure of the continuous phase, called turbulence modulation by Al Taweel & Landau (1977).

Parthasarathy et al. (1986) describe the initial phases of this investigation, while Parthasarathy and Faeth (1987, 1987a) present more abbreviated accounts of present findings. The report begins with a description of theoretical and experimental methods. This is followed by discussion of the particle drag calibration, measurements of near-injector flow properties to establish initial conditions for structure computations, and baseline results for single-phase water jets in still water. This portion of the report concludes with a description of structure measurements in particle-laden jets and their comparison with predictions.

## 2.2 Experimental Methods

### 2.2.1 Apparatus

The test arrangement has already been described (Parthasarathy et al. 1986); therefore, the following description will be brief. A sketch of the apparatus appears in figure 1. The flow was observed within a windowed test tank ( $410 \times 530 \times 910$  mm high) used during earlier studies of bubbly jets (Sun & Faeth 1986; Sun et al. 1986). The injector was a constant-area passage, 5.08 mm in diameter and 350 mm long, injecting vertically downward. This arrangement yielded nearly fully-developed pipe flow at the exit, for single-phase flow conditions. Instrumentation was mounted rigidly; therefore, the injector was traversed in three directions to measure flow properties. Positioning accuracies were  $100 \mu\text{m}$  in the horizontal plane and  $500 \mu\text{m}$  in the vertical direction.

Filtered water was supplied to the injector by a rotary gear pump. A valve, bypass and surge tank in the pump exhaust line were used to control and smooth the flow. Water flow rates were measured with a rotameter, which was calibrated by collecting water for timed intervals. Water injected into the test tank was removed by an overflow pipe and returned to a reservoir at the pump inlet.

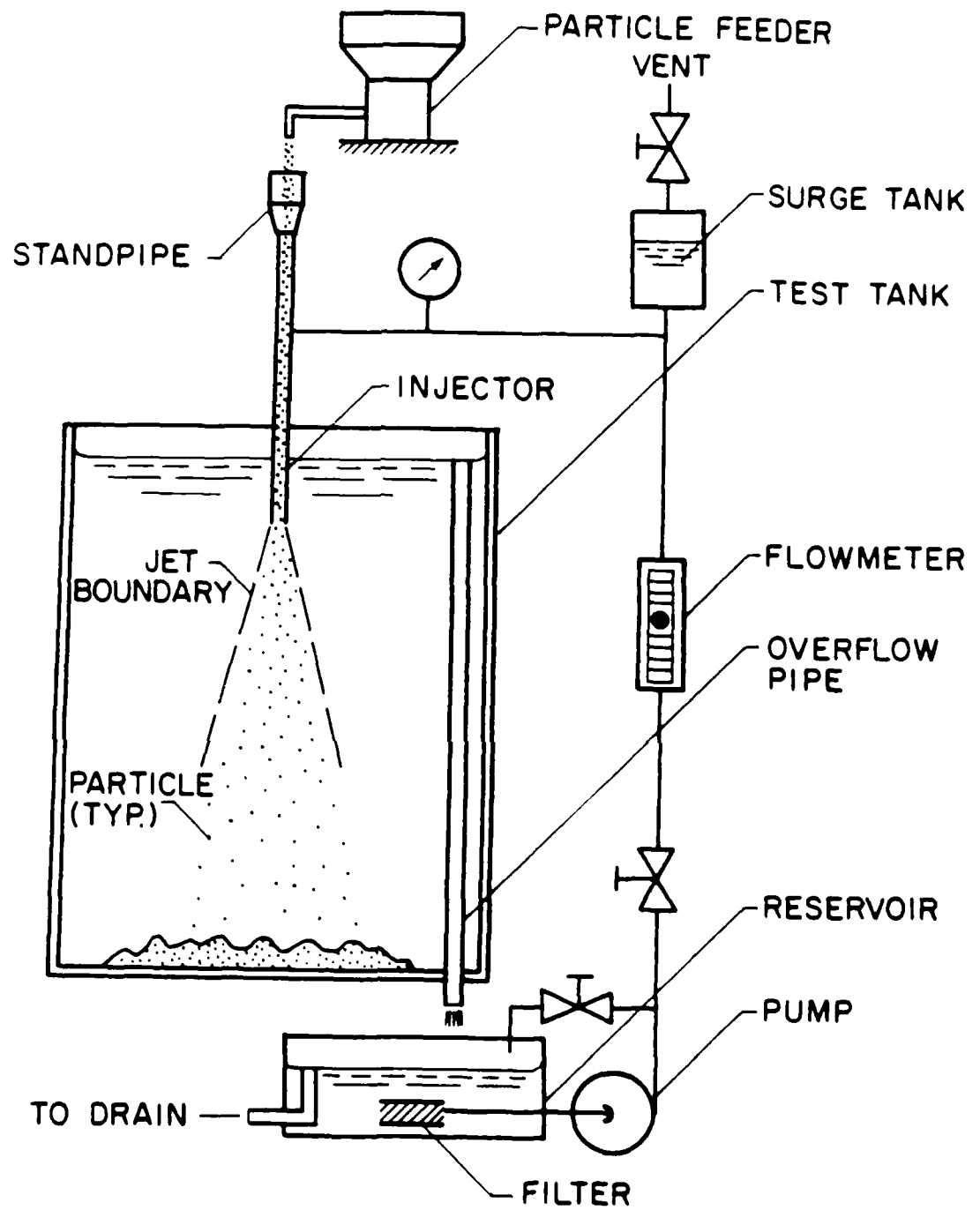


Figure 1. Sketch of the particle-laden jet apparatus.

Dried particles were fed by a screw feeder (maximum feed rate variations of 4%) to a standpipe located directly above the injector. While falling under the influence of gravity, the particles mixed with the water and entered the injector flow at a tee. After passing through the jet, the particles collected naturally at the bottom of the tank, where they were removed periodically by a suction system.

### 2.2.2 Instrumentation

Particle velocities. Mean and fluctuating particle velocities were measured with a laser-Doppler anemometer (LDA) which is sketched in figure 2. A dual-beam arrangement was used, based on the 514.5 nm line of an argon-ion laser operated at 200 mW optical power. Off-axis ( $45^\circ$ ) forward-scatter light detection was used for particle velocity measurements in order to control the size of the measuring volume. Directional bias and ambiguity were eliminated by use of a 40 MHz Bragg-cell frequency shifter. Output signals were downshifted to convenient frequency ranges for filtering and signal processing.

Signal amplitudes from the naturally-seeded water were much smaller than from particles; therefore, particle signals were identified by reducing the gain of the detector circuit until only signals from particles were recorded. This procedure was verified by stopping the flow of particles, which invariably resulted in no further signals being processed. Particle velocities were found using a burst-counter signal processor (TSI Model 1990C). The output of the burst counter was stored and subsequently processed by a microcomputer (IBM 9002) to yield particle-averaged mean and fluctuating velocities. Predictions of particle velocities were averaged in the same way, for comparison with the measurements. Streamwise and radial particle velocities were measured by appropriately orienting the optical plane of the LDA.

The LDA measuring volume for particle velocities was relatively large (0.6 mm diameter and 0.7 mm long) since grazing collisions of particles with the measuring volume were recorded. Nevertheless, gradient broadening was small and uncertainties of these measurements largely resulted from finite sampling times. Estimates of experimental uncertainties (95% confidence) are as follows: mean streamwise velocities, 5%; fluctuating streamwise and radial velocities, 10%; and mean radial velocities, 50%. Uncertainties of mean radial velocities are high due to their small magnitude.

Liquid velocities. Light scattered by natural seeding in the water yields lower-amplitude signals than light scattered by the glass beads; therefore, simple amplitude discrimination can help to distinguish between liquid-phase and particle velocity signals. As Modarress et al. (1984) point out, however, particles grazing the LDA measuring volume also yield low-amplitude signals, which can be interpreted as coming from the liquid phase, biasing the liquid velocity measurements.

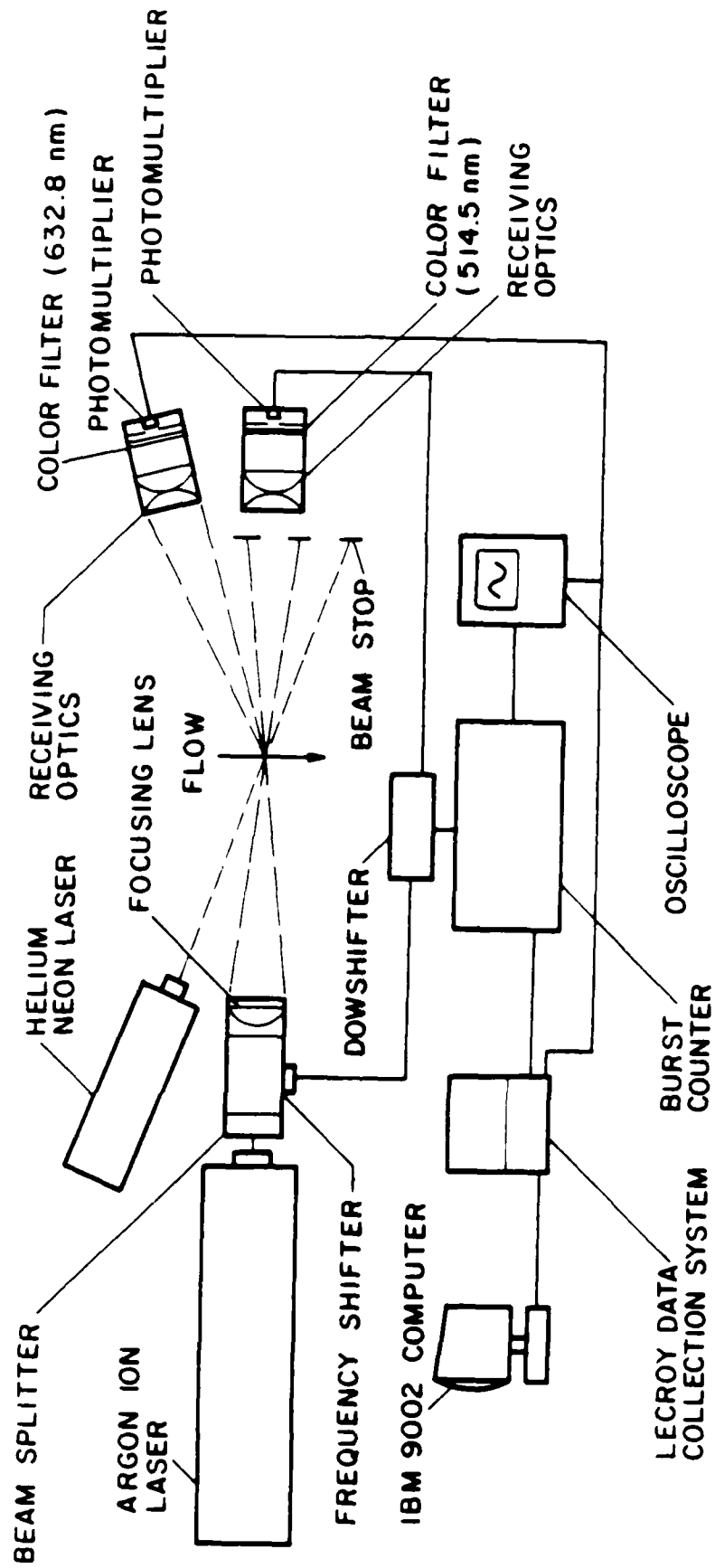


Figure 2. Sketch of the single-channel phase-discriminating LDA.

A phase-discriminator system sketched in figure 2 was used to avoid biasing from grazing particle collisions with the LDA measuring volume, similar to Modarress et al. (1984). The basic LDA arrangement was similar to the particle velocity measurements; but with on-axis forward-scatter light detection. The phase discriminator involved a third beam, from a 5 mW HeNe laser ( $18^\circ$  from the LDA axis) which was focussed at the LDA measuring volume and observed by off-axis ( $32^\circ$ ) detection through a laser-line filter. The discriminator optics were adjusted so that all grazing collisions were observed. The region viewed (0.6 mm diameter and 1.2 mm long) by the discriminator is illustrated in figure 3, yielding a discriminator volume with a diameter greater than the sum of the diameters of the LDA measuring volume and the largest particles. The discriminator signal was recorded simultaneously with the velocity signal from the burst counter. The data processing system was programmed to eliminate all velocity records where a pulse on the discriminator signal indicated the presence of a particle. The time between valid liquid velocity measurements was small in comparison to the integral time scales of the flow; therefore, the velocity signal was time averaged, ignoring periods when particles were present, to obtain unbiased time-averaged mean and fluctuating liquid velocities. Natural seeding in the water was sufficient to yield high data rates (3-8 kHz). Various velocity components and the Reynolds stress were obtained by rotating the optical plane of the LDA, as described by Durst & Whitelaw (1971).

The LDA measuring volume for liquid velocities was 0.1 mm in diameter and 1.3 mm long. Gradient broadening was negligible and experimental uncertainties were dominated by finite sampling times. Estimated experimental uncertainties (95% confidence) are as follows: mean streamwise velocities, 5%; fluctuating streamwise and radial velocities, 10%; turbulence kinetic energy, 20%; and Reynolds stress, 30% at its maximum and proportionately higher elsewhere.

Particle number fluxes. Mie scattering was used to measure particle number fluxes in the streamwise direction. A sketch of this system appears in figure 4. A small light sheet, having nearly uniform intensity, was produced at the measuring volume by passing the beam from a 5 mW HeNe laser through an aperture. The measuring volume was observed in the horizontal plane, normal to the laser beam. Particles passing through the measuring volume generated pulses in the detector output. The pulses were shaped and recorded by a pulse counter which had an adjustable threshold to control spurious background signals. Grazing collisions of particles with the optical measuring volume were recorded; therefore, the radius of the region observed was roughly the sum of the optical radius and the particle radius (total size roughly  $0.75 \times 0.75$  mm). The actual area of observation, however, was calibrated by collecting particles in a uniform flow. In general, more than 1000 particles were counted in order to find the mean particle number flux.

Experimental uncertainties for the particle number flux measurements were due to variable particle diameters, which influences the area actually observed; gradient broadening; and finite sampling times. The latter dominated the measurements, yielding uncertainties (95% confidence) of less than 15% along the axis and proportionately higher elsewhere.

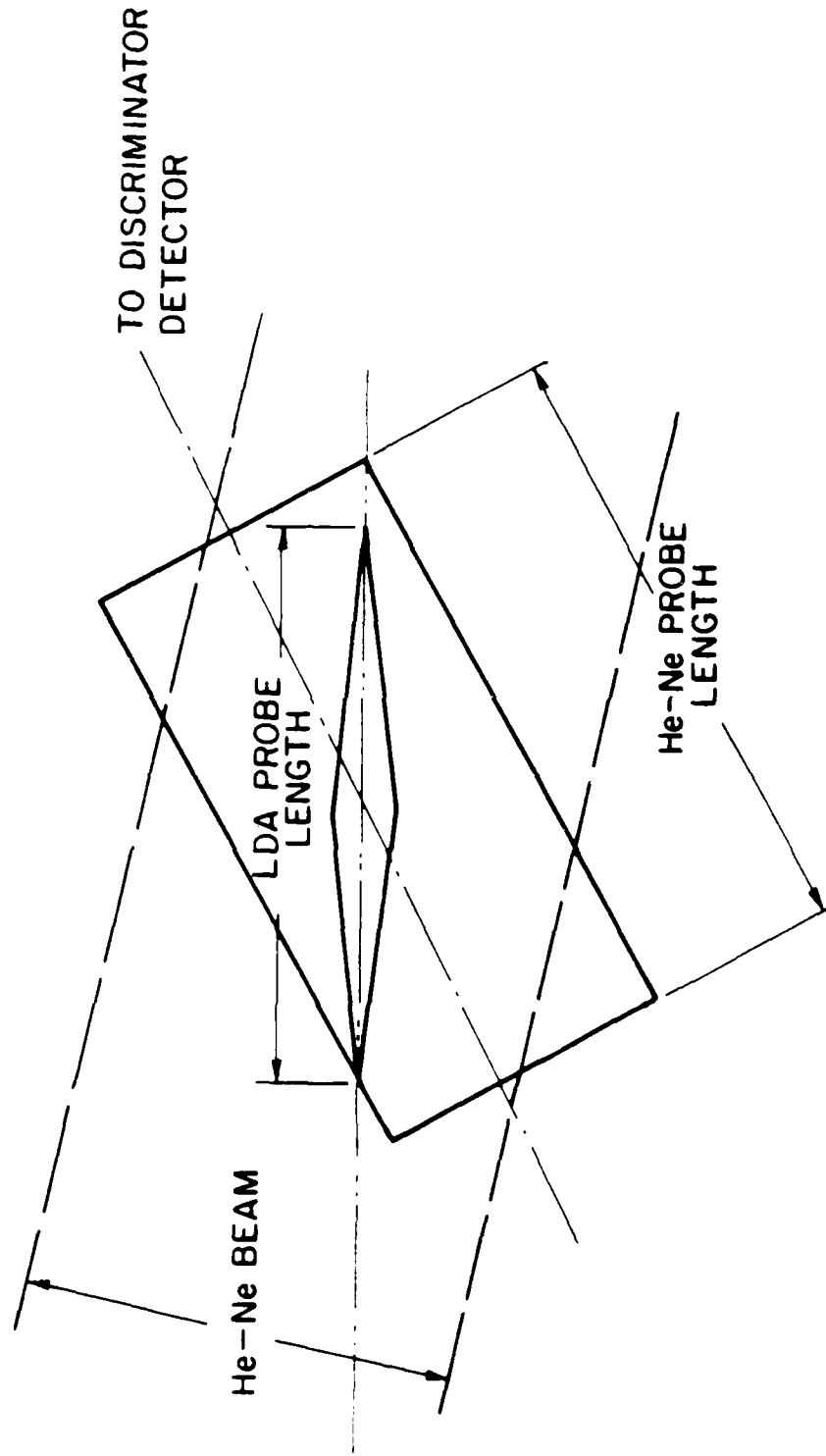


Figure 5. Sketch of the LDA measuring volume.

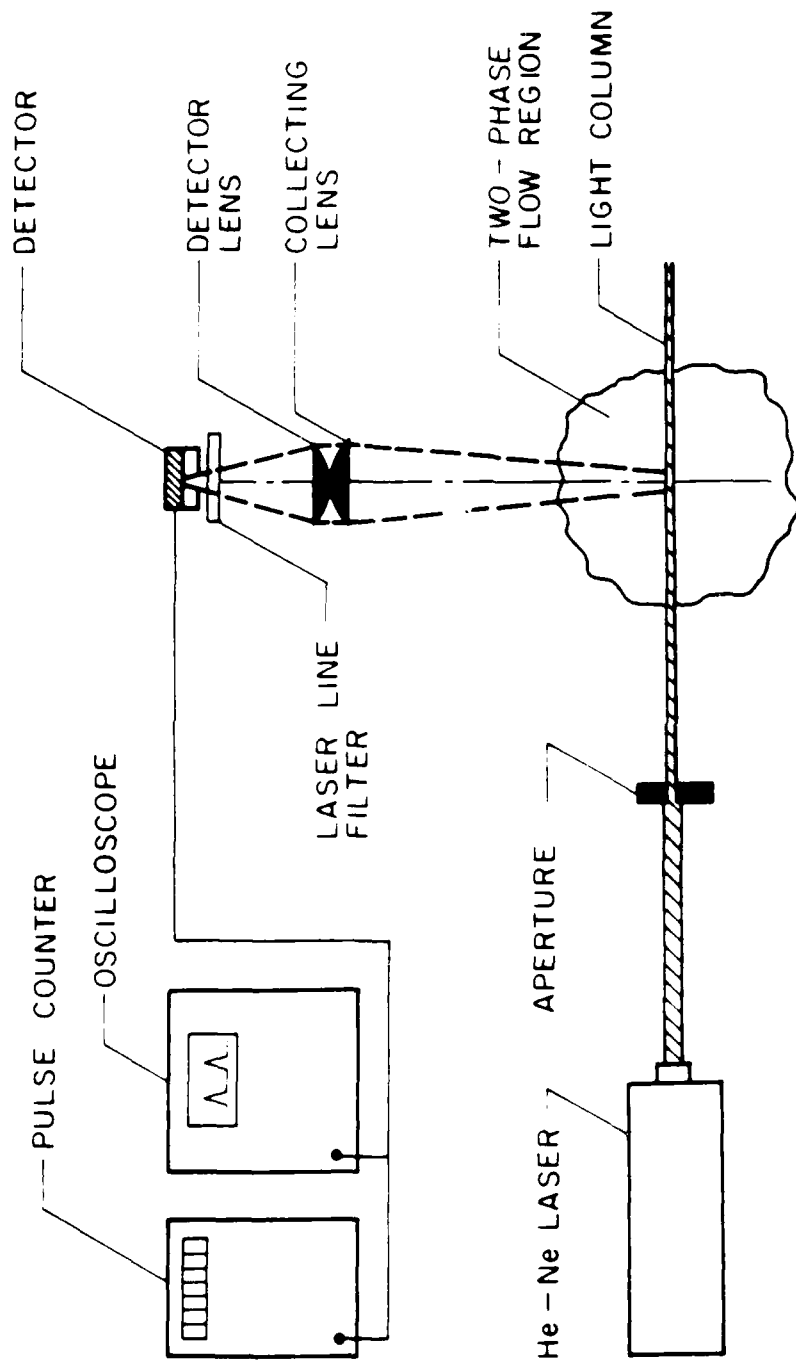


Figure 1. Sketch of the particle-flux measuring system.

### 2.2.3 Test Conditions

Test conditions are summarized in Table 1. Three flows were considered, a pure water jet, as a baseline, and two particle-laden jets. The particle-laden jets were dilute, having initial particle volume fractions of 2.4 and 4.8%. The flows were reasonably turbulent, with initial Reynolds numbers of roughly 8500. Initial flow velocities (ca. 1.6 m/s) were relatively low in comparison to terminal particle relative velocities (ca. 0.05 m/s); therefore, effects of buoyancy were significant. The size distribution of the particles, which were more-or-less round glass beads, is illustrated in figure 5. The particles had a number of mean diameter of roughly 500  $\mu\text{m}$ , with a standard deviation of 45  $\mu\text{m}$  (other particle properties are noted in Table 1). Particle properties were not distinguished by size during the measurements. The predictions were obtained by averaging calculated results over all particles, in the same manner.

Table 1. Summary of Test Conditions<sup>†</sup>

| Flow                                | Single-Phase | Particle-Laden Jet |      |
|-------------------------------------|--------------|--------------------|------|
|                                     | Jet          | I                  | II   |
| Mass loading ratio (%) <sup>†</sup> | 0            | 5.9                | 11.8 |
| Particle-volume fraction (%)        | 0            | 2.4                | 4.8  |
| Water flowrate (ml/s)               | 32.7         | 32.7               | 32.7 |
| Initial average velocity (m/s)      | 1.61         | 1.66               | 1.72 |
| Jet Reynolds number <sup>§</sup>    | 8530         | 8795               | 9115 |

<sup>†</sup>Initial conditions for a particle-laden water jet injected vertically downward in still water. Injector is a constant-area passage (diameter of 5.08 mm and length of 350 mm). Water temperatures of  $298 \pm 2\text{K}$ .

<sup>†</sup>Mass of particles per unit mass of water. Particles are round glass beads having a number mean diameter (NMD) of 501  $\mu\text{m}$ , a standard deviation from the NMD of 45  $\mu\text{m}$ , a Sauter mean diameter (SMD) of 505  $\mu\text{m}$ , and a density of 2450  $\text{kg m}^{-3}$ .

<sup>§</sup> $Re = u_0 d / \nu$ , where  $d$  is the injector diameter and  $\nu$  is the kinematic viscosity of water.

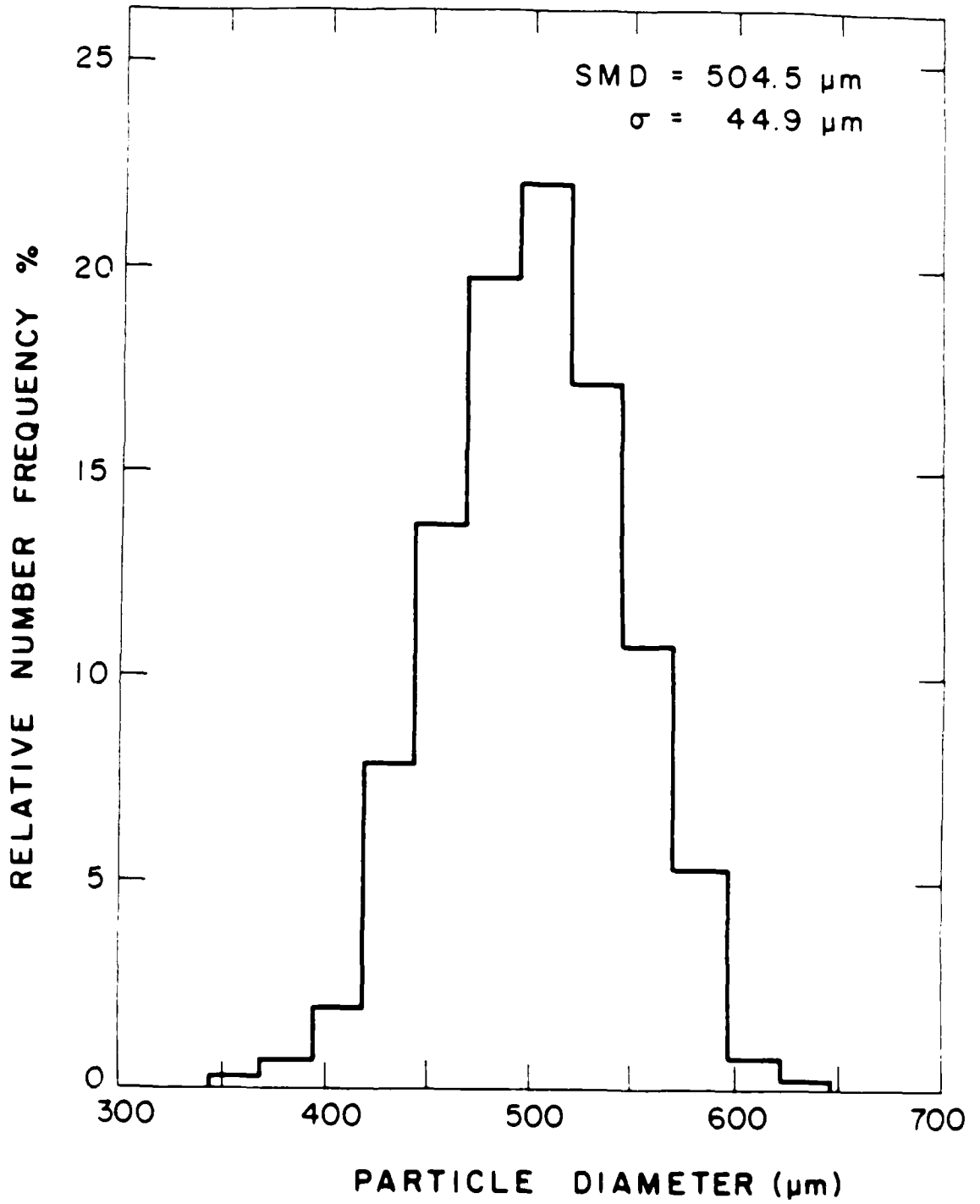


Figure 3. Particle-size distribution.

## 2.3 Theoretical Methods

### 2.3.1 General Description

The analysis considers steady, round, dilute, particle-laden turbulent jets, satisfying the boundary-layer approximations, in an infinite stagnant environment. Similar to past treatments of particle-laden jets in this laboratory (Shuen et al. 1983, 1983a, 1985; Sun & Faeth 1986; Sun et al. 1986), a  $k-\epsilon$  turbulence model was used to find continuous-phase turbulence properties. For present conditions, flow velocities were low and Reynolds numbers were reasonably high; therefore, the kinetic energy and viscous dissipation of the mean flow, as well as molecular transport, were ignored with little error. Both particle and liquid densities are constant, simplifying separated-flow analysis; however, variable-density effects must be considered during LHF analysis since changes in particle concentrations change local densities. Due to relatively low flow velocities, and density differences between the particles and water, buoyancy must be considered. The flows were dilute, with particle volume fractions never exceeding 5%; therefore, the dispersed-phase volume was ignored in the governing equations for the continuous phase, during separated-flow analysis.

The LHF and DSF formulations were very similar to Shuen et al. (1983, 1983a, 1985) and these methods will be described only briefly. However, the SSF approach was modified to treat anisotropy and turbulence modulation; therefore, the new formulation will be presented to facilitate later discussion.

### 2.3.2 Continuous Phase (SSF Formulation)

The turbulent flow analysis is similar to Lockwood & Naguib (1975), but employs mass-weighted (Favre) averages, following Bilger (1976). However, use of Favre averages is only important for LHF analysis, since the density of the continuous phase is constant. Present methods use the specific formulation and empirical constants of Jeng & Faeth (1984), which has been evaluated successfully for a variety of constant- and variable-density single-phase jets. Constants used, however, are not very different from Lockwood & Naguib (1975).

We use an axisymmetric coordinate system. The streamwise direction is vertically downward, aligned with the gravitational acceleration vector. With this arrangement, the general form of the governing equations is as follows:

$$\partial_x(\rho \tilde{u} \phi) + r^{-1} \partial_r(r \rho \tilde{v} \phi) = r^{-1} \partial_r \partial_r (r \mu_t \sigma_\phi \partial \phi / \partial r) + S_\phi + S_{p\phi} \quad (1)$$

where

$$\tilde{\phi} = \overline{\rho\phi} / \bar{\rho} \quad (2)$$

denotes a Favre average, while an overbar denotes a conventional time average. Governing equations are solved for conservation of mass ( $\phi = 1$ ), conservation of momentum ( $\phi = \tilde{u}$ ), turbulence kinetic energy ( $\phi = k$ ), and the rate of dissipation of turbulence kinetic energy ( $\phi = \epsilon$ ). The source terms,  $S_\phi$  and  $S_{p\phi}$ , are summarized in Table 2, along with the empirical constants,  $C_\phi$ , used during the computations. The  $S_\phi$  terms are conventional for a single-phase jet (Lockwood & Naguib 1975); the particle source terms,  $S_{p\phi}$ , will be discussed later. The turbulent viscosity was computed as usual:

$$\mu_t = C_\mu \rho k^2 / \epsilon \quad (3)$$

Table 2. Source Terms and Empirical Constants in Separated-Flow Analysis<sup>†</sup>

| $\phi$      | $S_\phi$  |                                   | $S_{p\phi}$  |                   |
|-------------|---|-----------------------------------|--|-------------------|
| 1           | 0   |                                   | 0  |                   |
| $\tilde{u}$ | 0   |                                   | $\bar{S}_{pu}^\dagger$                               |                   |
| k           | $\mu_t(\partial\tilde{u}/\partial r)^2 - \rho\epsilon$  |                                   | $\bar{u} \bar{S}_{pk} - \bar{u} \bar{S}_{p\epsilon}$ |                   |
| $\epsilon$  | $(C_{\epsilon 1} \mu_t (\partial\tilde{u}/\partial r)^2 - C_{\epsilon 2} \rho \epsilon) \epsilon / k$ |                                   | $C_{\epsilon 3} \bar{S}_{pk} \epsilon / k$           |                   |
| $C_\mu$     | $C_{\epsilon 1}$  | $C_{\epsilon 2} = C_{\epsilon 3}$ | $\sigma_k$   | $\sigma_\epsilon$ |
| 0.09        | 1.44  | 1.87                              | 1.0  | 1.3               |

<sup>†</sup> $S_{pk}$  only used for SSF-KMOD and SSF-EXT versions;  $S_{p\epsilon}$  only used for SSF-EXT version.

$$^\dagger \bar{S}_{pu} = \frac{\sum_{i=1}^n \dot{n}_i (m_p (u_{pin} - u_{pout}) + a(1 - \rho/\rho_p) \Delta t_p)_i}{V_j}$$

The flow leaving the injector was similar to fully-developed flow and had no potential core. Initial conditions for the computations were prescribed from measurements near the injector, as described later. Ambient values of  $\tilde{u}$ ,  $k$  and  $\epsilon$  are zero, while gradients of these quanti-

ties are zero at the axis of the flow, from symmetry.

### 2.3.3 Dispersed Phase (SSF Formulation)

The particle phase was treated by solving Lagrangian equations for the trajectories of a sample of individual particles ( $n$  groups defined by initial position, velocity, direction, and sample) as they move through the flow and encounter a random distribution of turbulent eddies. Results of these computations were averaged over all particle groups, to provide mean and fluctuating particle properties as well as the particle source terms,  $S_{po}$ , needed to solve the continuous-phase governing equations.

Several variations of the SSF analysis were considered, in order to examine effects of anisotropic turbulence properties and effects of particles on continuous-phase turbulence properties (turbulence modulation). The baseline version follows Shuen et al. (1983, 1983a, 1985), which is a modification and extension of a method proposed by Gosman and Ioannides (1981). In all cases, properties are assumed to be uniform within each eddy and to change randomly from one eddy to the next. At the start of particle/eddy interaction, the velocity of the eddy is found by making a random selection from the probability-density function (PDF) of velocity. A particle is assumed to interact with an eddy for a time which is the minimum of either the eddy lifetime or the time required for the particle to cross the eddy. Characteristic eddy sizes,  $L_e$ , and lifetimes,  $t_e$ , are estimated from the following expressions (Shuen et al. 1983a, 1985):

$$L_e = C_\mu^{3/4} k^{3/2} / \epsilon, \quad t_e = L_e / (2k/3)^{1/2} \quad (4)$$

Particles and eddies are assumed to interact as long as the time of interaction and the relative displacement of the particle and eddy are both less than  $t_e$  and  $L_e$ .

During baseline SSF analysis, the velocity PDF was taken to be isotropic and Gaussian, having standard deviations  $(2k/3)^{1/2}$  and mean values  $\bar{u}, \bar{v}$  with the tangential mean velocity  $\bar{w} = 0$ . However, the streamwise velocity fluctuations of particles in particle-laden jets are generally underestimated using this approach, an effect which has been attributed to ignoring the anisotropy of turbulent fluctuations generally observed in these flows (Shuen et al. 1985; Sun & Faeth 1986). For present initial considerations, anisotropy levels in the multiphase flows were correlated directly from the measurements and applied to the velocity PDFs, to minimize uncertainties in evaluation of the phenomenon.

Initial conditions for separated flow analysis were specified at  $x/d = 8$ , which was the position nearest the injector where all needed measurements could be made with acceptable spatial resolution and accuracy. Downstream of this position, particle volume fractions were less than 3%; therefore, particle collisions and effects of adjacent particles on particle transport

properties are negligible (Faeth 1986). Particle dimensions were less than 10% of the flow half width; therefore, particles were assumed to be in a locally uniform environment, based on liquid properties at their center. Particles were assumed to be spherical, and Magnus and Saffman-lift forces and static pressure gradients were neglected, similar to Shuen et al. (1983a).

Under these assumptions, particle motion was found using the formulation of Odar & Hamilton (1964), reviewed by Clift et al. (1978), as follows:

$$d x_{pi} / dt = u_{pi} \quad (5)$$

$$\begin{aligned} (\rho_p / \rho + \Delta_A / 2) d u_{ri} / dt = & a(\rho_p / \rho - 1) \delta_{li} - 3C_D |u_r| u_{ri} / (4d_p) \\ & - \Delta_H (81\nu / \pi d_p^2)^{1/2} \int_{t_0}^t (t-\xi)^{-1/2} (d u_{ri} / d\xi) d\xi \end{aligned} \quad (6)$$

where a Cartesian reference frame has been used with  $i=1$  denoting the vertical direction. The terms of the left-hand side of equation (6) represent accelerations due to particle and virtual mass, while the terms on the right-hand side represent buoyancy, drag and Basset-history forces.

The parameters  $\Delta_A$  account for particle acceleration; they were empirically correlated by Odar & Hamilton (1964), as follows:

$$\Delta_A = 2.1 - 0.123 M_A^2 / (1 + 0.12 M_A^2) \quad (7)$$

$$\Delta_H = 0.48 + 0.52 M_A^3 / (1 + M_A^3) \quad (8)$$

where  $M_A$  is the particle acceleration modulus

$$M_A = (d u_r / dt) d_p / u_r^2 \quad (9)$$

The values of  $\Delta_A$  and  $\Delta_H$  vary in the ranges 1.0-2.1 and 1.00-0.48, the former values being the correct limit for the Basset-Boussinesq-Oseen (B-B-O) formulation of equation (6) (Clift et al 1978).

For baseline computations, the B-B-O limit was used. Particle Reynolds numbers, based on the relative velocity of the particle and fluid, did not reach the supercritical flow regime; therefore, the standard drag coefficient for solid spheres was approximated as follows (Faeth, 1983):

$$C_D = 24(1 + Re^{2/3} / 6) / Re, \quad Re \leq 1000; \quad C_D = 0.44, \quad Re > 1000 \quad (10)$$

where  $Re$  denotes the particle Reynolds number.

Computations revealed that turbulent fluctuations of the continuous phase were often large in comparison to relative velocities; therefore, the extended version of the SSF analysis accounted for this effect following Clift et al. (1978) and Lopes & Dukler (1986). The expression for the drag coefficient in this case is as follows:

$$C_D = 162 I_r^{1/3} / Re, \quad Re \leq 50;$$

$$C_D = 0.133(1 + 150 / Re)^{1.565} + 4 I_r, \quad 50 < Re < 700 \quad (11)$$

where  $I_r$  is the relative turbulence intensity of the particles, taken as follows:

$$I_r = (2k/3)^{1/2} / u_r \quad (12)$$

assuming isotropic turbulence. These expressions were developed for  $I_r \leq 0.5$ ; however, they were used during the present calculations for  $I_r$  ranging up to 1.5, for lack of an alternative.

#### 2.3.4 Particle Source Terms (SSF Formulation)

The interaction between the particle and liquid phases yields source terms,  $S_{p\phi}$  in the governing equations for the liquid phase. For the baseline SSF analysis, this interaction is limited to the particle source term in the mean momentum equation ( $S_{pu}$  in Table 2), ignoring effects of turbulence modulation. The flow rate of particles along a given trajectory is conserved; therefore,  $\dot{n}_i$  is a constant specified near the injector to satisfy total particle flow rate requirements. The last term in  $S_{pu}$  accounts for effects of buoyancy on the flow; here  $\Delta t_p$  is the residence time of a particle in a computational cell (Sun & Faeth 1986).

Two approaches were examined to treat effects of turbulence modulation, denoted SSF-KMOD and SSF-EXT, similar to the limiting cases considered by Reitz & Diwakar (1987). Both versions adopt the source term  $S_{pk}$  given in Table 2, which is the same as Shuen et al. (1985). This term can be computed exactly from the SSF analysis and does not require modeling. The analogous term in the  $\epsilon$  equation has to be modeled. This term is simply ignored for the SSF-KMOD version, i.e.,  $S_{pe} = 0$ . For the SSF-EXT approach,  $S_{pe}$  is modeled by assuming that it is proportional to the source term in the  $k$  equation, similar to

treatments of this term by Reitz & Diwakar (1987) and in single-phase flows (Lockwood & Naguib 1975). This introduces a new empirical constant  $C_{\epsilon 3}$ . The value of  $C_{\epsilon 3}$  was chosen by considering equilibrium requirements in a homogeneous stationary flow where turbulence is only generated by particle motion; this implies that  $C_{\epsilon 3} = C_{\epsilon 2}$ .

### 2.3.5 Numerical Solution

Calculations for the liquid phase were performed using the GENMIX algorithm of Spalding (1977), which uses a second-order implicit central-difference scheme. The computational grid was similar to Shuen et al. (1983, 1983a, 1985): 33 crossstream grid nodes, with streamwise step sizes limited to 6% of the current flow width or an entrained flow increase of 5% – whichever was smaller. The particle phase was computed by a second-order finite-difference algorithm employing 7200 and 9600 trajectories for the case I and II flows.

### 2.3.6 Simplified Analysis

DSF method. All turbulence particle interactions are ignored using the DSF approach. Particle trajectories are found by integrating equations (5) and (6) with local mean liquid velocities replacing instantaneous eddy velocities. Thus, each initial condition yields a single deterministic trajectory and only  $S_{pu}$  is considered in the solution for liquid-phase properties. Particle drag was computed from equation (10), similar to the baseline SSF approach. The number of particle trajectories was also the same as for the SSF computations.

LHF method. This approximation implies that both phases have the same instantaneous velocity at each point; therefore, the flow corresponds to a variable-density single-phase flow whose density changes due to changes in particle concentration. Turbulent dispersion of particles is then equivalent to the turbulent diffusion of liquid, and particle inertia fully influences turbulence properties. Thus, the method allows for turbulence modulation, to the extent that negligible relative velocities between the phases is correct.

The formulation in this case is identical to Shuen et al. (1983, 1983a, 1985) and Sun and coworkers (1985, 1986). The procedure follows the conserved-scalar formalism which is widely-used for flows having variable scalar properties (Bilger 1976; Faeth 1986).

## 2.4 Results and Discussion

### 2.4.1 Drag Calibrations

Particle drag was calibrated by measuring the terminal velocities of single particles in still water. This was carried out by positioning a plate containing a small aperture below the particle feeder. The aperture plate collected most particles, allowing only an occasional particle to pass into the liquid and fall through the LDA measuring volume. The LDA was positioned

200 mm below the liquid surface; therefore, the particles were isolated and essentially at their terminal velocity condition when their velocity was measured.

Roughly 200 particle velocities were measured. Measurements yielded a mean terminal velocity of 0.05 m/s with a standard deviation of 0.01 m/s. Analysis showed that the particle drag coefficient was generally 1.5 times larger than the standard drag correlation provided by equation (10); therefore,  $C_D$  was increased by this amount for all separated-flow calculations. A possible reason for the increased  $C_D$  was the irregular shape of some of the particles (only roughly 60% were true spheres).

### 2.4.2 Near-Injector Properties

Initial conditions for separated-flow calculations were measured at  $x/d = 8$ , since high particle densities nearer to the injector tended to block LDA signals. The following measurements were made:  $\bar{u}$ ,  $\bar{u}'$ ,  $\bar{v}$  and  $\overline{u'v'}$  for the liquid phase;  $\tilde{u}_p$ ,  $\tilde{v}_p$ ,  $\tilde{u}_p'$  and  $\tilde{v}_p'$  for the particles, where the Favre-average denotes a particle-weighted average; and  $\dot{n}$ , the particle number flux. The symbols  $\bar{u}'$ ,  $\bar{v}'$ ,  $\tilde{u}_p'$ ,  $\tilde{v}_p'$  represent root-mean-square fluctuating velocities.

The measurements at  $x/d = 8$  were supplemented by other estimates in order to complete the specification of initial conditions. The tangential components of the mean liquid and particle velocities were assumed to be zero, since the particles gave no indication of swirling motion. Tangential velocity fluctuations of both phases were assumed to be equal to their respective radial velocity fluctuations. This approximation provided initial values of  $k$  for the liquid. Given the distributions of  $\bar{u}$ ,  $\overline{u'v'}$  and  $k$ , profiles of  $\epsilon$  were estimated from the expression for the turbulent viscosity, equation (3), e.g.

$$\epsilon = C_\mu k^2 \partial \bar{u} / \partial r / \overline{u'v'} \quad (13)$$

Liquid-phase properties for the single-phase and two particle-laden jets are illustrated in figure 6. Since the particle-laden jets were dilute, the values of  $\bar{u}$ ,  $\bar{u}'$  and  $\bar{v}'$  are not very different for the three flows. However,  $k$  and  $\overline{u'v'}$  are quadratic quantities which are more sensitive indicators of effects of particles. Near the axis,  $\overline{u'v'}$  becomes smaller in the particle-laden jets, while velocity fluctuations and  $k$  are increased. These effects tend to increase with increased particle loading and are evidence of turbulence modulation due to additional dissipation of potential energy of particles.

Mean and fluctuating particle velocities at  $x/d = 8$  are illustrated in figure 7. The properties of the two flows are essentially the same.  $\tilde{u}_p$  roughly parallels  $\bar{u}$ , while  $\tilde{v}_p$  increases near

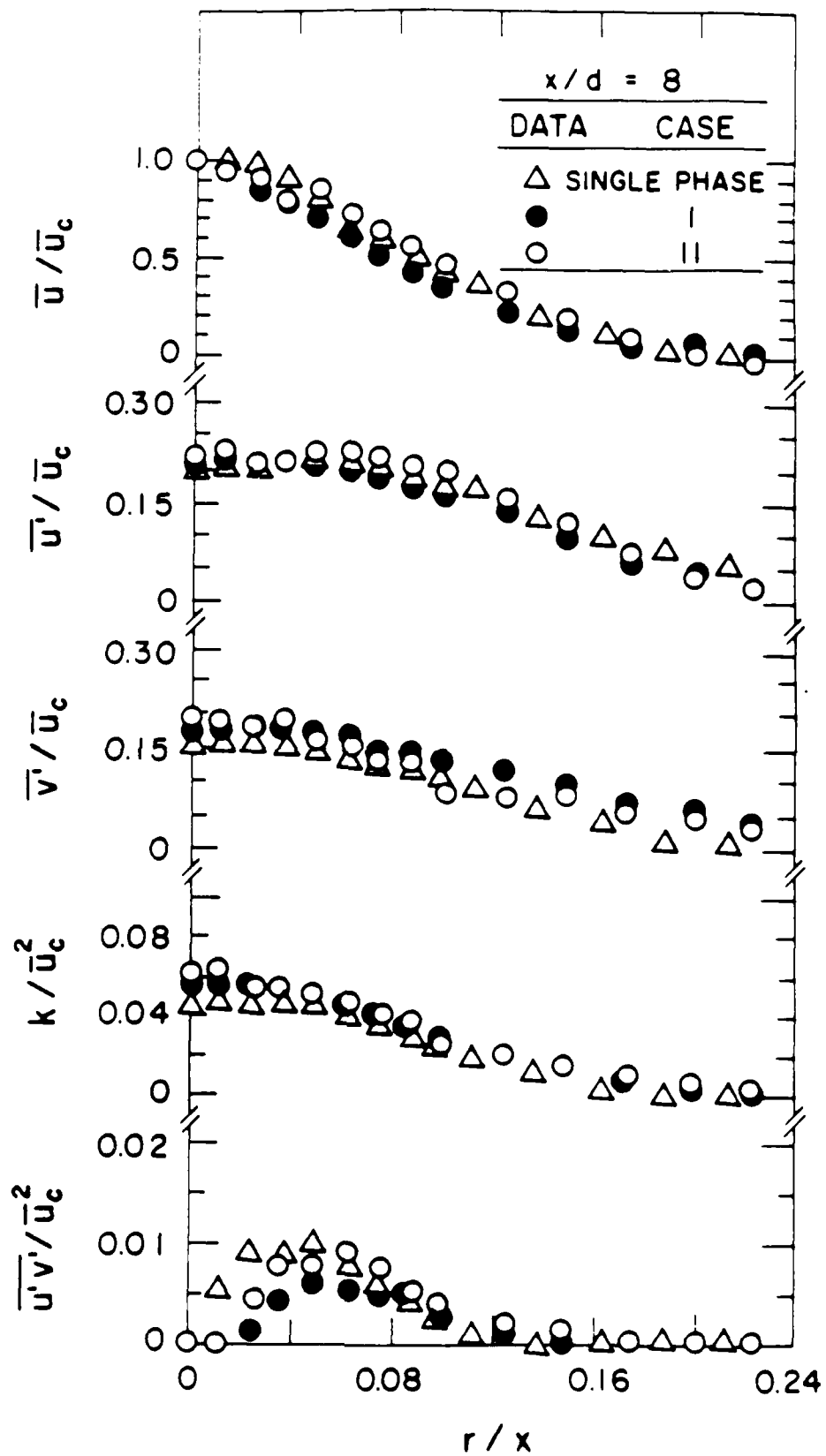


Figure 6. Mean and turbulent liquid properties at  $x/d = 8$ .

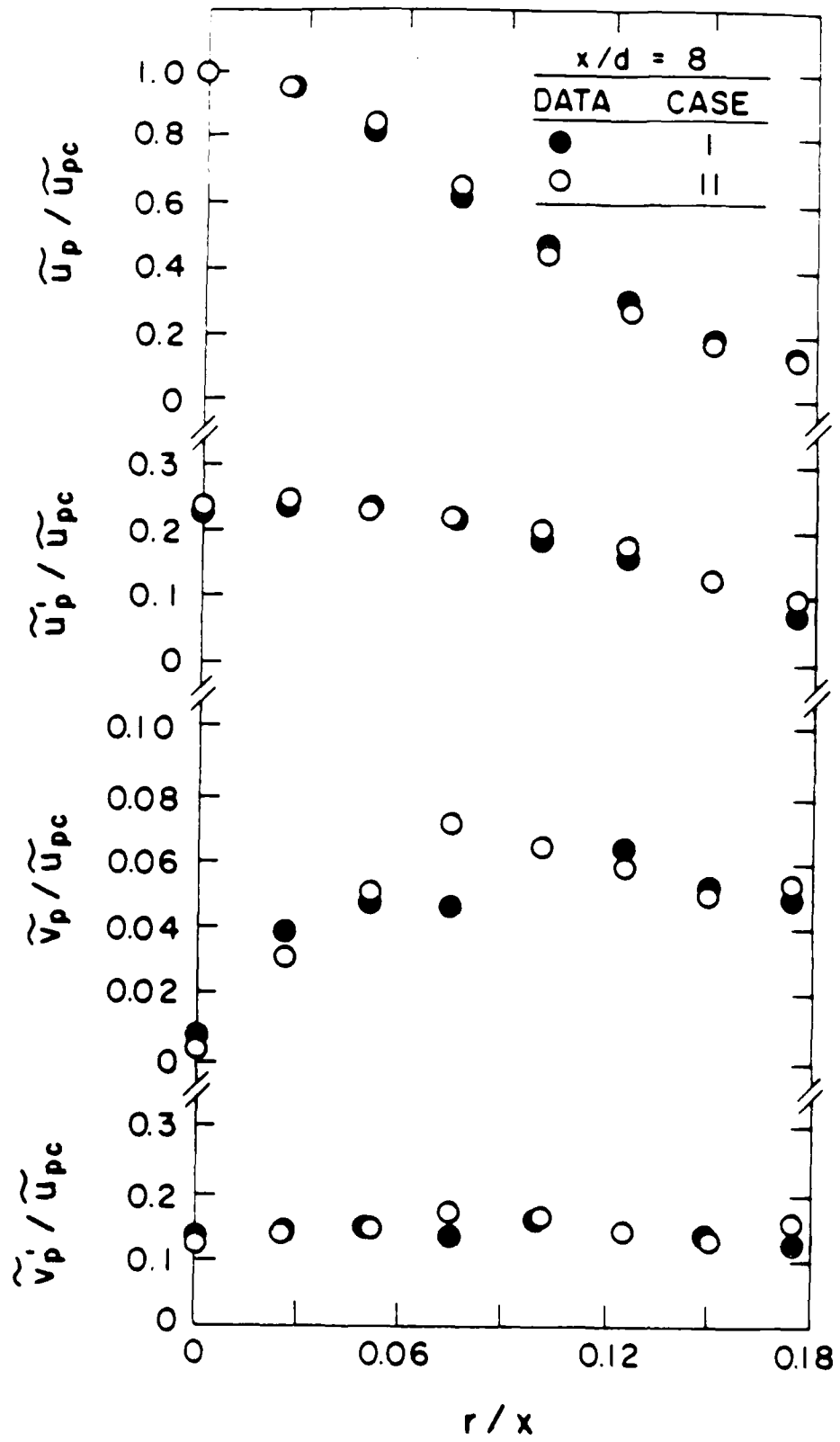


Figure 7. Mean and fluctuating particle velocities at  $x/d = 8$ .

near the axis and then remains relatively constant near the edge of the flow. Unlike mean radial liquid velocities (Wynanski & Fiedler 1969), there is no tendency for  $\tilde{v}_p$  to become negative near the edge of the flow, since particles are not entrained from the surroundings.  $\tilde{u}_p$  is greater than  $\tilde{v}_p$  near the axis, exhibiting greater anisotropy than fluctuating liquid velocities in this region (cf. figure 6). Similar to  $\bar{u}$  and  $\bar{v}$ , however,  $\tilde{u}_p$  and  $\tilde{v}_p$  are comparable near the edge of the flow.

Particle number flux distributions for the two particle-laden jets are illustrated in figure 8. The distributions are reasonably symmetric about the axis. The half-widths of the distributions are roughly  $r/x \sim 0.09$  and  $0.10$  for the case I and II flows.

In contrast to the separated-flow calculations, initial conditions for the LHF approach were specified at the injector exit. The flow was assumed to be fully developed at the exit, with the distribution of  $\bar{u}$  obtained from Schlichting (1979), and the distributions of  $k$  and  $\epsilon$  obtained from Hinze (1975), all at the Reynolds number range of the present experiments.

### 2.4.3 Properties Along Axis

Predicted and measured mean streamwise velocities along the axis are illustrated in figure 9. Results are shown for all methods of analysis – LHF, DSF, SSF-BASE (the baseline version), SSF-KMOD (accounting for turbulence modulation in the  $k$  equation), and SSF-EXT (accounting for turbulence modulation in both the  $k$  and  $\epsilon$  equations).

Only LHF calculations, initiated at the jet exit, were carried out for the single-phase flow. Since the initial flow was fully developed pipe flow, there is no potential core, although velocity changes along the axis are small for  $x/d < 3$ . Farther downstream, centerline velocities decay according to  $x^{-1}$ , which is expected for single-phase round jets. The comparison between predictions and measurements is excellent – well within experimental uncertainties. This was true for other properties of the single-phase flow, as will be discussed subsequently. These findings are typical of past experience concerning the performance of the present turbulence model for round jet flows (Jeng and Faeth 1984; Shuen et al. 1985; Sun & Faeth 1986), establishing a baseline for analysis of the particle-laden jets.

Mean liquid phase velocities along the axis are also illustrated for the two particle-laden jets in figure 9. The measurements are nearly identical to the single-phase jet, which is expected since the particle-laden flows were very dilute. The DSF, SSF-BASE and SSF-EXT predictions are the same and are represented by a single line for the particle-laden jet results illustrated in figure 9. Except for the SSF-KMOD version, all methods of analysis agree reasonably well with each other and with the measurements. However, mean continuous-phase properties are not strongly influenced by the dispersed phase in dilute

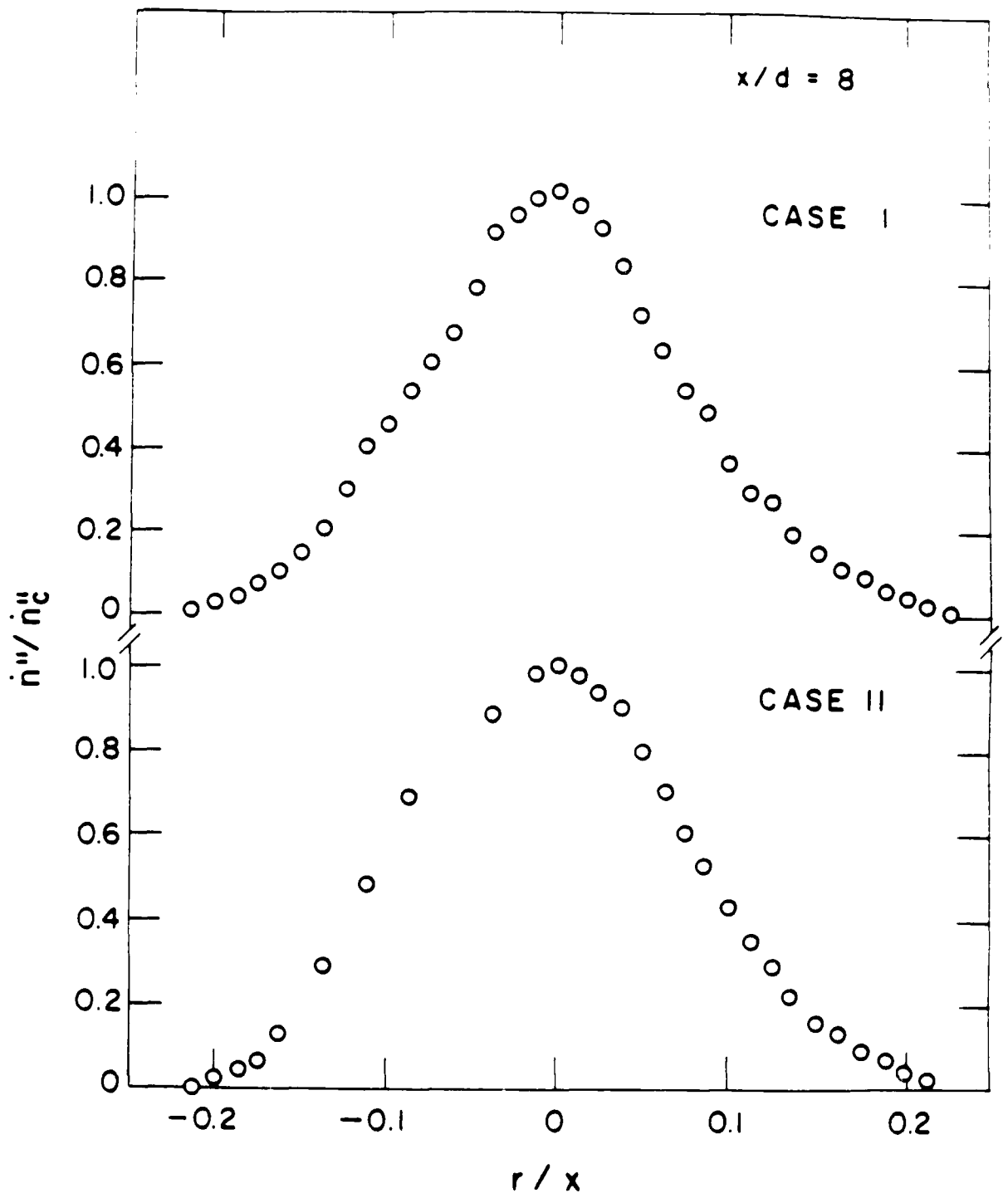


Figure 8. Mean particle number fluxes at x/d = 8.

multiphase jets; therefore, this observation is a relatively weak indicator of the performance of these methods (Shuen et al. 1983, 1983a, 1985).

In contrast to other methods pictured in figure 9, the SSF-KMOD predictions substantially underestimate the rate of decay of  $\bar{u}_c$  with distance along the axis. This behavior is similar to the findings of Sun et al. (1986) and Reitz & Diwakar (1987) for treatments of turbulence modulation limited to a source term in the governing equation for  $k$ . This term acts like a sink, reducing the turbulence kinetic energy of the flow, and thus, the rate of turbulent mixing. The problem appears to be an effect of scale, where the particles generally only influence the higher wave number end of the turbulence spectrum, rather than the large scale turbulence which is primarily responsible for turbulent mixing (Hinze 1972). The SSF-EXT approach avoids the problem through the use of a particle source term in the governing equation for  $\epsilon$ , which apparently results in unchanged gross mixing levels in the present flows. The SSF-BASE method achieves the same objective (more crudely) by neglecting turbulence modulation entirely, which is tantamount to assuming that these phenomena occur on scales that don't influence the low wave-number range of the turbulence spectrum which is responsible for mixing. This has been satisfactory for particle-laden flows considered in this laboratory (Shuen et al. 1983, 1983a, 1985; Sun & Faeth 1986), but it is clearly not a reliable approach. Earlier studies by Al Taweel & Landau (1977), Elghobashi & Abou-Arab (1983) and others (cf. Faeth 1986), have sought to include effects of scales on turbulence modulation. Based on present findings, additional theoretical and experimental work along these lines is clearly needed.

The variation of streamwise mean particle velocities along the axis of the two particle-laden jets is illustrated in figure 10. The measurements clearly show that mean particle velocities do not decay according to  $x^{-1}$  like the liquid, which is the rate given by the LHF predictions. This behavior is caused by the finite inertia of the particles, which only separated-flow analysis can treat. As before, the SSF-BASE and SSF-EXT methods yield very similar predictions which are in reasonably good agreement with the measurements. Other separated flow predictions are deficient to some extent. The SSF-KMOD approach underestimates the rate of decay of  $\bar{u}_{pc}$ , largely since it underestimates the rate of decay of  $\bar{u}_c$ . The DSF approach allows for particle inertia, but significantly underestimates the rate of decay of  $\bar{u}_{pc}$ , even though this approach yielded acceptable estimates of liquid velocities along the axis (cf. figure 9). This is an effect of the nonlinear drag law for present conditions. Drag is almost a quadratic function of the relative velocity for present conditions; therefore, when linearized, by using mean properties to represent the liquid phase properties, its magnitude is biased toward smaller values. This deficiency of DSF analysis has also been observed for nonevaporating sprays (Solomon et al. 1985).

Predictions and measurements of particle number fluxes along the axis are illustrated in figure 11. The measurements roughly follow an  $x^{-1}$  variation, rather than an  $x^{-2}$  variation that

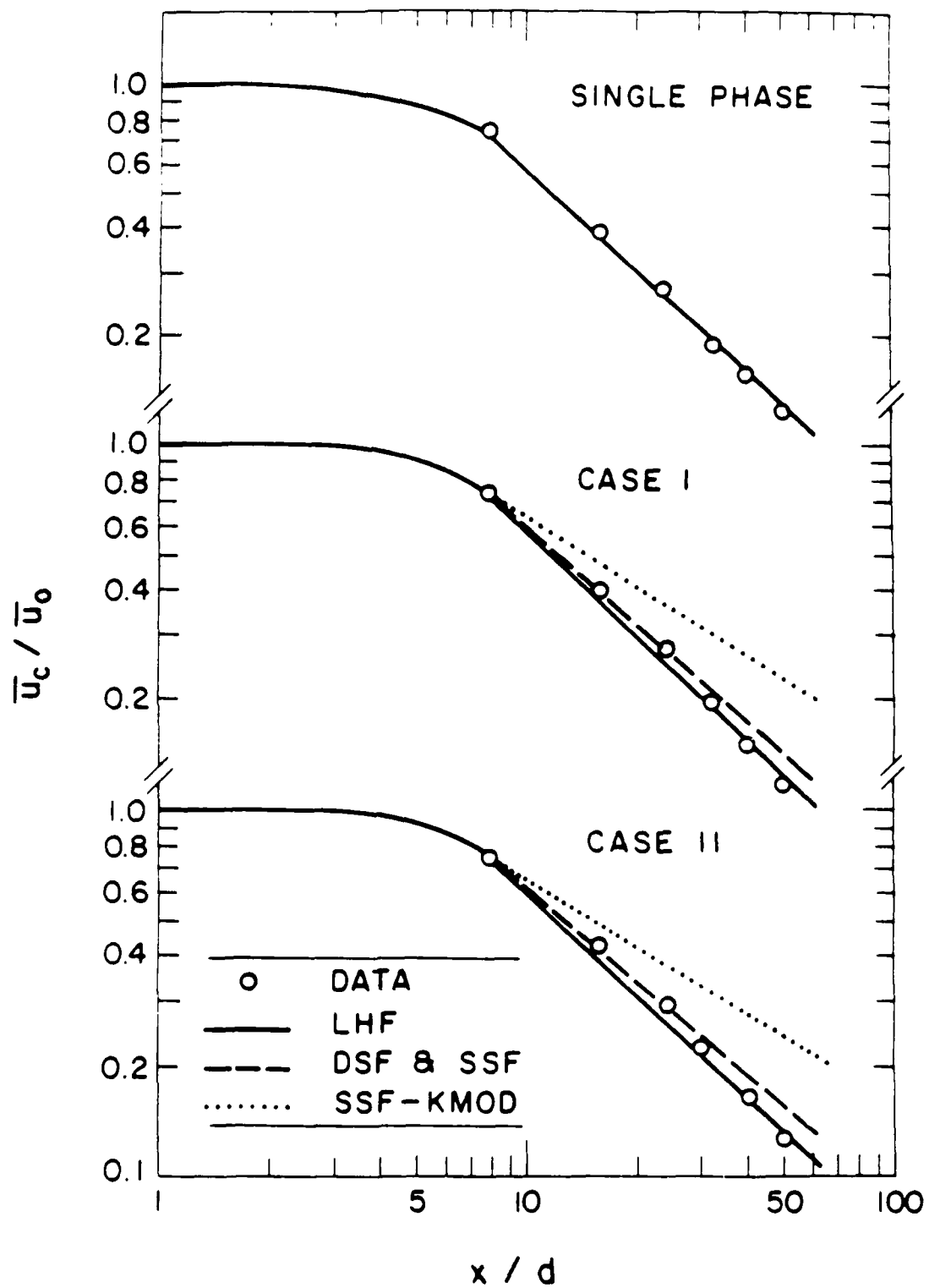


Figure 3. Mean liquid velocities along axis.

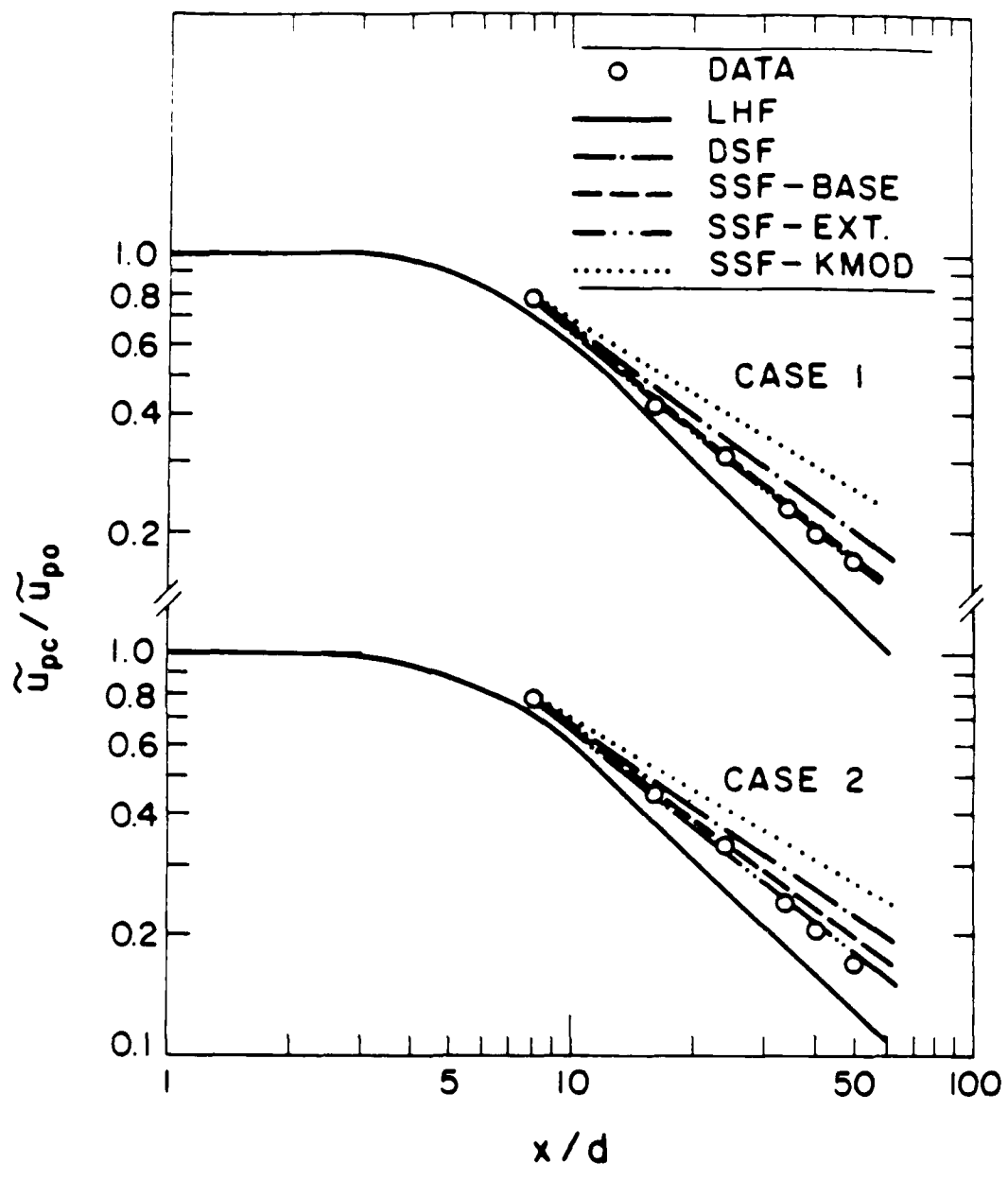


Figure 10. Mean particle velocities along axis.

would be expected for a passive contaminant in a round jet (which is similar to the LHF predictions illustrated in figure 11). This difference is due to effects of particle inertia, which inhibits particles from diffusing like the fluid. Particle number fluxes along the axis are sensitive indicators of capabilities for predicting the turbulent dispersion of the particles; therefore, it is encouraging that the SSF-BASE and SSF-EXT methods yield predictions which are in reasonably good agreement with the measurements. The DSF method yields good results for a short distance after  $x/d = 8$ , where initial conditions are specified. This is due to the imposition of measured mean particle radial velocities at the initial condition. Subsequently, the DSF method fails once these velocities decay in response to the mean liquid motion, due to neglect of particle/turbulence interactions responsible for turbulent dispersion. The SSF-KMOD results are even worse, due to poor predictions of liquid phase mixing and turbulence levels – both of which reduce particle spread rates.

#### 2.4.4 Liquid Properties

Radial profiles of  $\bar{u}$ ,  $\bar{u}'$ ,  $\bar{v}'$  and  $\bar{u}'\bar{v}'$  were measured at  $x/d = 16, 24$  and  $40$ . Predictions of  $\bar{u}'$  and  $\bar{v}'$  were estimated from  $k$ , assuming  $\bar{u}'^2: \bar{v}'^2 = k:k/2$ , which are the ratios usually observed near the axis of single-phase jets (Wyganski & Fiedler 1969). Similar to results along the axis, measured values of  $k$  were found by assuming  $\bar{v}' = \bar{w}'$  (since  $\bar{w}'$  was not measured) which is also reasonable for jets (Wyganski & Fiedler 1969). In the following, flow variables are plotted as a function of  $r/x$ , which is the similarity variable for fully developed jets and plumes (Hinze 1975), in order to indicate estimates of flow widths.

Predictions and measurements for the single-phase jet are illustrated in figures 12-14 for  $x/d = 16, 24$  and  $40$ . The comparison between predictions and measurements of most properties is quite good, suggesting reasonable baseline behavior of the turbulence model for present test conditions, as noted earlier. Exceptions are  $k$ , and to a lesser degree  $\bar{u}'$  and  $\bar{v}'$ , near the axis at  $x/d = 24$ . These measurements were rechecked several times, since they were unusual based on past experience, without resolving the difficulty. As a result, greater emphasis will be placed on results at  $x/d = 40$ , in the following, when drawing conclusions concerning flow phenomena.

Predictions and measurements of liquid properties for the two particle-laden jets at  $x/d = 16$  and  $40$  are illustrated in figures 15-20. LHF and SSF-BASE predictions are shown on the plots; however, SSF-EXT and DSF predictions were essentially identical to the latter. The LHF predictions appearing on the figures are essentially the same as results for the single-phase jet, due to the light particle loading of the present flows.

LHF and SSF predictions and the measurements at  $x/d = 24$  and  $40$ , are all in reasonably good agreement. This performance is similar to earlier results for particle-laden jets in gases (Shuen et al. 1983, 1983a, 1985) and bubbles in liquids (Sun & Faeth 1986). The LHF

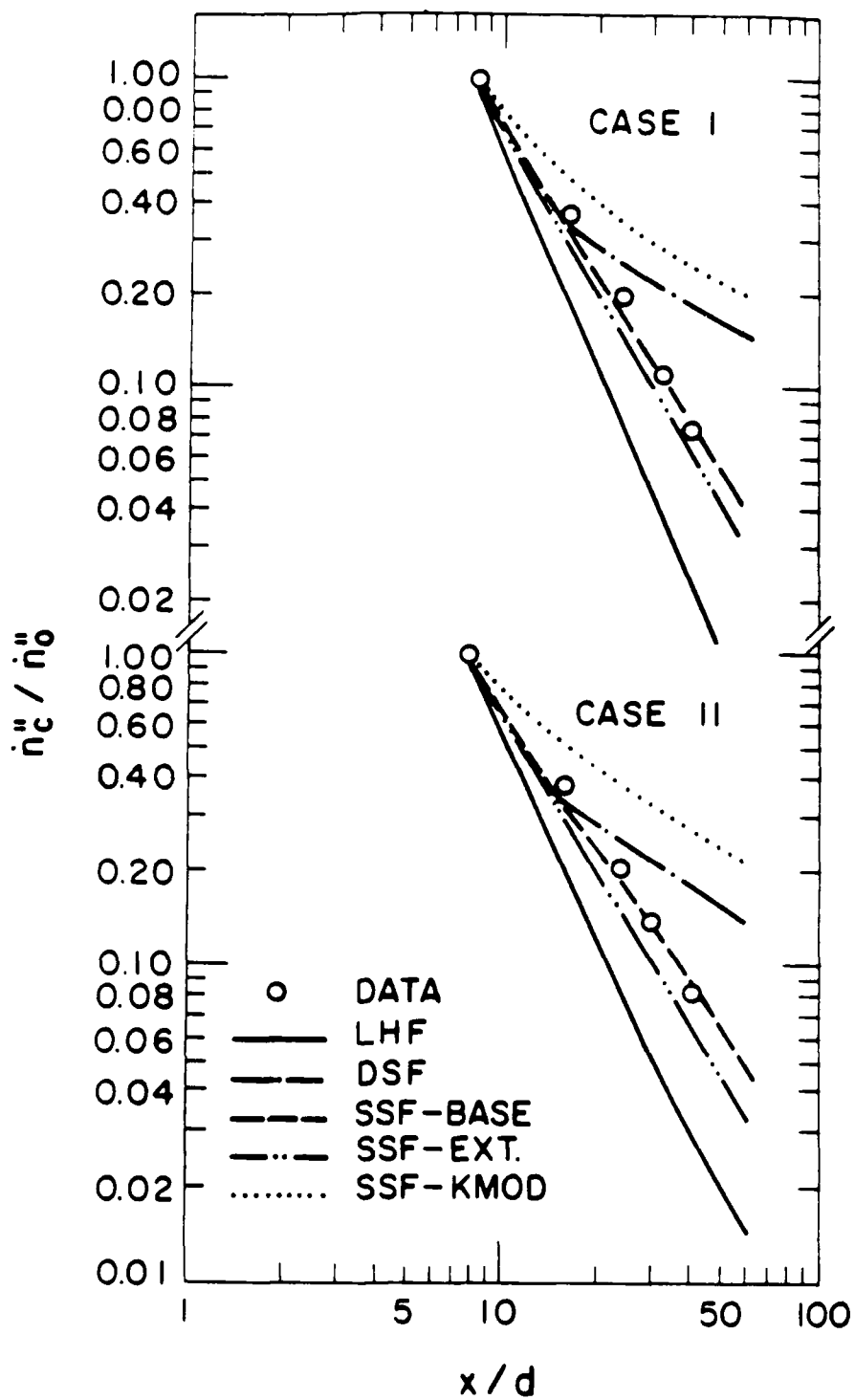


Figure 11. Mean particle number fluxes along axis.

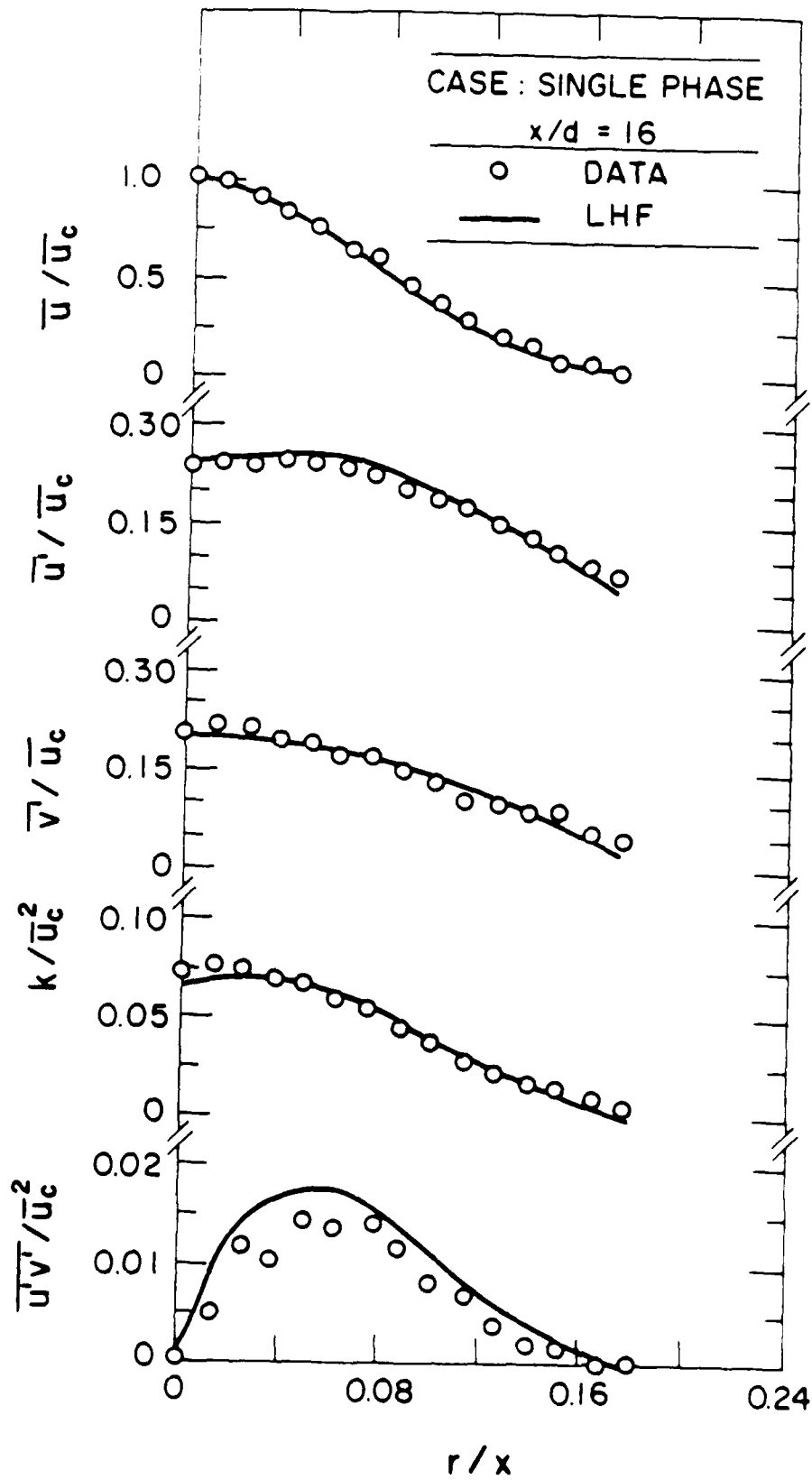


Figure 12. Mean and turbulent properties for single-phase jet ( $x/d = 16$ ).

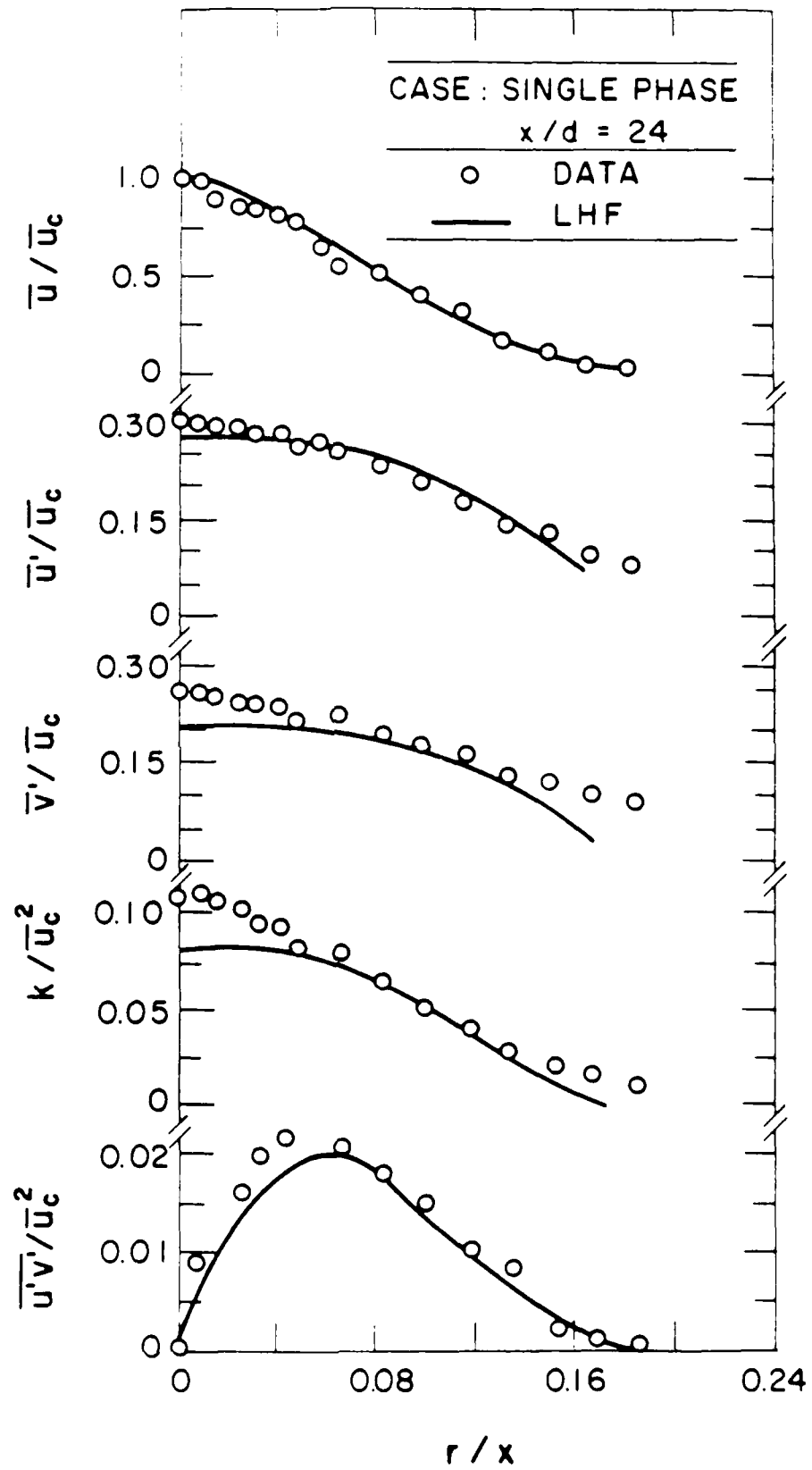


Figure 15. Mean and turbulent properties for the single-phase jet ( $x/d = 24$ ).

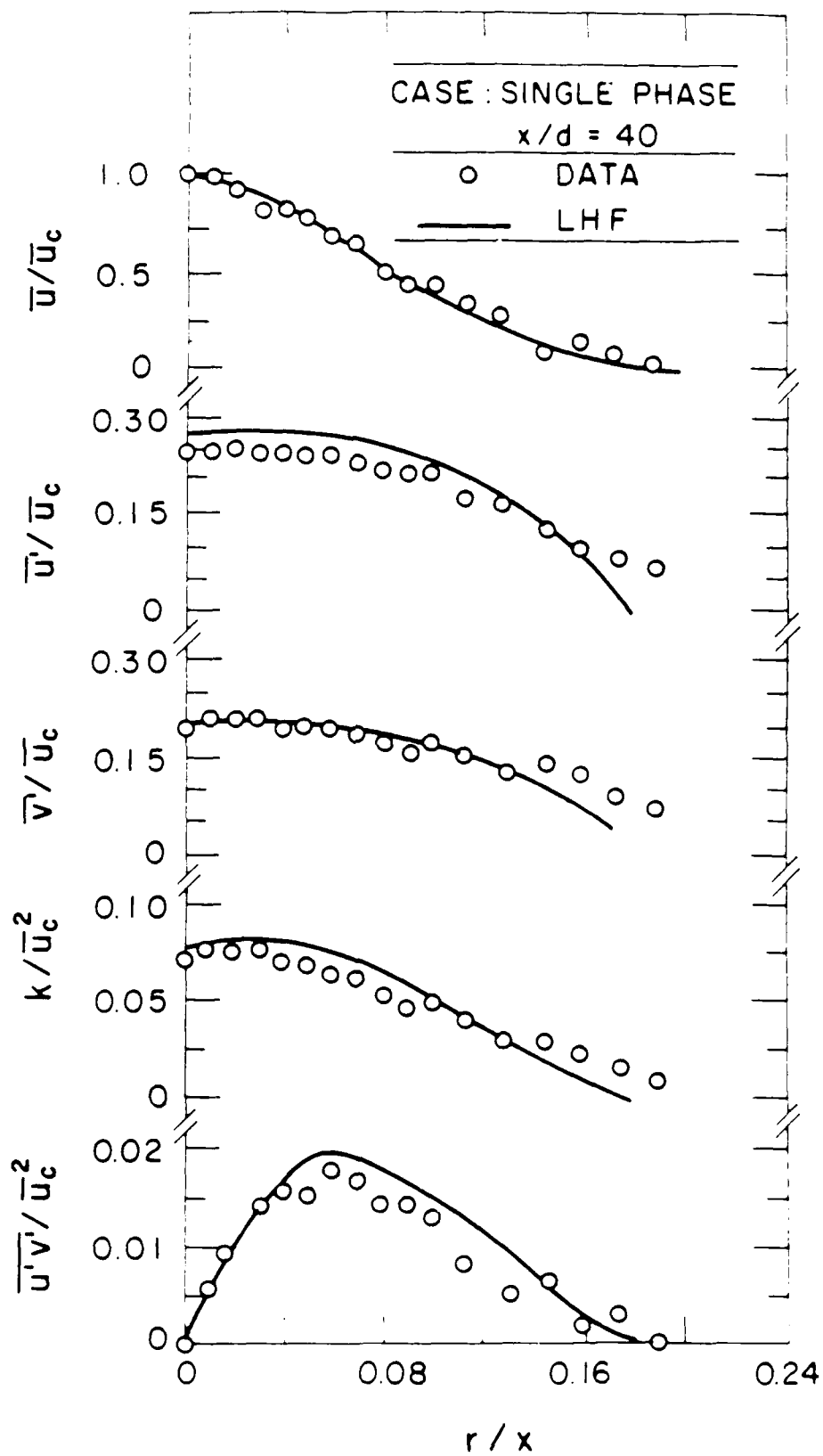


Figure 14. Mean and turbulent properties for the single-phase jet ( $x/d = 40$ ).

method also performs reasonably well at  $x/d = 16$ ; however, SSF predictions are not as satisfactory at this position, particularly for the case I jet. This problem is probably due to errors in the specification of initial conditions at  $x/d = 8$ . The approach used to estimate  $\epsilon$  is particularly problematical, since it involves several quadratic variables and the evaluation of a mean velocity gradient, leading to substantial uncertainties (the correctness of equation (3) aside). This view is supported by evaluation of the sensitivity of predictions to uncertainties in initial conditions, to be discussed later. In addition, LHF computations suggest relatively small effects of particles on liquid properties and yield better predictions, using initial conditions farther upstream, which provides more distance for errors in initial conditions to decay. Separated-flow predictions initiated at the injector exit (using estimated initial conditions), improve as well.

Another feature of the liquid-phase measurements is the progressive increase of  $k$  (above predictions) near the axis as distance and initial particle loading are increased. This phenomenon does not influence the gross mixing properties of the flow and is felt to be due to turbulence modulation. The effect on the turbulence spectra is probably limited to wave numbers somewhat higher than the energy-containing range, but direct measurements are needed to assess this hypothesis. The effect is most evident near the axis, since conventional turbulence production by shear forces in the continuous phase is small in this region. The enhancement of  $k$  grows with increasing distance from the injector, since liquid velocities are decreasing and becoming more comparable to velocity differences between the phases. Similar behavior has been observed in bubbly jets, far from the injector (Sun & Faeth 1986; Sun et al. 1986). Additional analysis and measurements concerning turbulence modulation are clearly needed in order to gain a better understanding of this type of particle/turbulence interaction.

#### 2.4.5 Particle Velocities

Predicted and measured mean and fluctuating particle velocities for the two particle-laden jets are illustrated in figures 21-26. Results are shown for  $x/d = 16, 24$  and  $40$ . Since deficiencies of the DSF and SSF-KMOD approaches have already been discussed, predictions are only shown for the LHF, SSF-BASE and SSF-EXT methods. LHF predictions are virtually identical to predictions of liquid properties for all methods.

The LHF method generally provides reasonably good predictions of particle properties, when normalized in the manner of figures 21-26. This is fortuitous, since the centerline velocities used to normalize the results are underestimated by the LHF approach, cf., figure 10. The separated-flow predictions are in best agreement with unnormalized particle velocities.

Both separated-flow methods tend to overestimate  $\tilde{u}_p / \tilde{u}_{pc}$  at  $x/d = 16$ , which is unusual since profiles of mean dispersed-phase velocities have generally been predicted reasonably well in the past (Shuen et al. 1983, 1983a, 1985; Sun & Faeth 1986). However, this difficulty disappears at greater distances from the injector, cf. figures 23 and 26 for  $x/d = 40$ , suggesting

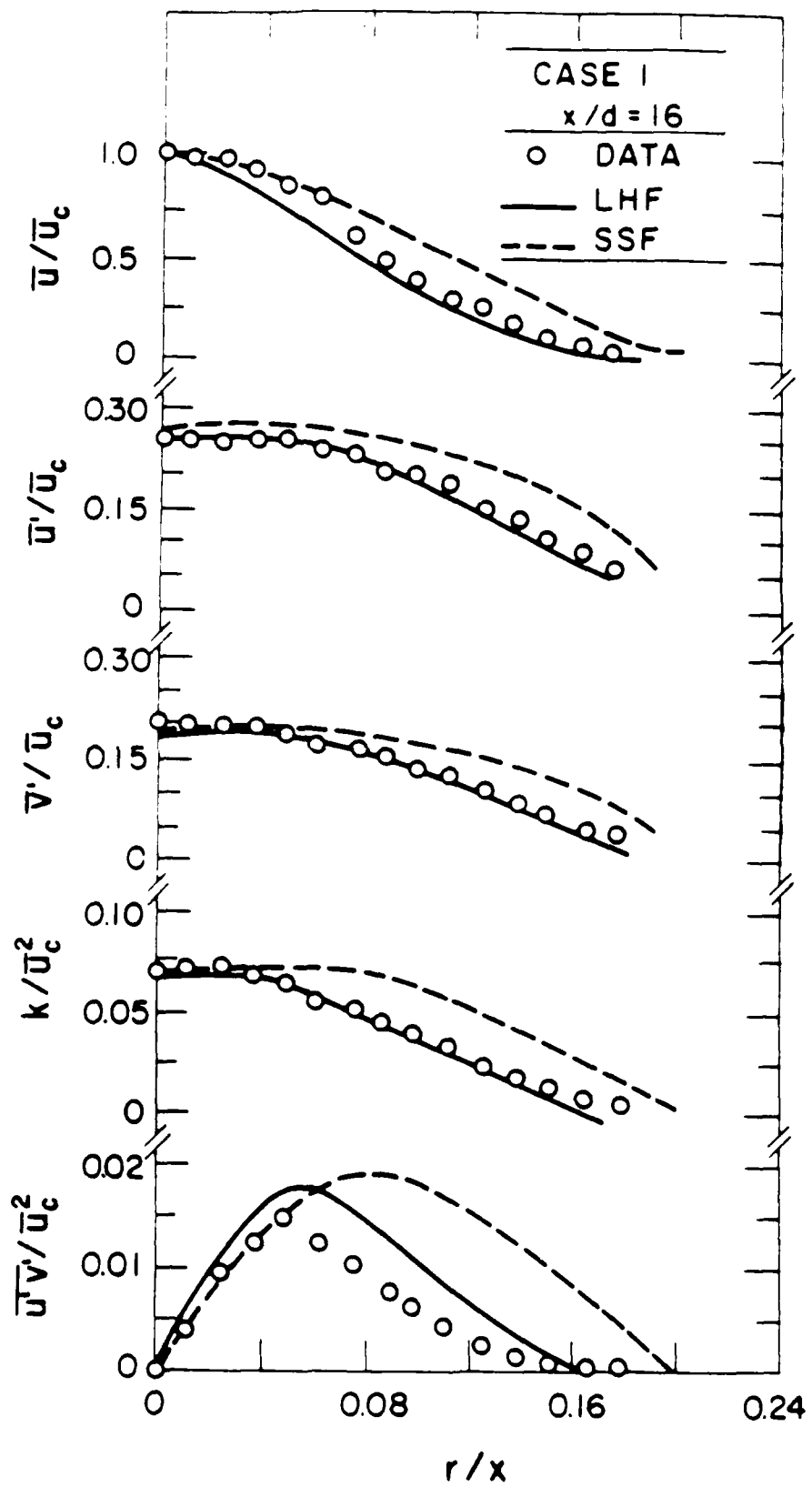


Figure 15. Mean and turbulent liquid properties (case I,  $x/d = 16$ ).

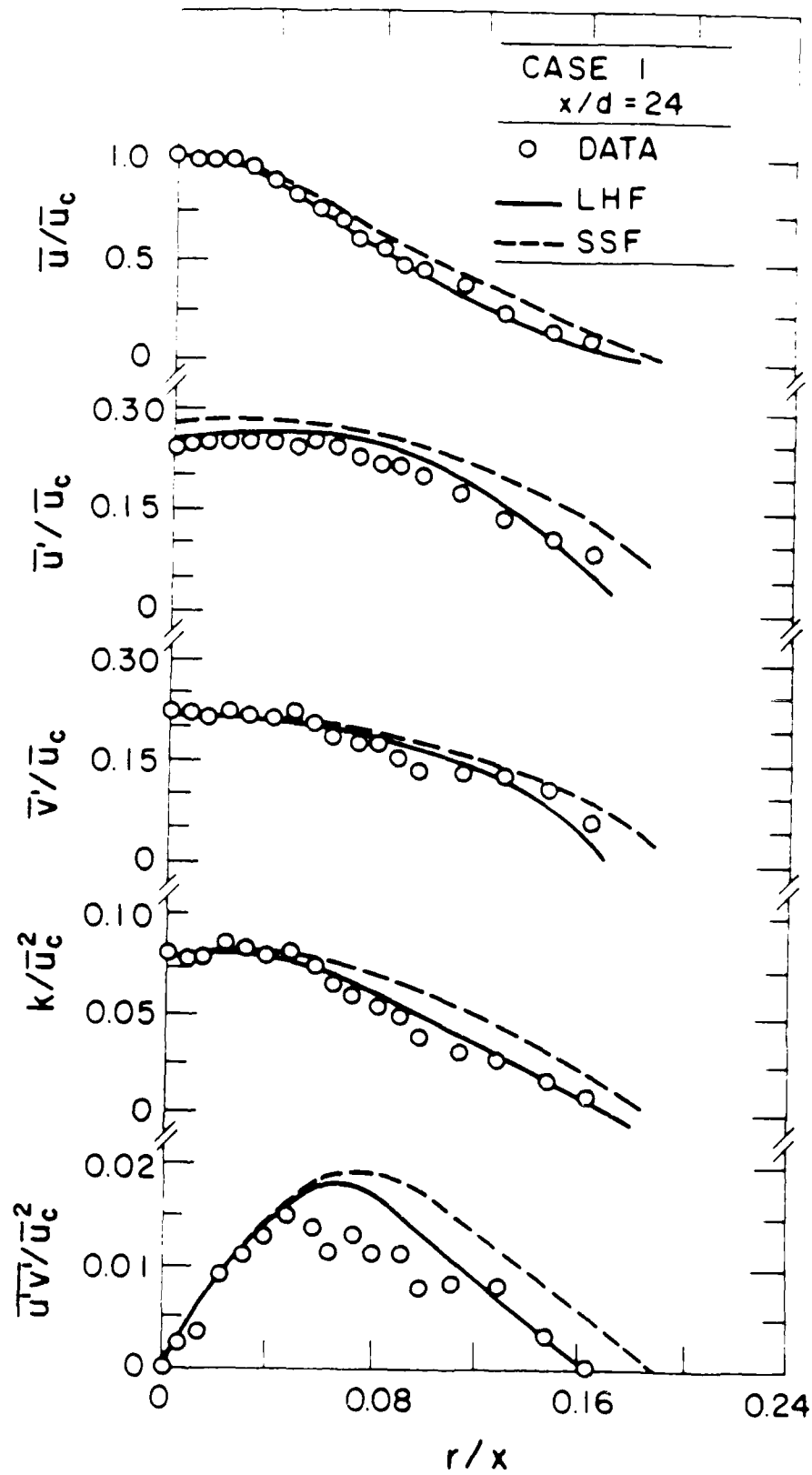


Figure 16. Mean and turbulent liquid properties (case I,  $x/d = 24$ ).

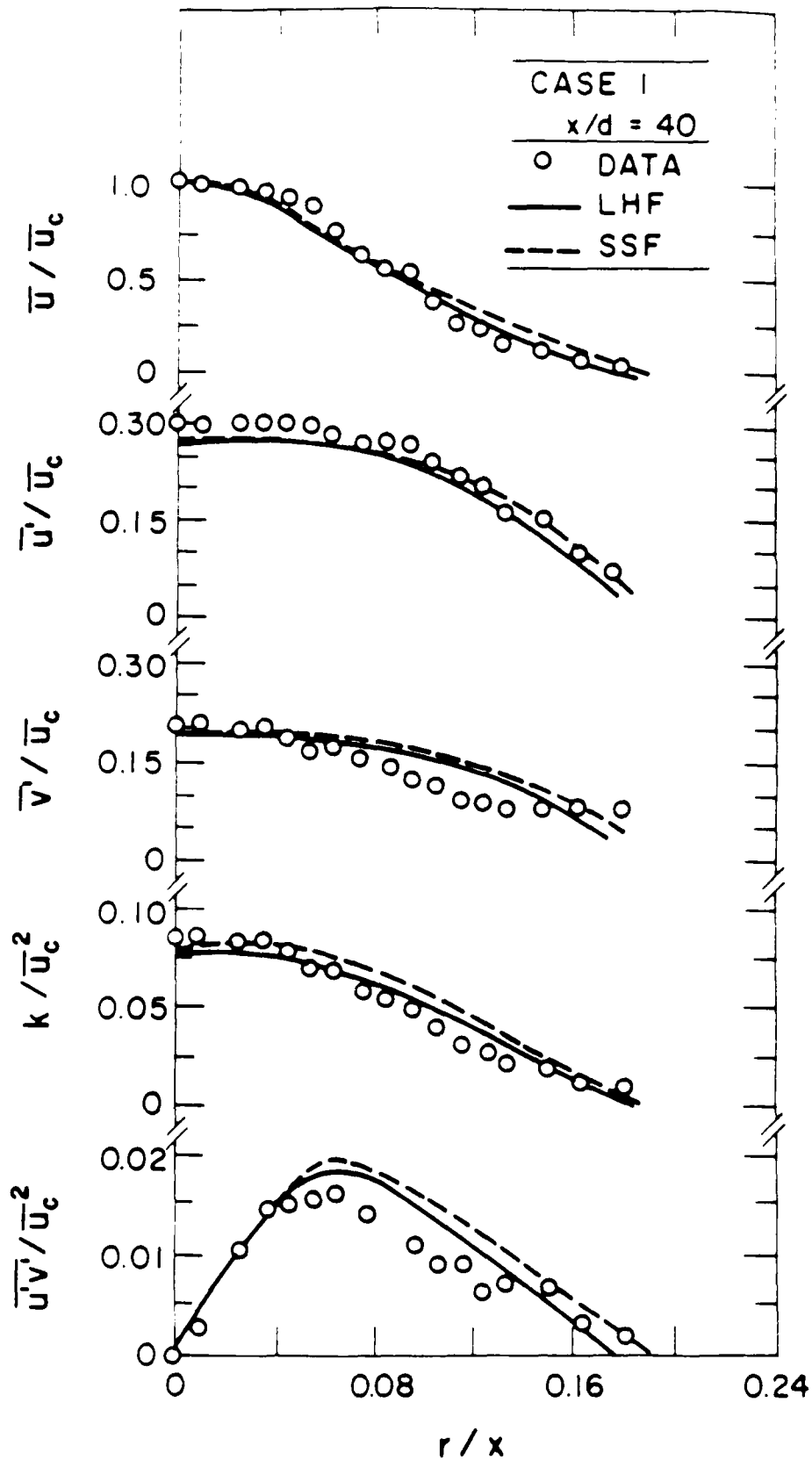


Figure 17. Mean and turbulent liquid properties (case I,  $x/d = 40$ ).

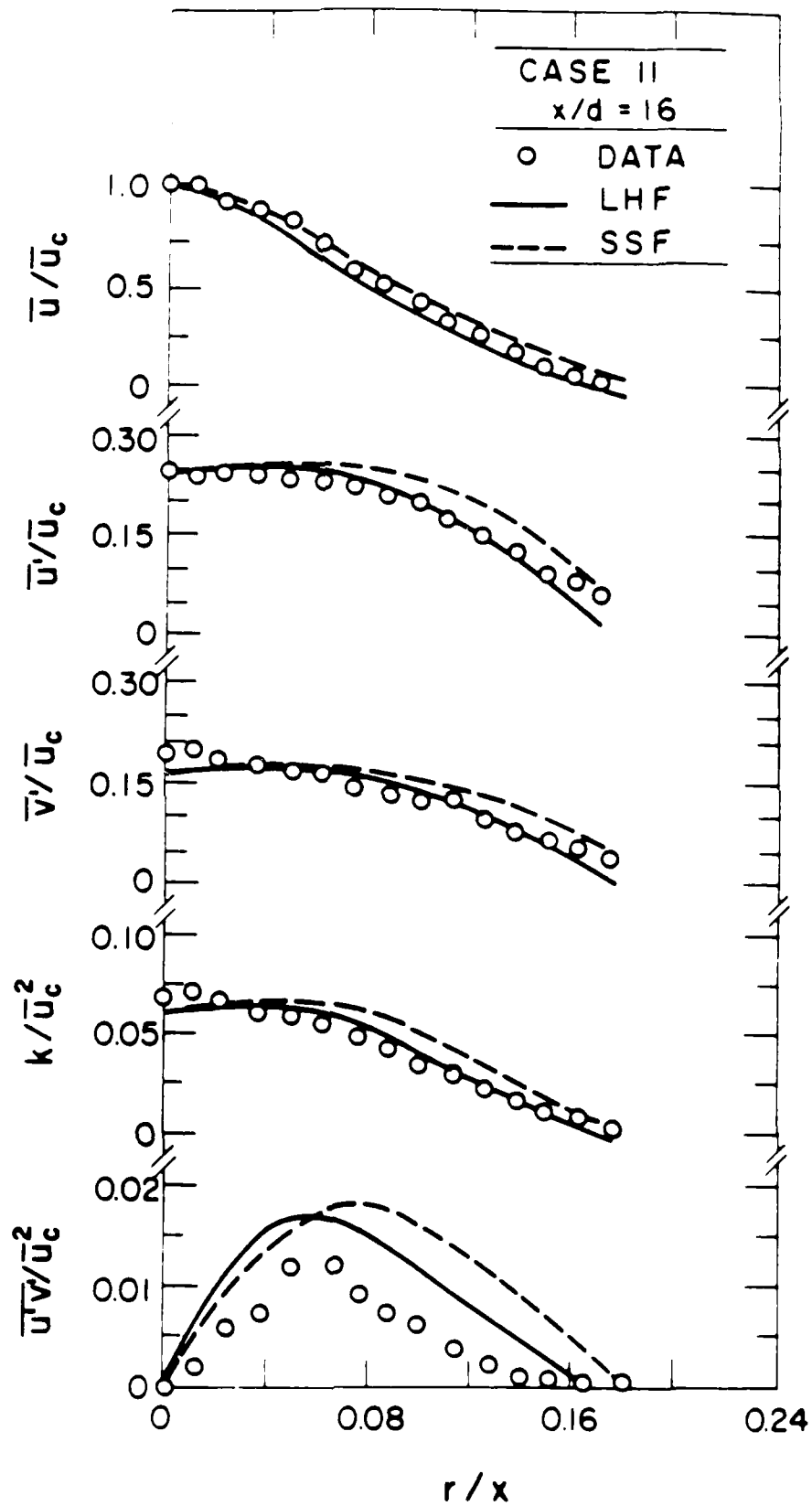


Figure 15. Mean and turbulent liquid properties (case II,  $x/d = 16$ ).

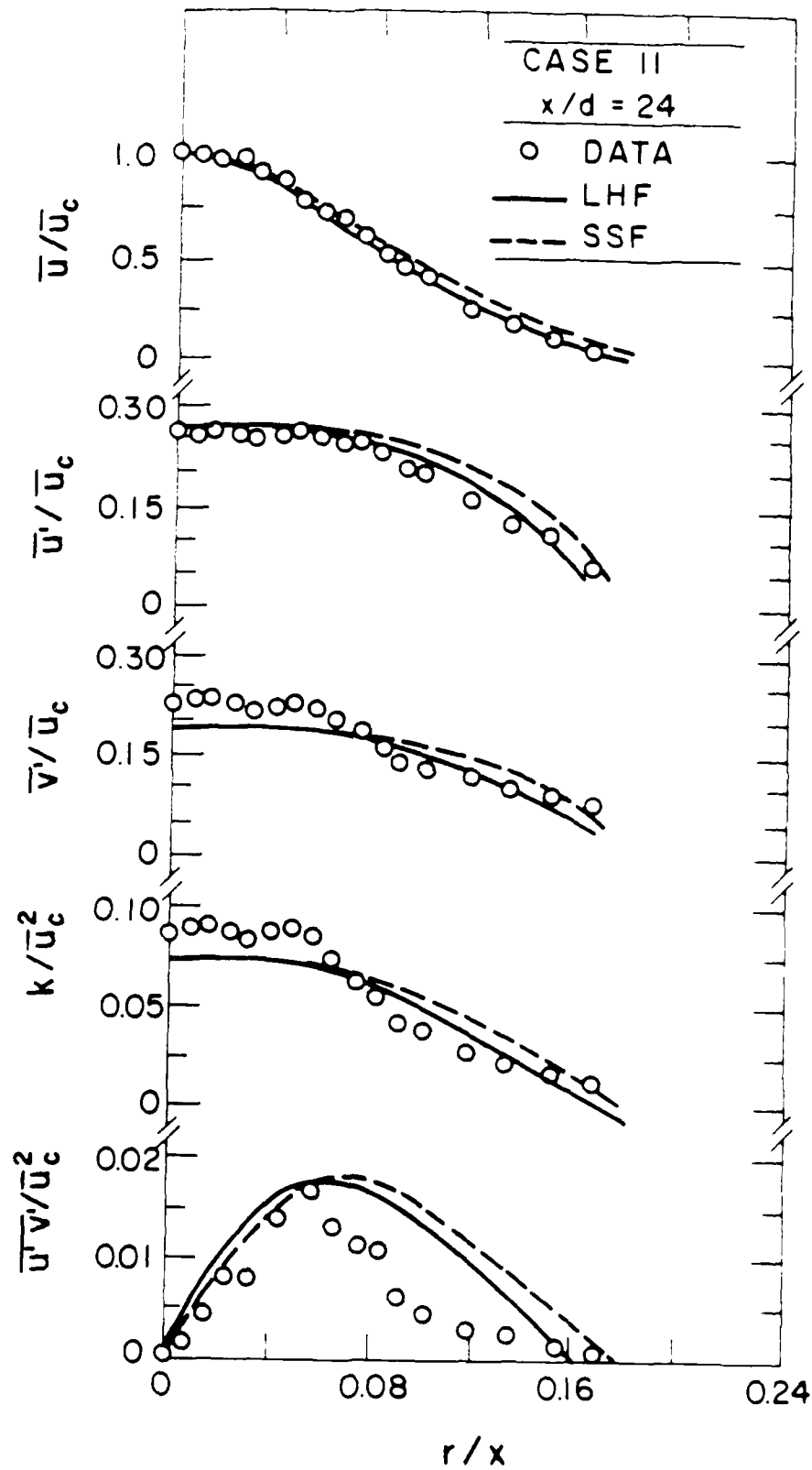


Figure 10. Mean and turbulent liquid properties (case II,  $x/d = 24$ ).

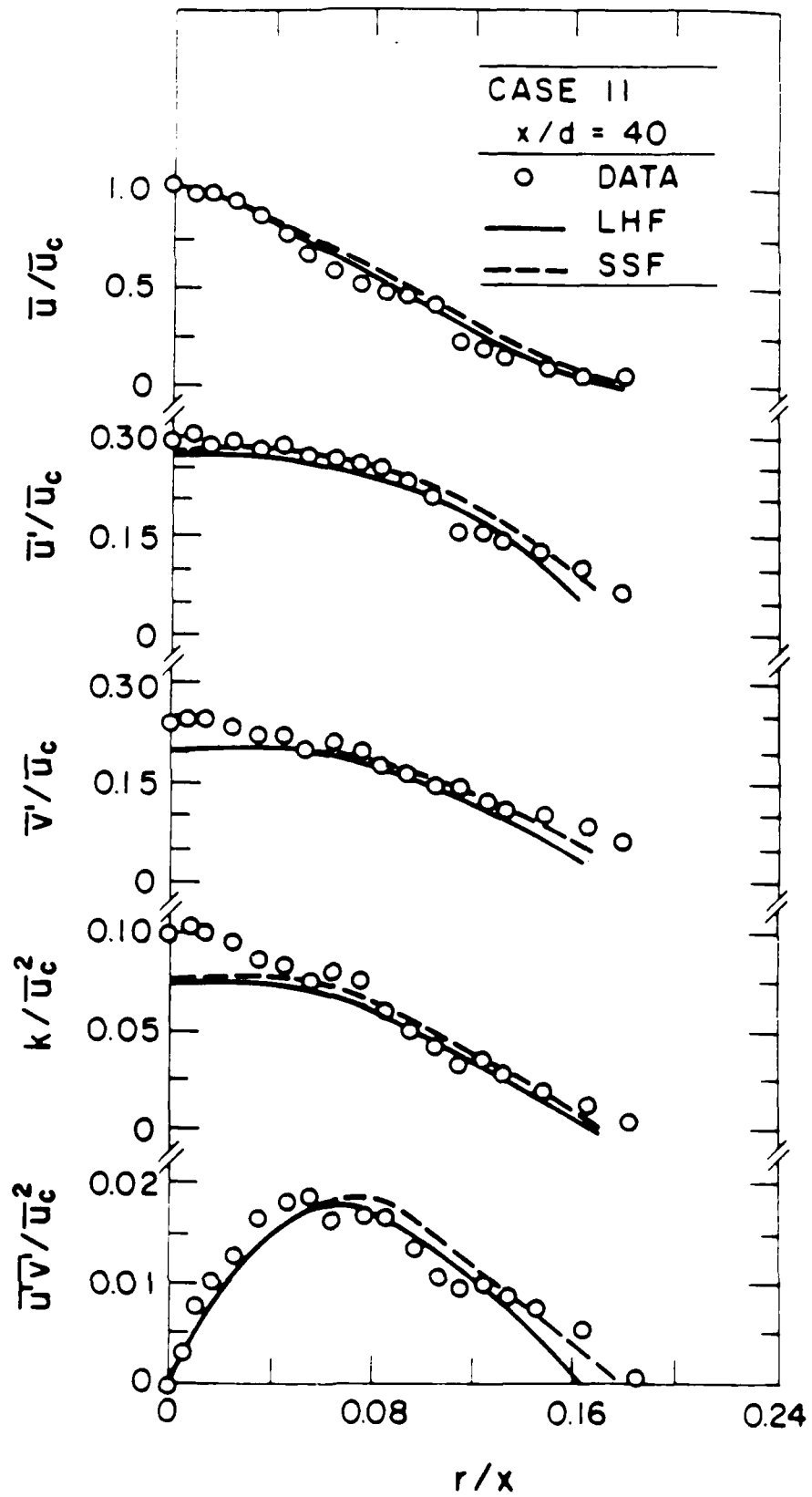


Figure 21. Mean and turbulent fluid properties - case II,  $x/d = 40$ .

that the discrepancy is probably due to deficiencies in specifying initial conditions at  $x/d = 8$ .

Of the two separated-flow analyses, the SSF-EXT version provides best agreement with measurements. This is not due to inclusion of effects of turbulence modulation, both SSF-BASE and SSF-EXT give very similar predictions of mean and fluctuating liquid-phase properties. The improvements are largely due to consideration of anisotropic liquid-phase velocity fluctuations and enhanced drag (resulting from large relative velocity fluctuations) by using equations (11) instead of equation (10) for particle drag predictions. For both particles in gases (Shuen et al. 1985) and bubbles in liquids (Sun et al. 1986), the assumption of isotropic velocity fluctuations for the continuous phase, during random-walk computations, was proposed as the reason for consistent underestimation of streamwise dispersed-phase velocity fluctuations. The present good predictions of the streamwise and radial particle velocity fluctuations, using the SSF-EXT method which allows for anisotropy of liquid velocity fluctuations, appears to confirm this hypothesis.

The predictions of the SSF-BASE method in figures 21-26, not only underestimate the anisotropy of particle fluctuations, by ignoring the anisotropy of liquid velocity fluctuations, but underestimate radial velocity fluctuations as well. This has not been observed during past work with particles in gases and bubbles in liquids, using the SSF-BASE approach, where radial velocity fluctuations of the dispersed phase have been predicted reasonably well – consistent with reasonably good predictions of the turbulent dispersion of the dispersed phase (Shuen et al. 1985; Sun et al. 1986). This effect is probably due to the unusually high relative velocity fluctuations encountered by particles in liquids, in comparison to the other cases where terminal relative velocities of the dispersed phase were roughly an order of magnitude larger (reducing relative velocity fluctuations by a similar amount). A measure of the predicted effect of enhanced drag due to large relative velocity fluctuations can be seen by comparing predictions of  $\tilde{v}_p'$  and  $\tilde{u}_{pc}$  for the SSF-BASE and SSF-EXT methods, since the latter allows for the phenomenon. It is seen to be quite significant, roughly yielding a 40% increase in radial particle velocity fluctuations. However, the reasonably good results obtained here with the SSF-EXT method does not provide an adequate justification of the drag expression of equation (11). The character of the continuous-phase turbulence spectrum and the size and response properties of the dispersed phase probably play a role in drag enhancement, and these properties are not considered in the drag correlation of equation (11). Rather, present results show that drag enhancement due to large relative velocity fluctuations can be important in particle-laden flows, and that this phenomenon deserve further study. Lopes & Dukler (1986) also find enhanced drag effects, at high relative turbulence intensities, in annular two-phase flows.

#### 2.4.6 Particle Number Fluxes

Predictions and measurements of particle number flux distributions, for the two particle-laden jets, are illustrated in figures 27 and 28. Results are shown for  $x/d = 16, 24$  and

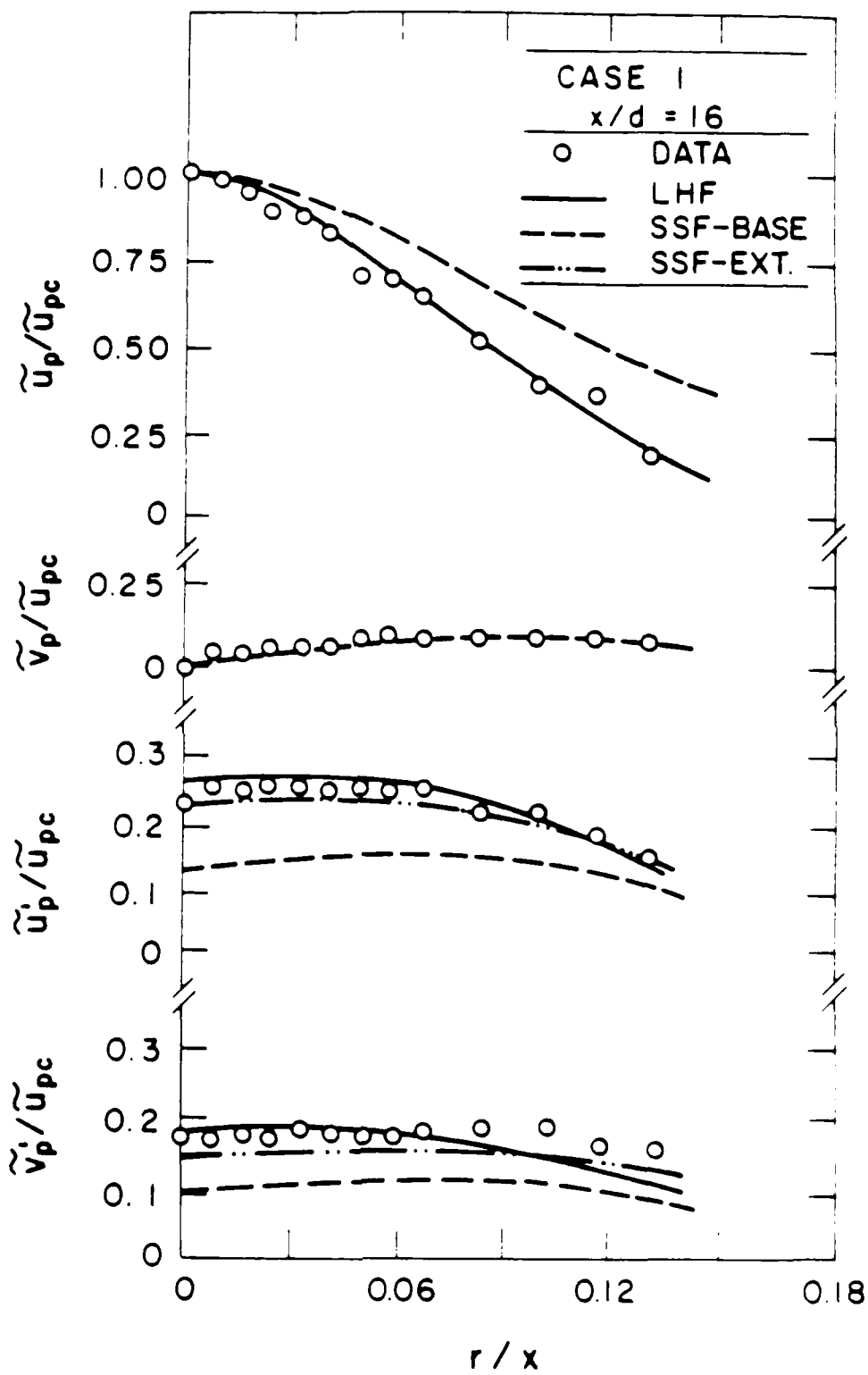


Figure 21. Mean and fluctuating particle velocities (case 1,  $x/d = 16$ ).

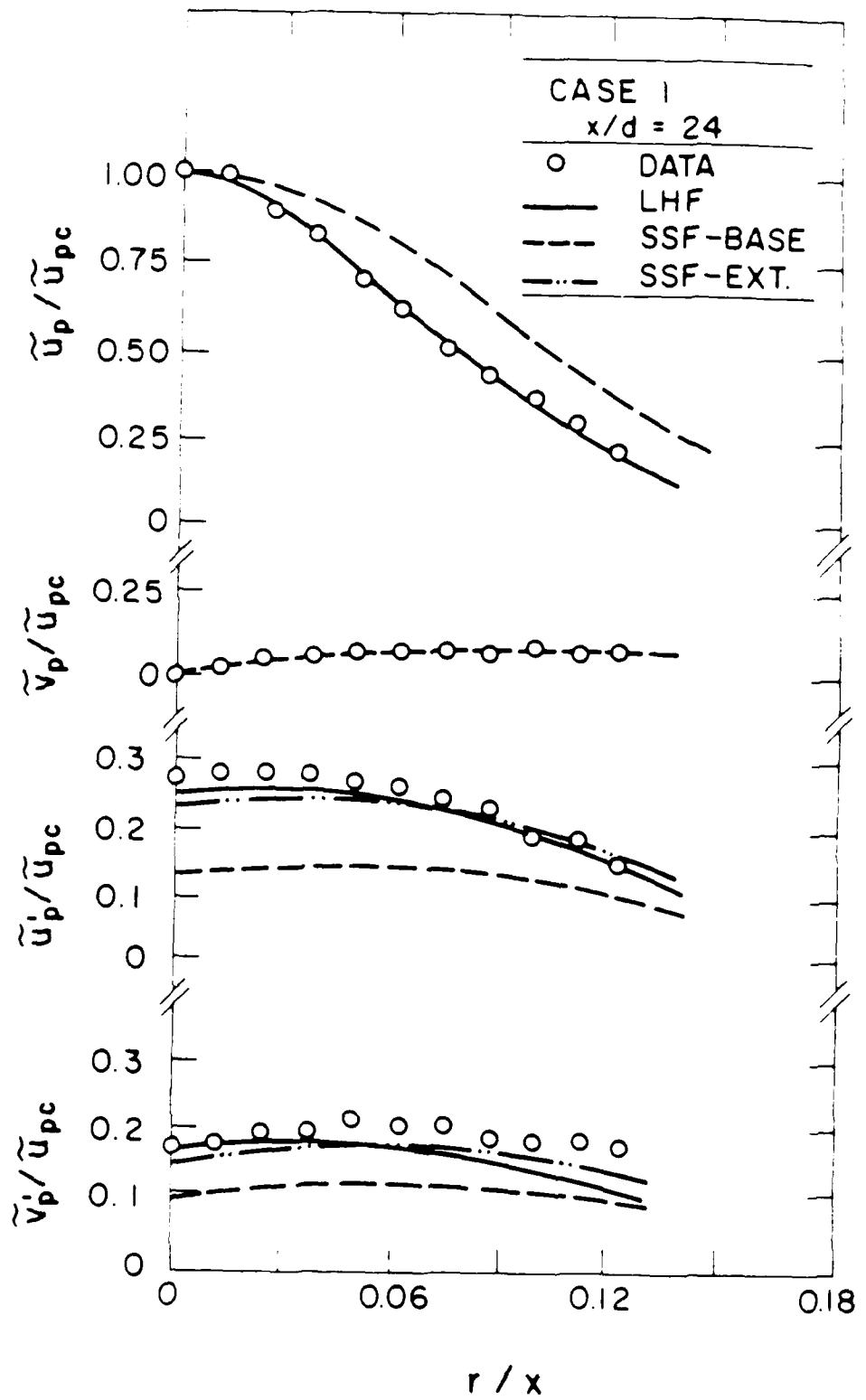


Figure 10. Mean and fluctuating particle velocities (case 1, x/d = 24).

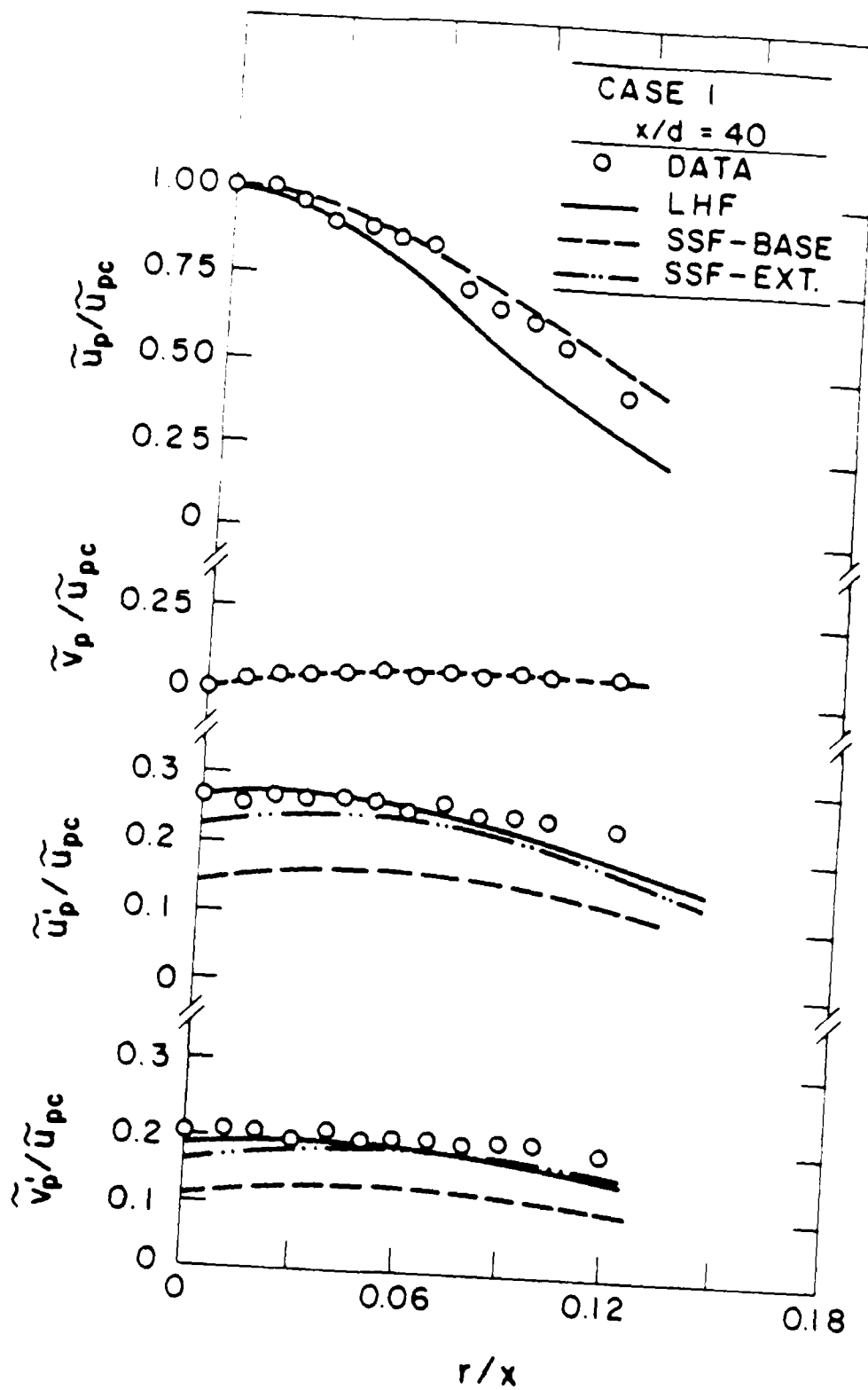


Figure 23. Mean and fluctuating particle velocities, case I,  $x/d = 40$ .

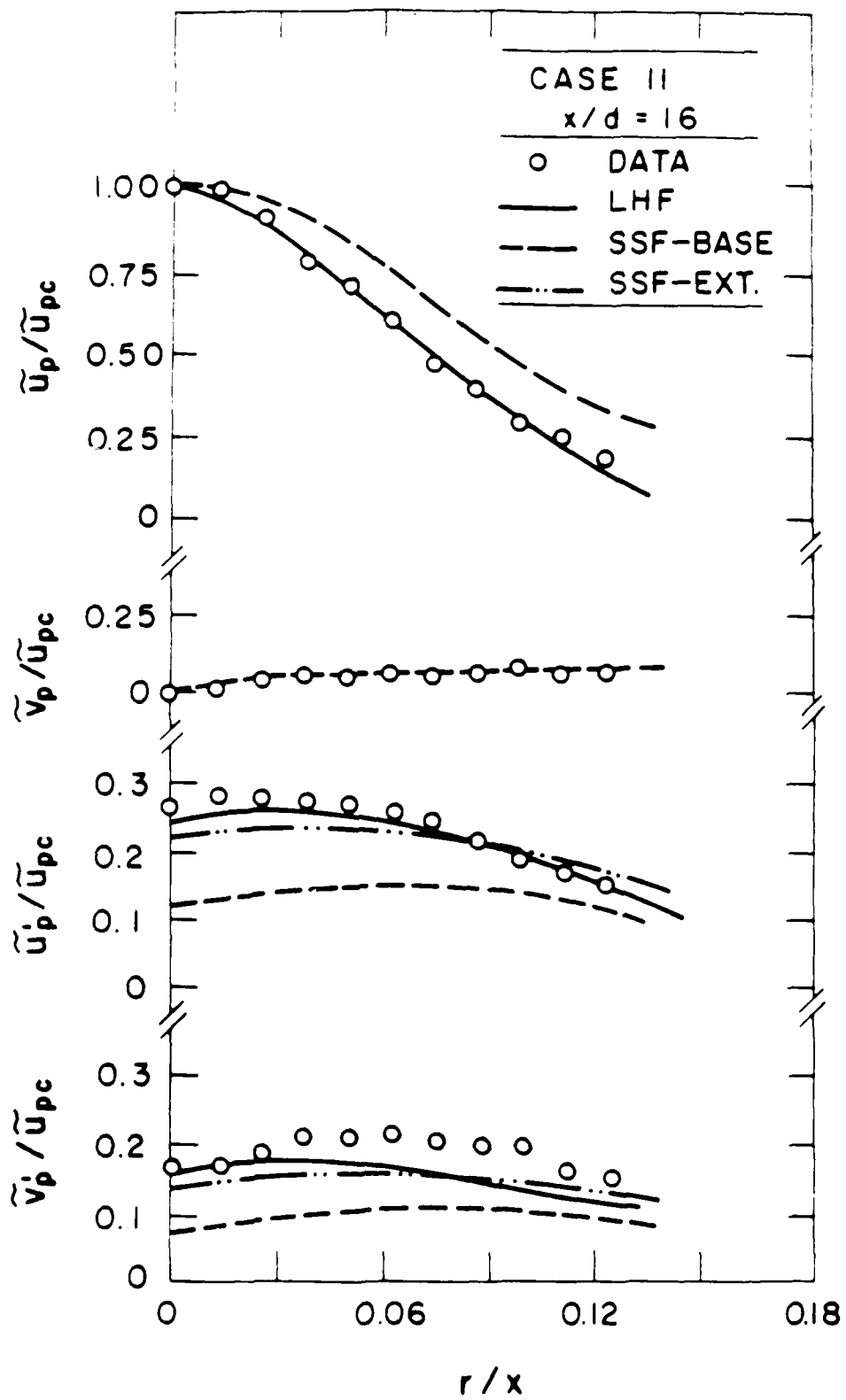


Figure 24. Mean and fluctuating particle velocities (case II,  $x/d = 16$ ).

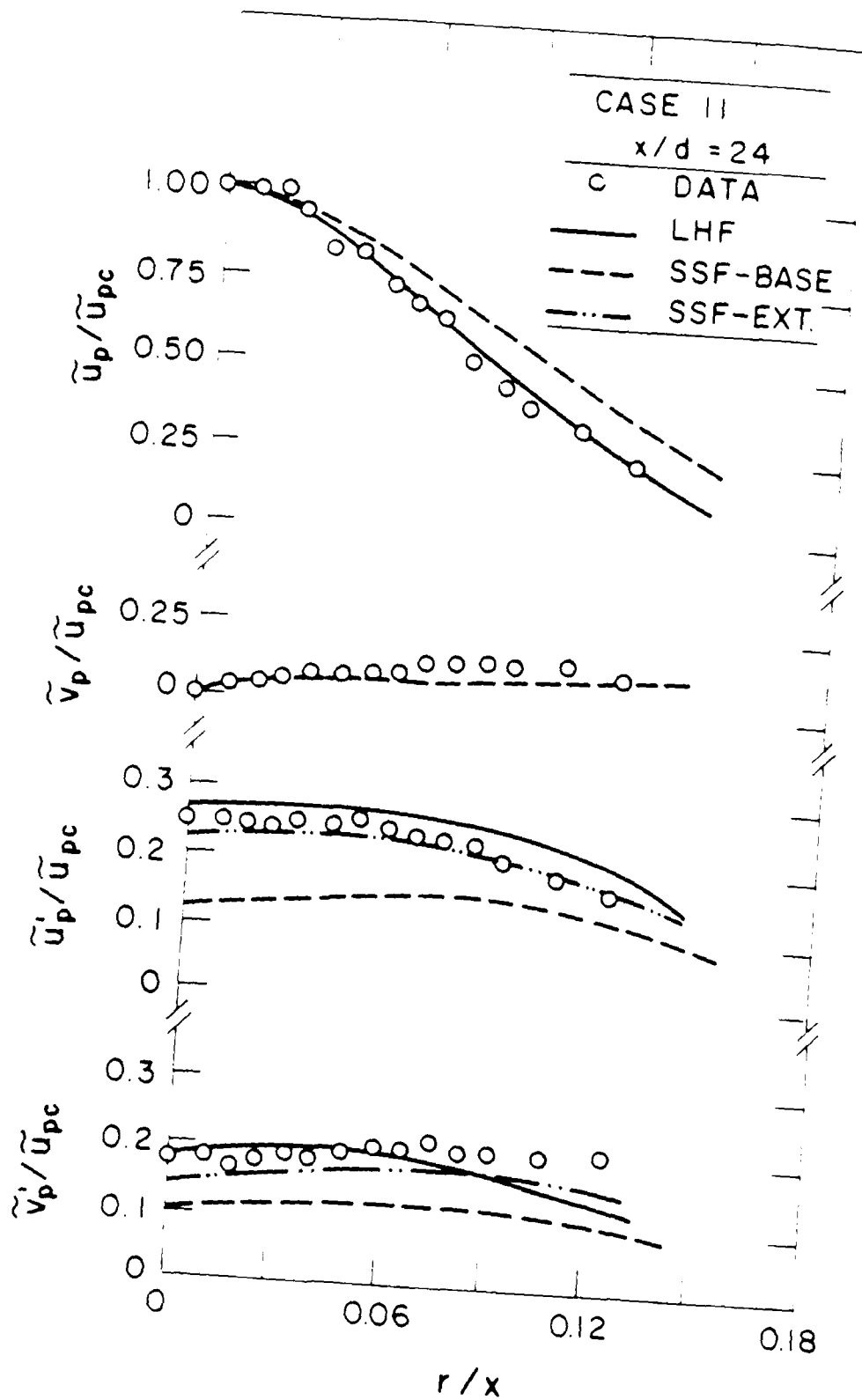


Figure 2. Mean and fluctuating particle velocities (case II, x/d = 24).

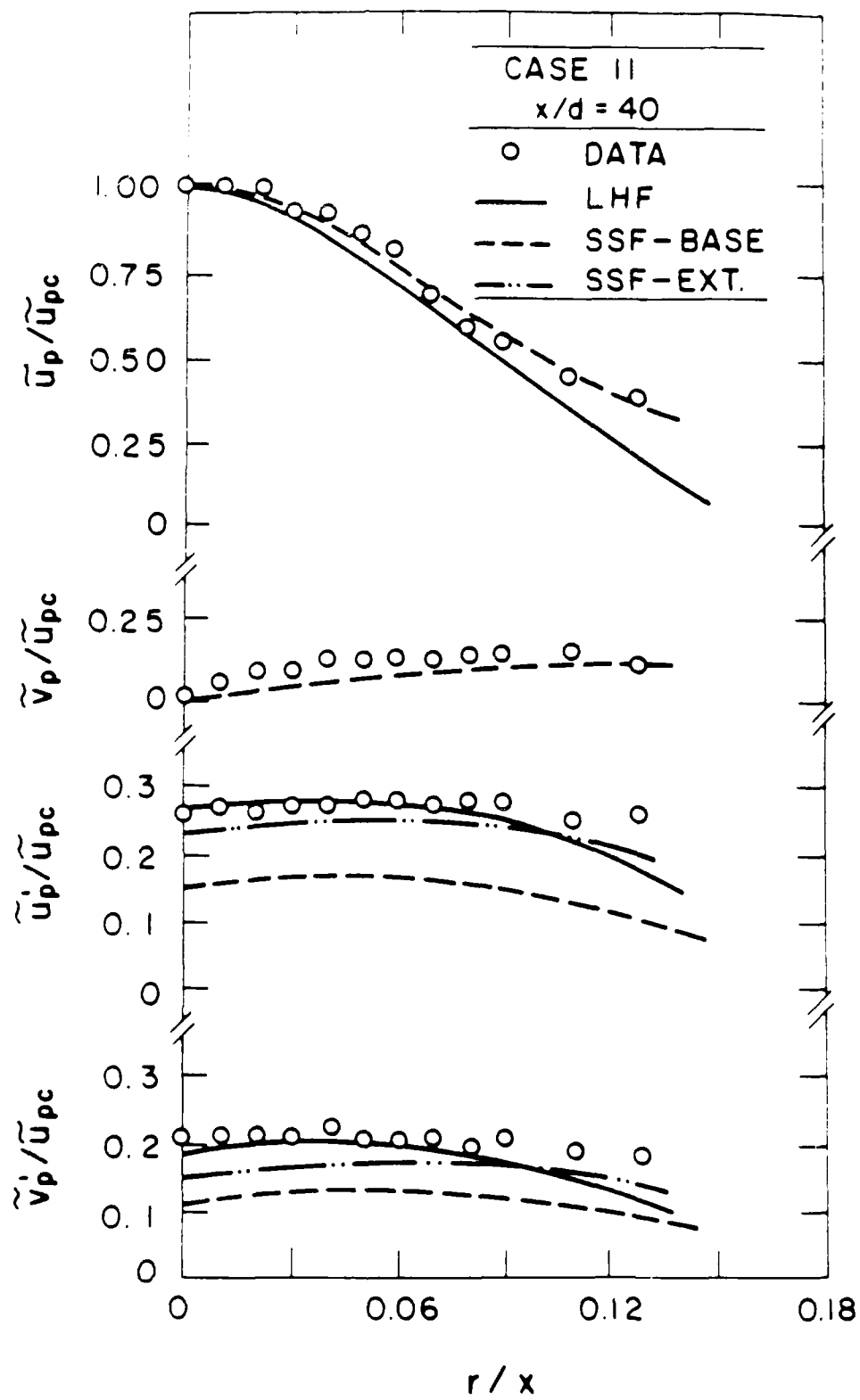


Figure 2. Mean and fluctuating particle velocities (case II,  $x/d = 40$ )

40. Predictions are presented for the LHF, DSF, SSF-BASE and SSF-EXT methods; however, the two separated-flow predictions were essentially the same and are simply denoted SSF on the figures.

Measurements on either side of the axis, illustrated in figures 27 and 28, are reasonably symmetric, indicating good uniformity of particle distributions during the experiments. The LHF and SSF predictions are in good agreement with the measurements. However, the apparently good performance of the LHF method is an artifact of the method of plotting used in figures 27 and 28. Centerline concentrations, illustrated in figure 11, clearly show that the LHF approach overestimates the rate of turbulent dispersion of the particles, due to neglect of their inertia. Similarly, the DSF method is also unsatisfactory, due to neglect of particle/turbulence interactions. In contrast, the stochastic separated-flow methods yield reasonably good results, consistent with their performance in figure 11. It appears that this approach can effectively treat effects of turbulent dispersion in jets for a wide range of conditions, e.g., the method has been reasonably successful for particles in gases, bubbles in liquids and now particles in liquids, which involves density ratios,  $\rho_p / \rho$ , in the range  $10^{-3}$  -  $10^4$ .

#### 2.4.7 Sensitivity Study

Evaluation of methods of predicting multiphase flows is always uncertain, since numerous theoretical and experimental parameters must be specified. Therefore, in order to place the evaluation of predictions in perspective, the sensitivity of predictions to changes in theoretical and experimental parameters was investigated. This involved increasing various parameters by 100% and finding changes in the dependent variables at  $x/d = 16$  and 40 for the two particle-laden jets.

Table 3 is a summary of the main results of sensitivity analysis. Changes in  $\bar{u}_c$ ,  $k_c / \bar{u}_c^2$ ,  $\tilde{u}_{pc}$  and  $\tilde{u}_{pc} / \tilde{u}_{pc}$ , the most sensitive output parameters, are tabulated for 100% increases in  $k_o$ ,  $\epsilon_o$ ,  $C_D$  and  $L_e$ . Errors in specification of initial conditions,  $k_o$  and  $\epsilon_o$ , are very significant, particularly at  $x/d = 16$ . This probably accounts for some of the deficiencies of SSF predictions noted at this position. Estimates of  $C_D$  have a small influence on liquid properties, consistent with the fact that present flows were dilute.  $C_D$  also has relatively small effect on particle velocities, largely due to the fact that relative velocities are not large in the present flows, and drag is nearly a quadratic function of velocity.  $C_D$  has a much greater influence on particle velocity fluctuations, a finding already evident from the discussion of the results illustrated in figures 21-26. The parameter,  $L_e$ , was specified in a relatively ad hoc manner (Shuen 1983), but has served reasonably well for predictions of turbulent dispersion (Faeth 1986). Results summarized in Table 3 indicate that most parameters of the flow are relatively insensitive to the actual value of  $L_e$ .

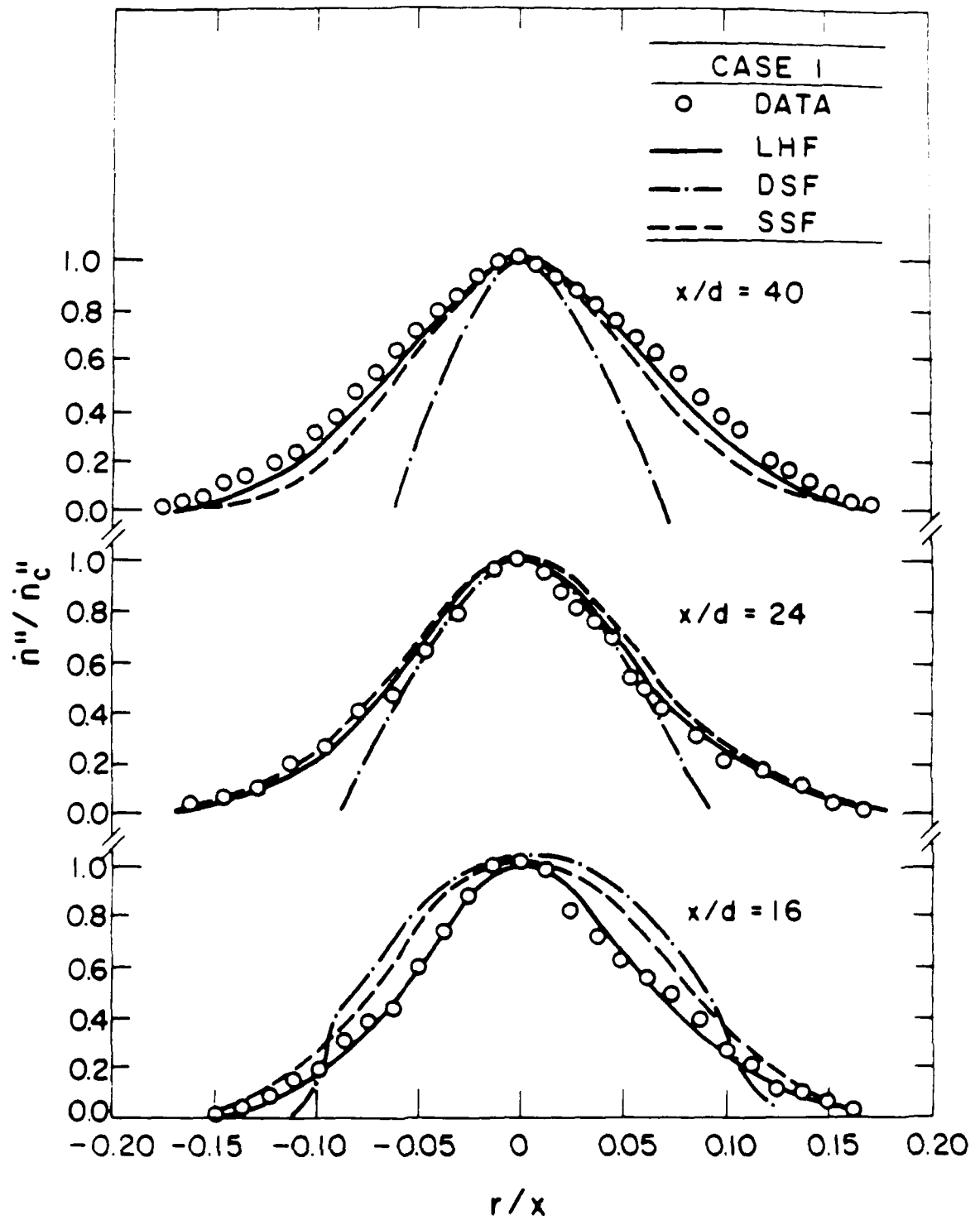


Figure 27. Mean particle number flux distributions (case I).

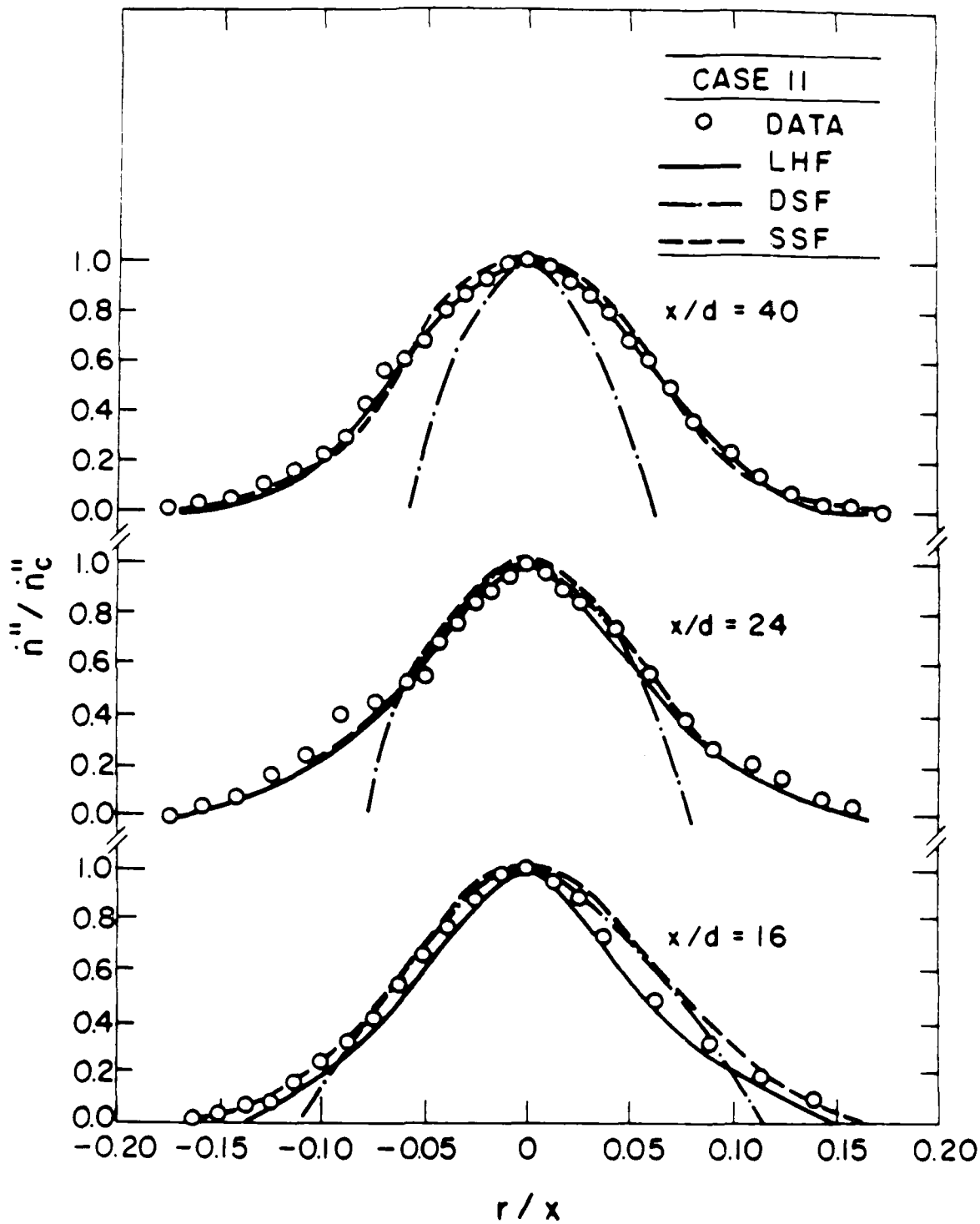


Figure 28. Mean particle number flux distributions (case II).

Table 3. Sensitivity Study of SSF Analysis<sup>†</sup>

| Input<br>Parameter | Output Parameter |                     |                  |                                    |
|--------------------|------------------|---------------------|------------------|------------------------------------|
|                    | $\bar{u}_c$      | $k_c / \bar{u}_c^2$ | $\tilde{u}_{pc}$ | $\tilde{u}_{pc}' / \tilde{u}_{pc}$ |
| Case I:            |                  |                     |                  |                                    |
| $k_o$              | -36, -24         | 219, 24             | -21, 25          | 126, 17                            |
| $\epsilon_o$       | 24, 17           | -58, -8             | 12, 16           | -27, -1                            |
| $C_D$              | ~ 0, -1          | ~ 0, -2             | ~ 0, -3          | 15, 16                             |
| $L_e$              | -1, -1           | 1, -6               | -2, -4           | 12, 15                             |
| Case II:           |                  |                     |                  |                                    |
| $k_o$              | -35, -23         | 219, 14             | -20, -23         | 117, 98                            |
| $\epsilon_o$       | 22, 15           | -56, -5             | 16, 15           | -32, -4                            |
| $C_D$              | -1, ~ 0          | 1, -4               | 2, -3            | 4, -1                              |
| $L_e$              | -2, -2           | 1, -7               | 1, -2            | 21, 5                              |

<sup>†</sup>Percent increase in output parameter for a 100% increase of the input parameter at  $x/d = 16, 40$ .

## 2.5 Conclusions

The major conclusions of the study are as follows:

- (1) Stochastic separated flow analyses yielded estimates of mixing and turbulent dispersion for particle-laden liquid jets that were comparable to past performance for particle-laden gas jets and bubbly jets – with no changes in the prescriptions for turbulence properties and turbulence/dispersed-phase interactions. Thus, the approach appears to be useful for a wide range of multiphase flows and merits further development.
- (2) Effects of turbulence modulation were observed, evidenced by increased turbulence levels near the axis, where turbulence production by conventional continuous-phase mechanisms is small. The phenomenon did not appear to influence the overall mixing and turbulent dispersion properties of the flow, since effects of particles on continuous-phase turbulence properties are probably limited to wave numbers which are higher than the energy-containing range of the turbulence spectrum which is largely

responsible for mixing. Several proposals for treating turbulence modulation were examined; however, none was particularly successful since they did not incorporate effects of turbulence scale and the response of the dispersed phase. Additional measurements and analysis are clearly needed, in order to gain a better understanding of turbulence modulation in multiphase flows.

- (3) Present flows exhibited higher relative turbulence intensities of the particles than in the past. This resulted in significant increases in particle drag from estimates based on the standard drag curve. An existing method, reported by Clift et al. (1978), exhibited some capabilities to treat this phenomenon; however, since the method does not include effects of turbulence scale and particle response, its general use is suspect. Additional study of drag, virtual mass forces, Basset history forces, and effects of particle acceleration rates at high relative turbulence intensities is needed to gain a better understanding of this phenomenon.
- (4) Earlier deficiencies in estimating levels of anisotropy of dispersed-phase velocity fluctuations (Shuen et al. 1985; Sun & Faeth 1986, Sun et al. 1986) were eliminated by considering measured levels of the anisotropy of continuous-phase velocity fluctuations. While this deficiency did not influence predictions of turbulent mixing and dispersion to a great degree for flows considered thus far, consideration of anisotropy of the continuous phase should be incorporated into stochastic separated methods, since this may not always be the case.
- (5) Predictably, the locally homogeneous flow approximation yielded better results for the present particle-laden liquid jets, than for past work with particle-laden gas jets and bubbly jets, since relative velocities were smaller in comparison to continuous-phase velocities. Similar conditions are frequently encountered in high pressure sprays, which are difficult to treat using current present separated-flow analyses; therefore, LHF methods merit further evaluation for such applications.

This concludes all work that is currently planned for the particle-laden liquid jets. Subsequent work dealing with turbulence/dispersed-phase interactions has been limited to homogeneous particle flow – to be discussed next.

### 3. HOMOGENEOUS PARTICLE FLOW

#### 3.1 Introduction

Work on this phase of the investigation has just begun. Thus far, the test arrangement has been designed and assembled, test conditions have been established, and measurements initiated. These activities will be discussed in the following, but findings at this stage are only

preliminary.

The study of homogeneous particle flows is a direct outgrowth of the investigation of particle-laden liquid jets. This portion of the investigation seeks to gain a better understanding of turbulence modulation, i.e., the direct modification of continuous-phase turbulence properties by transport from the dispersed phase.

Turbulence modulation effects have been anticipated for some time (Al Taweel & Landau, 1977; Hinze, 1972), and effects attributed to turbulence modulation have been observed during past studies of dispersed jets in this laboratory (Faeth, 1983, 1987; Parthasarathy & Faeth, 1987, 1987a; Shuen et al., 1985; Solomon et al. 1985, 1985a; and Sun et al. 1986), as well as during the study of particle-laden liquid jets, discussed in the previous section. The difficulty with studying turbulence modulation in jets is that effects of turbulence modulation are strongest where the particle concentration is high; however, measuring accuracy also deteriorates at the same conditions.

Results illustrated in figures 15-20 show a way around the problem of measuring turbulence modulation, which is exploited during the present investigation. It can be seen that turbulence modulation effects actually are most evident far from the injector, where relative velocities of the particles become large in comparison to liquid velocities. In this instance, mechanisms of turbulence modification by particle motion begin to dominate the process, since conventional mechanisms of turbulence production by shear forces in the liquid phase have become small.

The previous observation suggests that turbulence modulation might best be studied where production of turbulence by the continuous phase is formally zero, i.e. a homogeneous continuous phase. This is the approach taken here: considering a uniform flux of particles settling through a nearly stagnant liquid bath, at their terminal velocities. In this case, the particles are the direct source of turbulence in the flow and all turbulence properties are an effect of turbulence modulation. The problem becomes one of understanding the properties of this turbulence field and the relationship between the turbulence field and the properties of the dispersed phase, e.g., particle terminal velocities, particle concentrations, etc.

Progress on this phase of the investigation is discussed in the following. The report begins with a description of experimental methods, and concludes with a discussion of initial (preliminary) findings.

## **3.2 Experimental Methods**

### **3.2.1 Apparatus**

Figure 29 is a sketch of the homogeneous particle-flow apparatus. The test configuration involves nearly monodisperse round glass particles, settling with a uniform flux

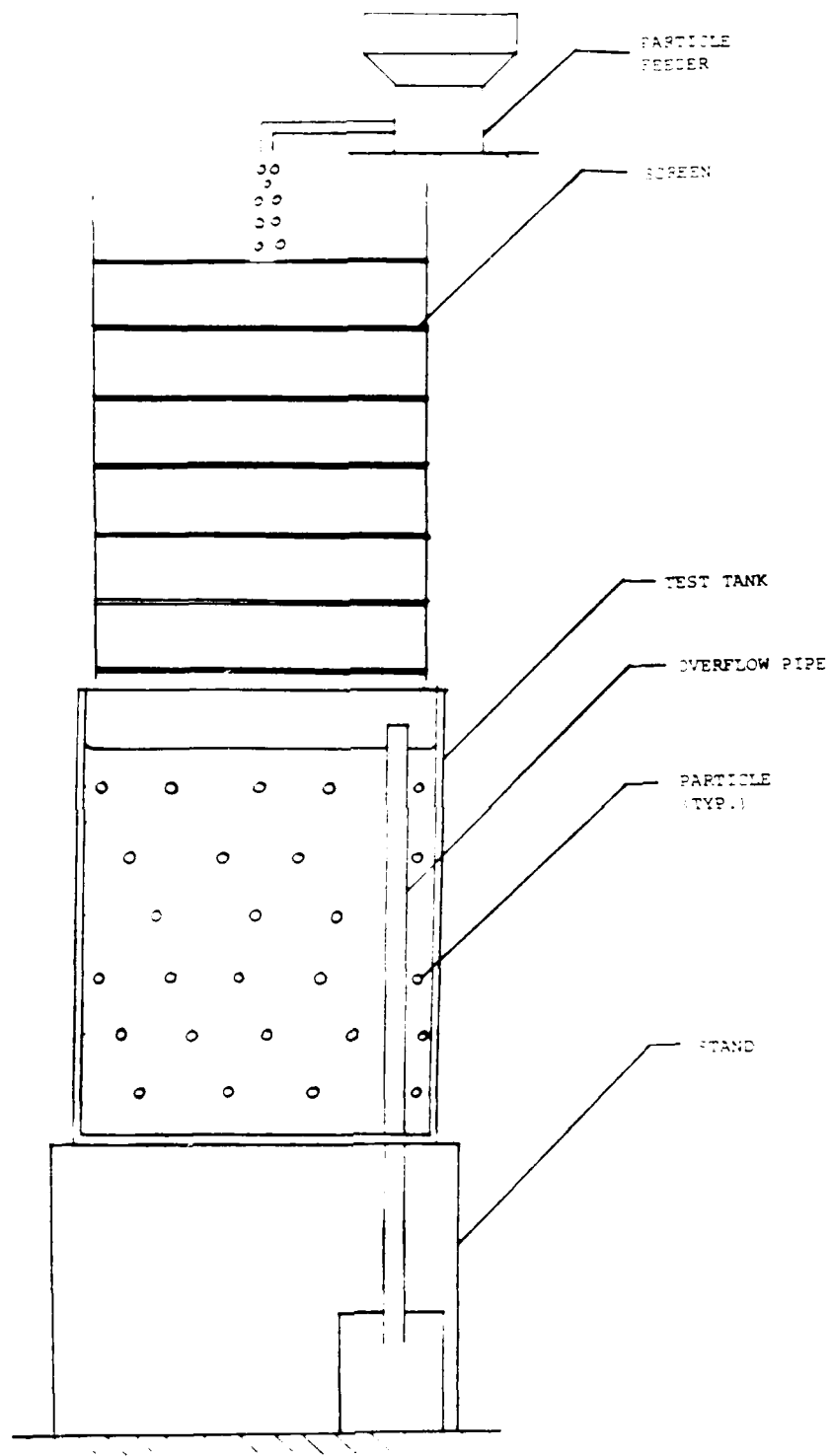


Figure 24. Sketch of the homogeneous particle flow apparatus.

in a nearly stagnant water bath. Measurements include phase velocities, using a phase-discriminating LDA, and particle number fluxes, using Mie scattering.

The particle flow is initiated by a particle feeder (AccuRate, Model 310, with a 19 mm diameter helix with center rod). The particles then fall through an array of 9 screens (0.58 mm diameter wire, stainless steel square mesh wire cloth, spaced 1.52 mm apart, 52.4 mm percent open area), each spaced 190 mm apart. The particles then fall into a windowed tank (410 × 535 × 910 mm high) which is filled with water, to a depth of 800 mm. After a deceleration distance of 100-200 mm, the particles reach a steady (in the mean) terminal velocity. Observations are made near the center of the tank (roughly at a depth of 400 mm). The particles then collect naturally at the bottom of the tank, with little rebound upon impact. The particles are removed from time-to-time using a suction system.

The test arrangement is conceptually simple, and yields a homogeneous dilute dispersed flow where all turbulence in the system is produced directly by the particles. The particle feed system was evaluated for dry operation, showing essentially uniform particle fluxes across the exit, within experimental uncertainties. Results to be discussed later show that uniform particle fluxes are preserved in the liquid phase.

Mean liquid motion in the test tank results from water displaced by particles which are collecting at the bottom of the tank: this contribution is very small, ca. 0.01 mm/s. LDA measurements of continuous-phase velocities exhibit somewhat higher mean velocities, ca. 1 mm/s; however, these are still small in comparison to velocity fluctuations, ca. 10 mm/s, and are essentially zero within the uncertainties of velocity measurements. Based on these findings, the test arrangement appears to be satisfactory with flow properties largely resulting from effects of turbulence modulation.

The mean liquid motion that is observed, appears to be largely caused by effects of buoyancy forces, due to thermal nonuniformities, rather than nonuniformities in the particle fluxes. Buoyancy intrudes since the liquid bath has an appreciable thermal capacity while the laboratory has relatively poor temperature control. As a result, the bath is invariably either heating up or cooling down. These thermal motions are best seen when there is no particle flow: mean velocity levels at this condition are on the order of 10 mm/s. However, once the flow of particles is initiated, the thermal motions are nearly destroyed with particle effects dominating the flow in the bath. The effects of buoyant circulation, however, prevent useful operation at very low particle loadings. This is not a very significant limitation, since turbulence modulation phenomena are not very strong at these conditions.

Round glass beads, having a diameter of 1 mm and a density of 2450 kg/m<sup>3</sup> are used in the tests. The size distributions is nearly monodisperse, with a standard deviation of 50 μm. The particles are nearly round, with differences between the major and minor diameters of less than 10 percent. This size was chosen to provide reasonable levels of velocity fluctuations in the bath, e.g., calculations of terminal velocities in still water yielded a value of 149 mm/s.

The particles enter the bath dry; however, little difficulty has been encountered with particles becoming trapped in air bubbles (less than 1 percent).

### 3.2.2 Instrumentation

Measurements are similar to those used for the particle-laden jet tests: phase-discriminating LDA for phase velocities and Mie scattering for particle number fluxes; therefore, the following discussion of instrumentation will be brief.

Figure 30 is a sketch of the phase-discriminating LDA. This system is unique, since it exploits the properties of the present homogeneous flow while circumventing difficulties due to the fact that the flow has negligible mean velocities. Desired quantities include phase velocities, and one- and two-point velocity correlations of the continuous phase. Two-point correlations are particularly sought, since turbulence scales produced by the particles are a major issue, and scales cannot be found, even in the streamwise direction, since Taylor's hypothesis is not applicable when there is no mean motion. Streamwise and cross-stream properties are not necessarily the same in a homogeneous flow; therefore, provision must be made for two-point measurements in both directions – although azimuthal variations in a horizontal plane are irrelevant.

The LDA arrangement to execute these measurements involves one fixed channel and one channel that can be traversed in both the streamwise and crossstream directions. A sketch of the arrangement appears in figure 30. The two channels are based on the green (514.5 nm) and blue (488 nm) lines of an argon-ion laser. Each channel has a separate phase discriminator based on a HeNe laser (632.8 nm), with discrimination of these two beams found by amplitude discrimination by operating one beam at higher power than the other. The orientation of beams and detectors is still being modified as part of preliminary tests; therefore, specific details concerning measuring volumes and orientations will not be given. The main objective, however, is to achieve measuring volumes which are comparable in size, or smaller, than the Kolmogorov microscales, which are ca. 300-500  $\mu\text{m}$  for present test conditions. Such sizes are achievable, by off-axis detection, using the components illustrated in figure 30.

The green and blue lines of the argon-ion laser are separated using a dichroic (green) mirror. The blue line, for the traversable channel, is then transmitted to the sending optics using an optical fiber. This keeps the traversing portion of this channel relatively light, simplifying the design of the traverse system, while maintaining optical alignment with little difficulty. The sending and receiving optics of the traversing channel, including the phase-discriminator for this channel, are all mounted on a single traversing optical breadboard, to maintain alignment. The two channels are perpendicular to each other, in order to simplify the arrangement of the components around the apparatus. This presents no problem for a homogeneous flow, since flow properties are independent of direction in horizontal planes.

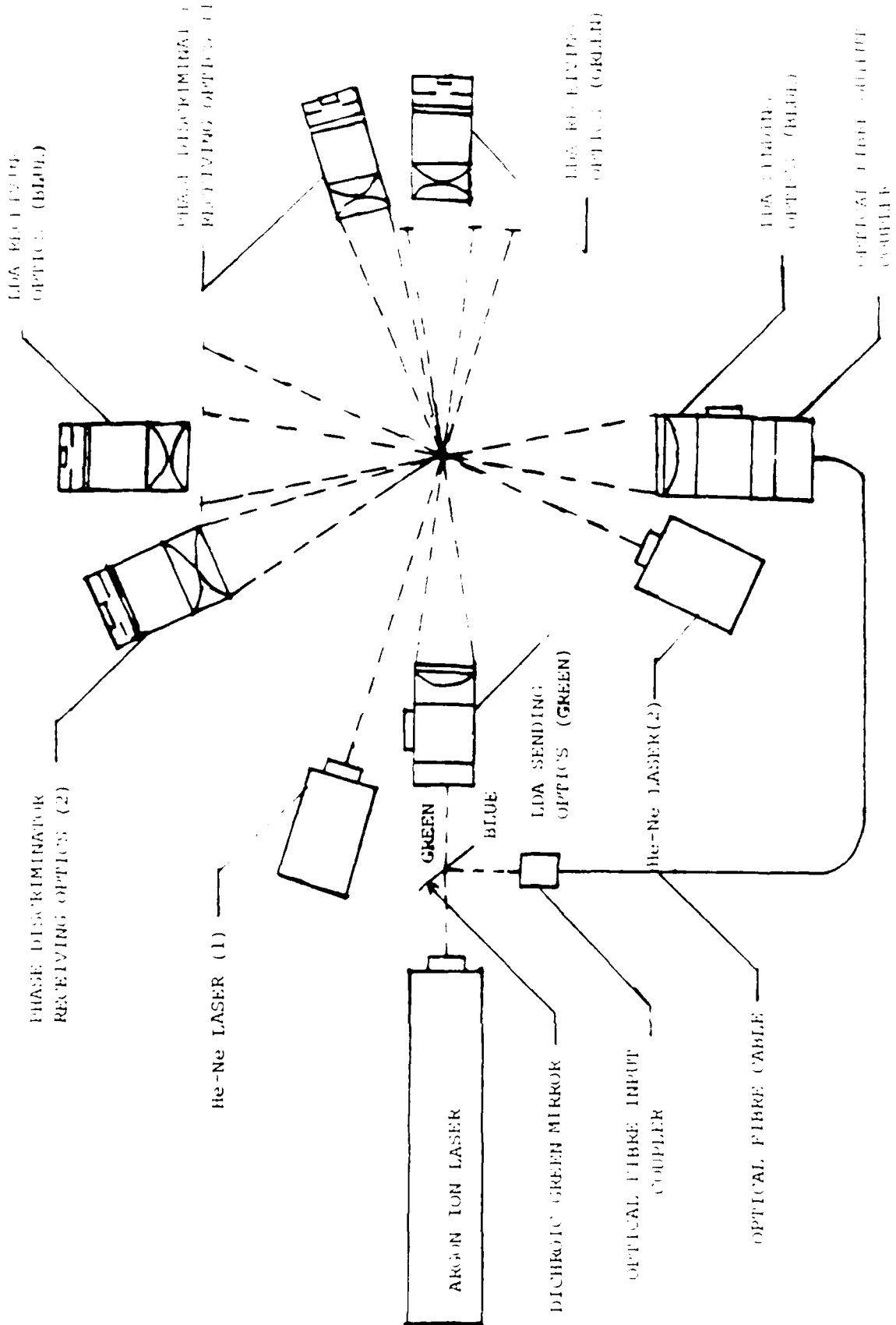


Figure 30. Sketch of the two-point phase discriminating LDA.

Signal processing and the use of the discrimination signals is the same as the single-channel instrument discussed earlier. Burst counters are used for signal processing; therefore, operation in the low burst density and high data density regime is desired. This presents little problem, since seeding particles can be added to the fixed inventory of water until data sampling rates are optimum.

The Mie scattering system for particle number flux measurements was identical to the arrangement used for the particle-laden jets. The details of this system were discussed in Section 2.2.2

### 3.2.3 Test Conditions

Test conditions are summarized in Table 4. Three particle flow conditions have been considered thus far, designated low, medium and high. Particle fluxes are roughly doubled from one test condition to the next. Particle spacings are in the range 18-33 mm; therefore, the flows are dilute, e.g., particle volume fractions are less than 0.009 percent. Streamwise velocity fluctuations of the liquid are in the range 5-11 mm/s, which is roughly an order of magnitude larger than mean streamwise velocities and roughly an order of magnitude smaller than the terminal velocity of the particles in still water, which is 149 mm/s.

Within the region where measurements are made, the mean velocity of the particles is constant. Then the rate of dissipation of the flow as a whole is simply equal to the rate of loss of potential energy of the particles as they fall, yielding

$$\epsilon = \pi n'' a d_p^3 (\rho_p - \rho) / (6\rho) \quad (14)$$

where the small volume fraction of the particles has been neglected in deriving equation (14). Knowing the rate of dissipation of turbulence kinetic energy,  $\epsilon$ , the Kolmogorov microscales of length, time and velocity can be calculated as follows:

$$l_k = (v^3 / \epsilon)^{1/4} \quad (15)$$

$$t_k = (v / \epsilon)^{1/2} \quad (16)$$

$$u_k = (\epsilon v)^{1/4} \quad (17)$$

The scales given by equations (15)-(17), the mean terminal velocity of the particles,  $\bar{u}_p$ , and the mean particle spacing,  $\bar{\lambda}_p$ , can be used to find some of the frequency scales characteristic of the particle turbulence field. Low-frequency scales are given by the Kolmogorov frequency,  $f_k$ , and the particle passing frequency,  $f_p$ , as follows:

Table 4. Summary of Turbulence Modulation Test Conditions<sup>†</sup>

| Flow   | Low    | Medium | High   |
|--|--------|--------|--------|
| Particle flux (part. m <sup>2</sup> s)                 | 3670   | 9160   | 20930  |
| Particle spacing (mm)                                  | 32.7   | 24.1   | 18.3   |
| Particle volume fraction (percent)                     | 0.0015 | 0.0037 | 0.0085 |
| Streamwise velocity fluctuations (mm/s)                | 5.1    | 8.0    | 10.6   |
| Rate of dissipation (mm <sup>2</sup> /s <sup>3</sup> ) | 27.3   | 68.2   | 155.8  |
| Kolmogorov microscales                                 |        |        |        |
| Length (mm)  | 0.422  | 0.336  | 0.273  |
| Time (s)   | 0.178  | 0.113  | 0.075  |
| Velocity (mm/s)  | 2.37   | 2.98   | 3.66   |
| Characteristic frequencies (Hz)                        |        |        |        |
| Kolmogorov   | 5.6    | 8.8    | 13.3   |
| Fluid Passing  | 0.16   | 0.33   | 0.58   |
| Particle Passing                                       | 4.6    | 6.2    | 8.2    |
| High   | 355    | 445    | 545    |

<sup>†</sup>Glass beads, 1 mm diameter with a density of 2450 kg/m<sup>3</sup>, falling in a stagnant water bath at 298 ± 2K. Terminal velocity of particles in still water is 149 mm/s.

$$f_k = t_k^{-1} \quad (18)$$

$$f_p = \bar{u}_p / \bar{l}_p \quad (19)$$

Another low frequency scale is the fluid passing frequency, defined as follows:

$$f_p = \bar{u} / \bar{l}_p \quad (20)$$

The highest frequencies are represented by the terminal velocity of the particles, which is the highest velocity in the system, and the Kolmogorov micro-length scale, which is representative of the smallest length scales in the system, as follows

$$f_{pk} = \bar{u}_p / \bar{l}_k \quad (21)$$

The various turbulence properties given by equations (14)-(20) are also summarized in Table 4. Since the particle locations are random, the largest length scales in the system are comparable to the particle spacing. The smallest length scales are comparable to the Kolmogorov microscale of length, which is roughly two orders of magnitude smaller than the particle spacing. Thus, the present flows cannot be treated by current exact numerical simulations, even if the details of the flow around each particle were ignored. The smallest length scales are somewhat smaller than the particle diameter; therefore, it is probable that turbulence produced by the particles influences the drag properties of the particles, aside from the large-scale effects of the time-varying velocity field seen by the particles (Faeth, 1987). The Kolmogorov velocity scale is comparable to the streamwise velocity fluctuations measured in the flows. The fluid passing frequency is the lowest frequency scale of the system. The Kolmogorov and particle frequency scales are intermediate, having values on the order of 10 Hz. The high frequency scale is roughly three orders of magnitude higher than the lowest frequency scale, on the order of 500 Hz. All frequency scales increase with increasing particle loading.

### 3.3 Results and Discussion

#### 3.3.1 Number Fluxes

Number fluxes, and their uniformity, are of major importance for the proper design of the present experiment. Measurements of number fluxes for the present three test conditions are illustrated in figure 31. The mean particle number fluxes vary less than 10 percent across the central portion of the test tank. Even this variation, however, is comparable to the experimental uncertainties of the measurements due to finite sampling times and particle feed rate variations over the lengthy test times needed to establish good mean values. Thus, it is likely that particle number fluxes are more uniform at any instant, than the results illustrated in figure 31. It is concluded that the particle feed system provides a sufficiently uniform spatial distribution of particles for present needs.

#### 3.3.2 Flow Visualization

Two types of flow visualization have been used to characterize the present tests: particle tracks and particle-wake tracks. The particle tracks were obtained by taking motion picture shadowgraphs of the particles as they fall through the central region of the test tank.

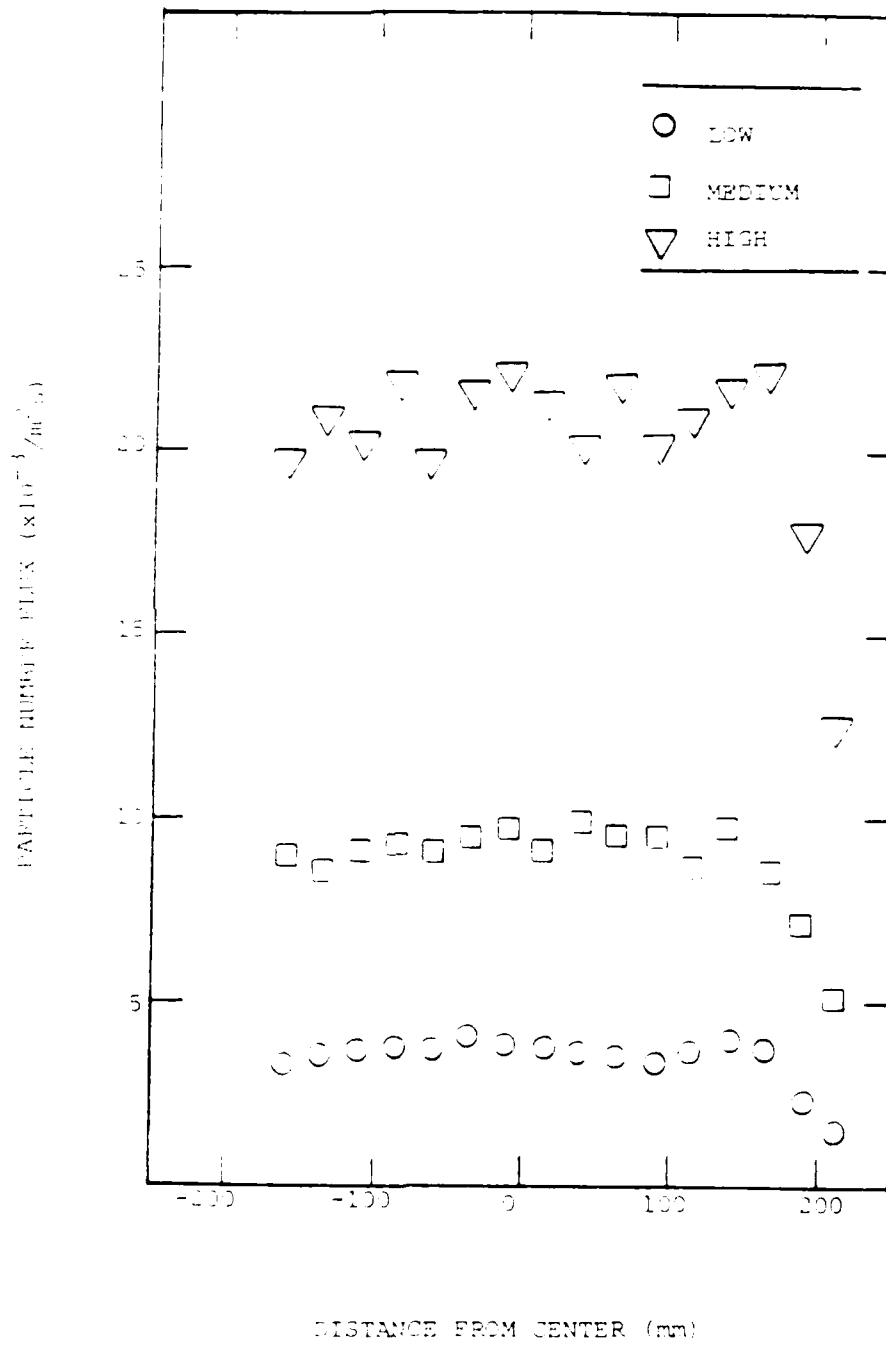


Figure 31. Particle number flux measurements.

Typical projections of particle tracks for the three test conditions are illustrated in figure 32. Shadowgraph insets of particles in  $4.5 \text{ mm} \times 4.5 \text{ mm} \times 400 \text{ mm}$  (width of the tank) are provided at each condition, to give a general idea of particle concentrations. The number of tracks shown for each test condition have also been varied proportional to the particle spacing, to suggest particle concentrations. The properties of the tracks shown, however, are representative of the behavior of the flow as a whole, for each test condition.

For the low particle loading condition, illustrated in figure 32, the particles generally fall straight down, similar to isolated particles falling in a still liquid. As the particle loading increases, however, the particle paths become more erratic, with larger random deflections in the lateral direction. Such behavior is expected for particles moving in a turbulent continuous phase, and is a manifestation of turbulent particle dispersion. The remarkable feature of the results illustrated in figure 32, however, is that the turbulence field causing turbulent dispersion is entirely due to turbulence generated by the particles themselves (or turbulence modulation). More often than not, particles are displaced randomly back and forth across the mean vertical position of their projected trajectory. Occasionally, however, a particle undertakes a rather continuous deflection in a single lateral direction. We have not analyzed the flow as yet; therefore, whether this effect is systematic cannot be quantitatively determined. Such behavior, however, is relatively rare and is thought to be due to the finite probability of this type of deflection during any random-walk trajectory.

Turbulence modulation is often discussed as a mechanism through which dispersed phases add to the dissipation of turbulence in the continuous phase (Al Taweel & Landau, 1977; Faeth, 1983, 1987; Hinze, 1972). The results illustrated in figure 32, however, show another manifestation of turbulence modulation: namely, the creation of a turbulence field by particle motion, with the particles undergoing turbulent dispersion by their own turbulence. In fact, this phenomena must always be present in a particle (drop, bubble)-containing flow. If shear forces, or turbulent diffusion in the continuous phase, are creating a turbulence field, the particles will generally extract turbulence energy from the flow, since their sizes are usually small in comparison to the largest turbulence scales. However, in doing this, they also create their own turbulence field, like the flows being studied here. Thus, particles act like a turbulence frequency shifter, extracting turbulence energy at large scales and feeding it back at small scales. The implications of this behavior can be very significant, once the process is understood, since small-scale motion enhances micro-mixing which is important for many practical applications.

The second type of flow visualization involved coating the particles with a fluorescein dye and observing laser-induced fluorescence (LIF) from the dye track left by the particle. This was done by dissolving the powdered dye in water, wetting the particles with this solution and then allowing the solution to dry on the particle surface. This left a coating of the dye solution on the particle, which would redissolve as the particle passed through the water bath, leaving a dye track.

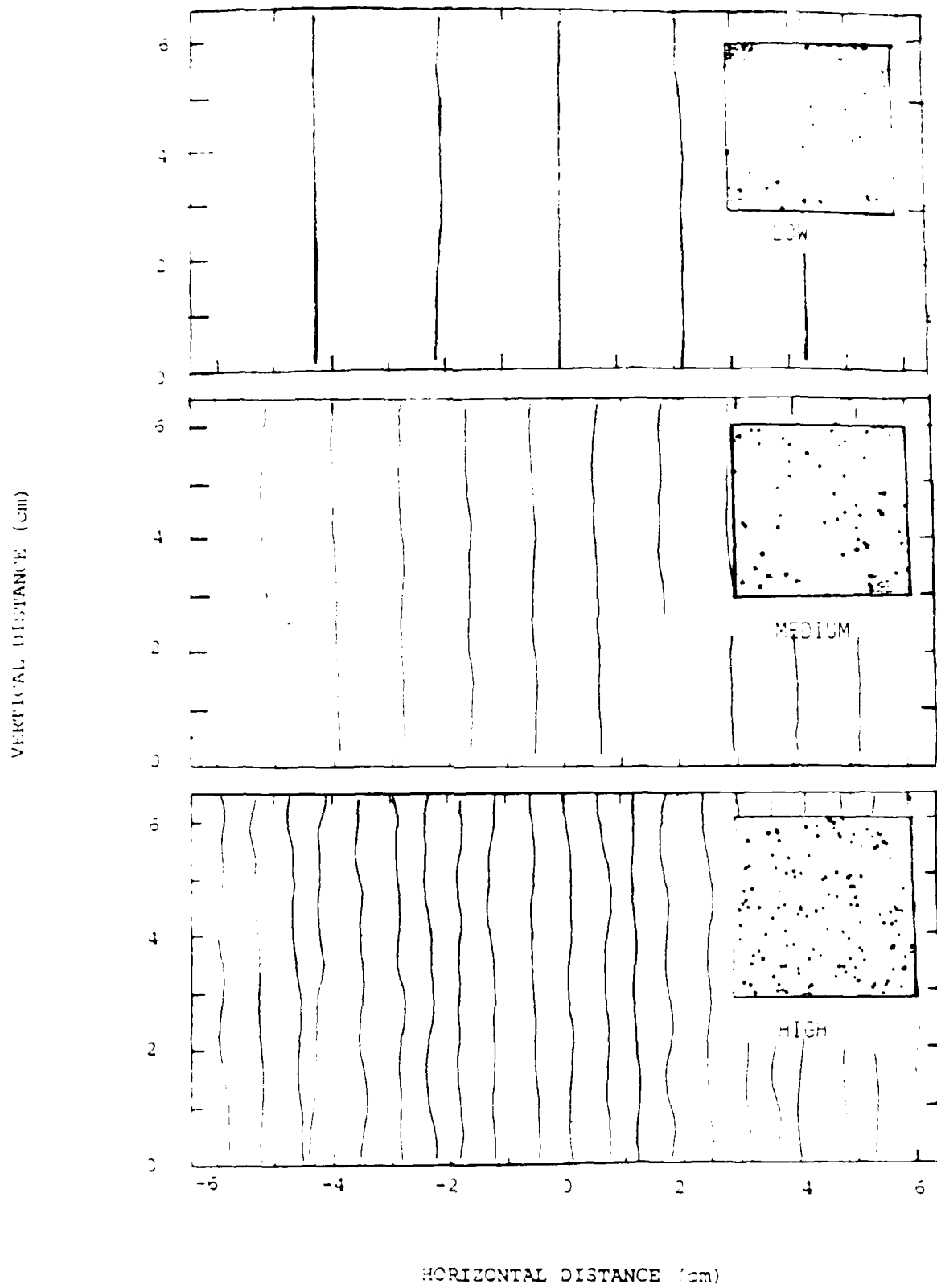


Figure 52. Particle tracks for the three particle loadings

This LIF technique worked satisfactorily. Examples of the results will be deferred for a more complete later report of this phase of the investigation, after other measurements are available. In general, the dye tracks exhibited greater degrees of lateral deflection than the particle tracks. This suggests greater degrees of turbulent dispersion for the liquid than the particles, which is generally the case for particle-laden flows having large relative velocities between the phases. Since the liquid is nearly stagnant, in the mean, the dye tracks remain within the field of view and continue to disperse within the turbulent field.

### 3.3.3 Phase Velocities

Velocity fluctuations of the continuous phase are summarized in Table 4 for the three particle loadings. As noted earlier, velocity fluctuations are comparable to the Kolmogorov velocity scales, and both tend to increase as the particle loading is increased.

Another property of interest for characterizing the turbulence field produced by the particles is the power spectrum of the continuous-phase velocity fluctuations. Measurements of power spectra, based on streamwise velocity fluctuations, for the three flows are illustrated in figures 33-35. Measured power spectra are plotted directly as a function of frequency on each figure. The slopes of the power spectra in the inertial range of conventional turbulence,  $E(f) \sim f^{-5.3}$ , are also shown on the plots, for reference. Finally, the various frequency scales, drawn from Table 4, are marked on the plots. It should be noted that these results are preliminary, with irregularities of the spectra that are largely due to insufficient samples for fully representative results. Nevertheless, the findings provide some insight concerning the turbulence properties of these flows and will be considered in the following.

The power spectra illustrated in figures 33-35 are similar to spectra found in single-phase flows. Maximum turbulence energy is found at low frequencies, characteristic of the fluid passing frequency. At somewhat higher frequencies, characteristic of the Kolmogorov and particle-passing frequencies, the power spectra decrease with a slope that approximates the inertial range of conventional turbulence (Hinze, 1975). The inertial range is most prominent for the highest loading, which exhibits the highest effective Reynolds number of the flow, i.e. this flow has the highest frequency scales. Finally, the magnitude of the power spectral density becomes small as the high characteristic frequency scale is approached. The spectrum does not show a cut-off, typical of turbulence near the microscales, at high frequencies, but actually trails off probably as a result of measurement noise. Additional work on the LDA arrangement, and examination of higher seeding levels so that the smallest scales can be resolved, is being undertaken in order to improve the measurements at high frequencies.

In spite of the preliminary nature of the power spectral density measurements, the findings suggest that the particles are generating a very respectable turbulent flow and that the cascade of turbulence energy from large to small scales in this field is similar to conventional turbulence. This behavior is expected, since the volume fraction of particles is very small, cf. Table 4. For such conditions, once the particle produces the turbulence, the likelihood of the

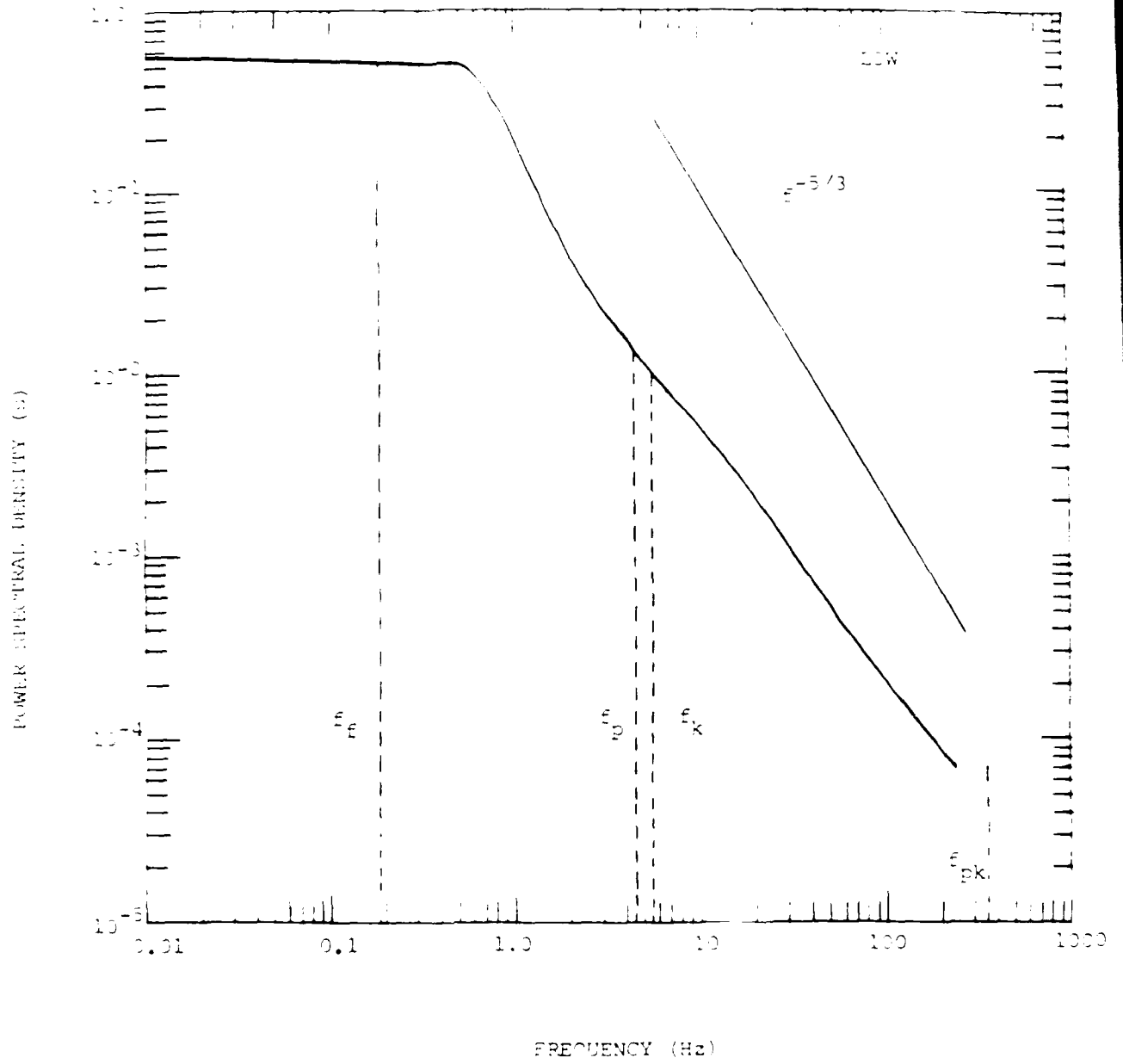


Figure 53. Lower spectrum of streamwise velocities (low condition).

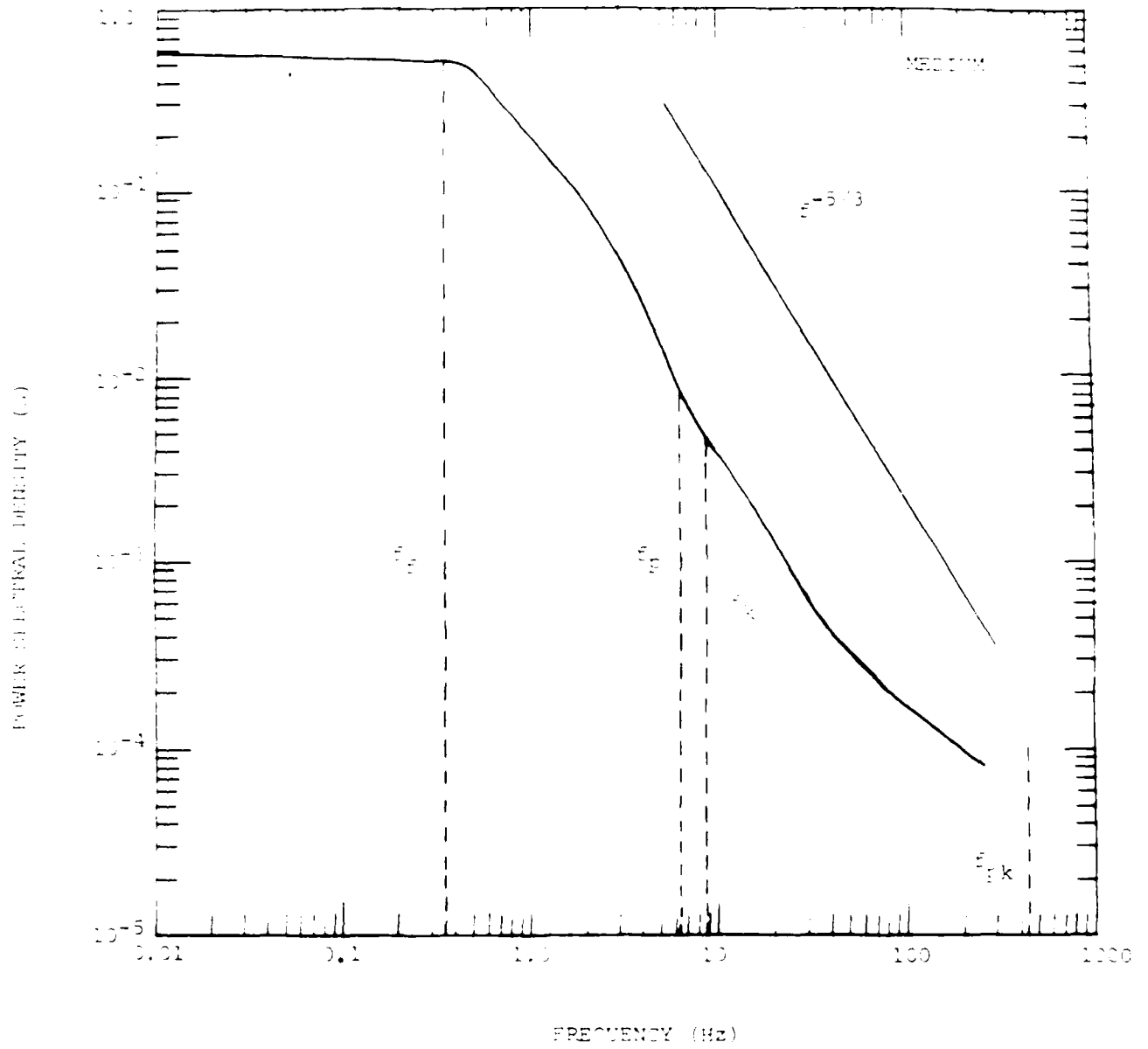


Figure 14. Power spectrum of streamwise velocities (medium condition).

POWER SPECTRAL DENSITY (s)

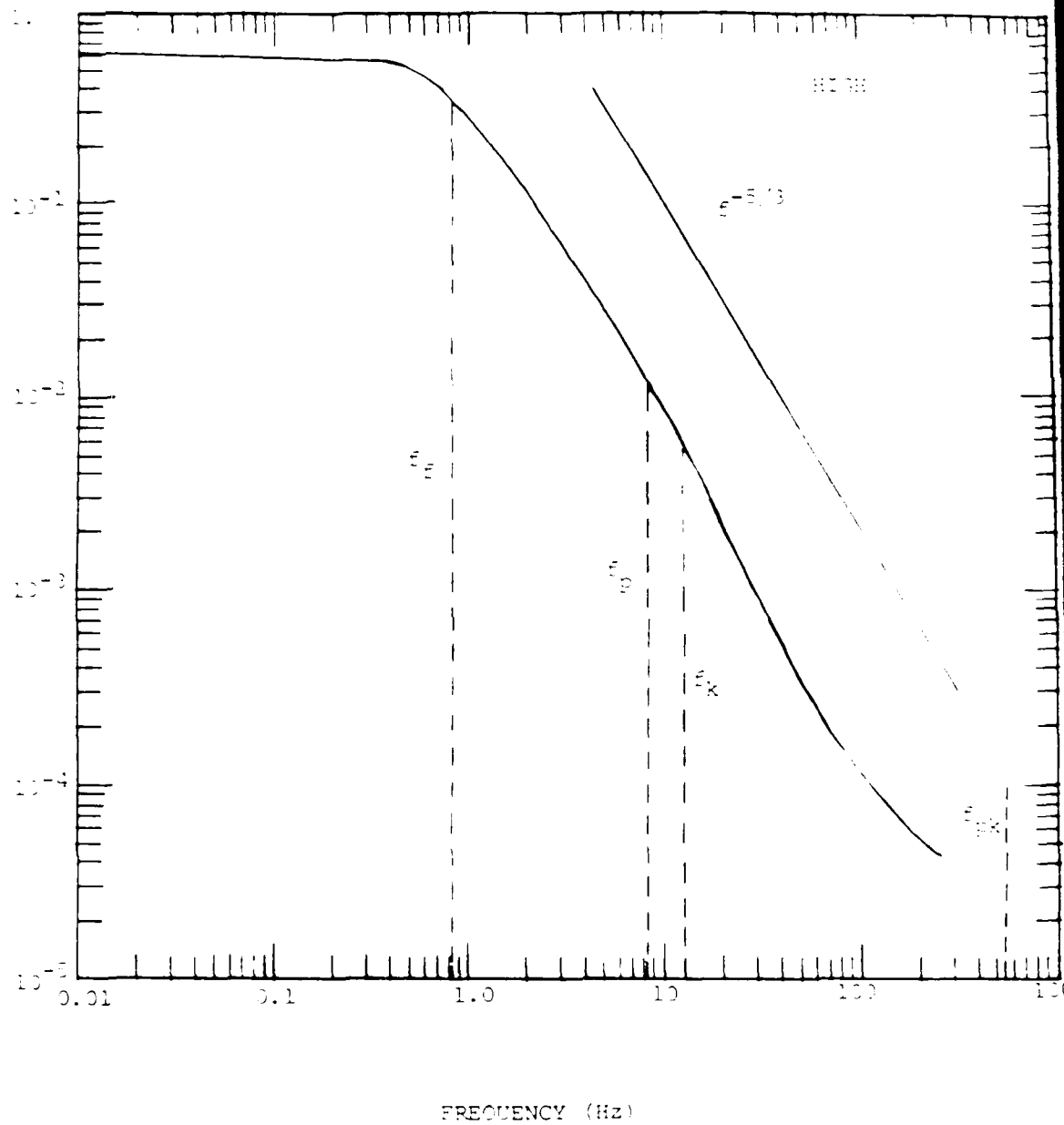


Figure 52. Power spectrum of streamwise velocities (high condition).

resulting turbulent fluid encountering another particle in the characteristic time of decay, the Kolmogorov time scale, is relatively small. Thus, the main novel feature of the turbulence being studied here is the mode of production, the rest of the decay process is probably conventional.

### 3.4 Summary

The test arrangement for the homogeneous particle flow experiments has been completed. Preliminary tests, to examine the performance of the arrangement, have also been undertaken. These results show that a uniform particle number flux has been achieved, that the bath is relatively stagnant in the mean, and that the particles generate a reasonably turbulent flow field in the continuous phase, i.e., the turbulence has a significant band of frequencies in the inertial range. The flows also produce effects of turbulent mixing in the continuous phase, and turbulent dispersion of the dispersed phase. Thus, the apparatus and the test conditions appear to be suitable for investigation of effects of turbulence modulation.

Measurements and analysis concerning homogeneous particle flows will be completed during the next report period. Measurements will include single-point phase velocities, single- and two-point velocity correlations for the continuous phase, and power spectra for the continuous phase. This data will be reduced to provide single point moments, two-point correlations, and temporal and spatial scales of the flow. Turbulent particle dispersion can be inferred from particle velocity fluctuations; however, particle deflections along projected particle tracks will also be measured to yield direct information on turbulent particle dispersion.

Measurements and analysis concerning homogeneous particle flows will be completed during the next report period. Measurements will include single-point phase velocities, single- and two-point velocity correlations for the continuous phase, and power spectra for the continuous phase. This data will be reduced to provide single point moments, two-point correlations, and temporal and spatial scales of the flow. Turbulent particle dispersion can be inferred from particle velocity fluctuations; however, particle deflections along projected particle tracks will also be measured to yield direct information on turbulent particle dispersion. Other test conditions will be examined during subsequent work, once some insight concerning these flows has been obtained from present tests.

The process will be analyzed to gain insight concerning the measurements. The first phase of the analysis will involve stochastic simulation of the flow, using measured continuous-phase properties to find particle phase velocities, etc., for comparison with the measurements. This work should disclose the degree of approximation needed to predict particle properties, e.g., whether first moments, like current stochastic separated flow models are satisfactory, or whether higher moments are needed. The results should also provide information on whether the particle drag properties are being influenced by the turbulence field, since turbulence scales are smaller than the particle diameter. This is of interest, since effects of turbulence on drag properties was suspected during earlier work with particle-laden jets

(Parthasarathy & Faeth, 1987, 1987a). The second phase of analysis will be more difficult: namely to quantify the turbulence field of the continuous phase. Plans for this phase of analysis will be undertaken after a better understanding of the flow is obtained from the measurements and the analysis of particle properties.

#### 4. SUMMARY OF INVESTIGATION

##### 4.1 Articles and Papers

Bulzan, D. L., Shuen, J.-S. & Faeth, G. M. (1987) Particle-laden swirling free jets: measurements and predictions. AIAA Paper No. 87-0303.

Faeth, G. M. (1987) Mixing, transport and combustion in sprays. Prog. Energy, Combust. Sci., in press.

Faeth, G. M. (1987) Structure of nonpremixed and premixed combusting pressure-atomized sprays. Proceedings of the Twentieth Fall Technical Meeting, Eastern Section of the Combustion Institute, Pittsburgh, invited.

Faeth, G. M. (1987) Turbulent multiphase flows. Proceedings of the U.S.-France Workshop on Turbulent Reactive Flows, Springer-Verlag, Berlin, in press.

Parthasarathy, R.N. & Faeth, G. M. (1987) Structure of particle-laden turbulent water jets in still water. Int. J. Multiphase Flow, in press.

Parthasarathy, R. N. & Faeth, G. M. (1987) Structure of turbulent particle-laden jets having comparable phase densities. Proceedings of the 1987 Spring Technical Meeting, pp. 64.1-64.4, Central States Section of the Combustion Institute, Pittsburgh.

Ruff, G. A., Sagar, A. D. & Faeth, G. M. (1987) Structure of large-scale pressure-atomized sprays. First Annual Conference of ILASS-Americas, Madison, WI.

Ruff, G. A., Sagar, A. D. & Faeth, G. M. (1987) Structure and mixing properties of pressure-atomized sprays. AIAA 26th Aerospace Sciences Meeting, Reno, NV, submitted.

##### 4.2 Participants.

G. M. Faeth, Principal Investigator; Professor, The University of Michigan.

R. N. Parthasarathy, Graduate Assistant, Doctoral Candidate, The University of Michigan.

G. A. Ruff, Graduate Assistant, pre-Ph.D., The University of Michigan.

#### 4.3 Oral presentations.

G. M. Faeth, "Turbulence/Drop Interactions in Sprays," Southwest Mechanics Seminar Series: Southwest Research Institute, San Antonio; University of Houston, Houston; and Shell Development Company, Houston, October 1986.

G. M. Faeth, "Turbulence/Particle Interactions in Dilute Particle-Laden Liquid Jets," Department of Mechanical Engineering, Carnegie-Mellon University, Pittsburgh, February 1987.

G. M. Faeth, "Particle-Laden Jets having Comparable Phase Densities," Chemical and Physical Sciences Laboratory Seminar Series, Ford Scientific Research Laboratories, Dearborn, MI, March 1987.

G. M. Faeth, "Turbulent Multiphase Flows," U.S.-France Workshop on Turbulent Reactive Flows, University of Rouen, France, July 1987.

G. M. Faeth, "Structure of Nonpremixed and Premixed Combusting Pressure-Atomized Sprays," Fall Technical Meeting, Eastern Section of the Combustion Institute, Gaithersburg, MD, November 1987.

R. N. Parthasarathy, "Structure of Turbulent Particle-Laden Jets having Comparable Phase Densities," Spring Technical Meeting, Central States Section of the Combustion Institute, Argonne, IL, May 1987.

R. N. Parthasarathy, "Structure of Turbulent Particle-Laden Water Jets in Still Water," Seminar, Department of Aerospace Engineering, The University of Michigan, Ann Arbor, MI, March 1987.

G. Ruff, "Structure of Large-Scale Pressure-Atomized Sprays," First Annual Conference of ILASS-Americas, Madison, WI, May 1987.

#### REFERENCES

Al Taweel, A. M. & Landau, J. (1977) Turbulence modulation in two-phase jets. Int. J. Multiphase Flow 3, 341-351.

Bilger, R. W. (1976) Turbulent jet diffusion flames. Prog. Energy Combust. Sci. 1, 87-109.

- Clift, R., Grace, J. R. & Weber, M. E. (1978) Bubbles, Drops and Particles, pp. 266-269, 296-302. Academic Press, New York.
- Durst, F. & Whitelaw, J. H. (1971) Measurements of mean velocity, fluctuating velocity and shear stress in air using a single channel optical anemometer. DISA Information 12, 11-16.
- Elghobashi, S. E. & Abou-Arab, T. W. (1983) A two-equation turbulence model for two-phase flows. Phys. Fluids 26, 931-938.
- Faeth, G. M. (1983) The evaporation and combustion of sprays. Prog. Energy Combust. Sci. 9, 1-76.
- Faeth, G. M. (1987) Mixing, transport and combustion in sprays. Prog. Energy Combust. Sci., in press.
- Gosman, A. D. & Ioannides, E. (1981) Aspects of computer simulation of liquid-fueled combustors. AIAA Paper No. 81-0323.
- Hinze, J. O. (1972) Turbulent fluid and particle interaction. Progress in Heat and Mass Transfer, Vol. 6, pp. 433-452. Pergamon Press, Oxford.
- Hinze, J. O. (1975) Turbulence, 2nd Edition, pp. 427 and 724-734. McGraw-Hill, New York.
- Jeng, S.-M. & Faeth, G. M. (1984) Species concentrations and turbulence properties in buoyant methane diffusion flames. J. Heat Transfer 106, 721-727.
- Lockwood, F. C. & Naguib, A. S. (1975) The prediction of fluctuations in the properties of free, round-jet turbulent diffusion flames. Comb. Flame 24, 109-124.
- Lopes, J. C. & Dukler, A. E. (1986) Droplet dynamics in vertical gas-liquid flow. A.I.Ch.E. J. submitted.
- Modarress, D., Tan, H. & Elghobashi, S. (1984) Two-component LDA measurements in a two-phase turbulent jet. AIAA J. 22, 624-630.
- Odar, F. & Hamilton, W. S. (1964) Force on a sphere accelerating in a viscous fluid. J. Fluid Mech. 18, 302-314.
- Parthasarathy, R. N., Sagar, A. & Faeth, G. M. (1986) Dense-spray structure and phenomena. Annual Report for Grant No. AFOSR-85-0244, Department of Aerospace Engineering, The University of Michigan, Ann Arbor, MI.

- Parthasarathy, R.N. & Faeth, G. M. (1987) Structure of particle-laden turbulent water jets in still water. Int. J. Multiphase Flow, in press.
- Parthasarathy, R. N. & Faeth, G. M. (1987a) Structure of turbulent particle-laden jets having comparable phase densities. Proceedings of the 1987 Spring Technical Meeting, pp. 64.1-64.4, Central States Section of the Combustion Institute, Pittsburgh.
- Reitz, R. D. & Diwakar, R. (1987) Structure of high-pressure fuel sprays. SAE Paper No. 870598.
- Ruff, G. A. & Faeth, G. M. (1987) Dense-spray structure and phenomena: Part II - Pressure-atomized sprays. Annual Report for Grant No. AFOSR-85-0244, Department of Aerospace Engineering, The University of Michigan, Ann Arbor, MI.
- Ruff, G. A., Sagar, A. D. & Faeth, G. M. (1987) Structure and mixing properties of pressure-atomized sprays. AIAA 26th Aerospace Sciences Meeting, Reno, NV, submitted.
- Ruff, G. A., Sagar, A. D. & Faeth, G. M. (1987a) Structure of large-scale pressure-atomized sprays. First Annual Conference of ILASS-Americas, Madison, WI.
- Schlichting, H. (1979) Boundary Layer Theory, pp. 599, McGraw-Hill, New York.
- Shuen, J.-S., Chen, L.-D. & Faeth, G. M. (1983) Evaluation of a stochastic model of particle dispersion in a turbulent round jet. A.I.Ch.E. J. 29, 167-170.
- Shuen, J.-S., Chen, L.-D. & Faeth, G. M. (1983a) Predictions of the structure of turbulent, particle-laden, round jets. AIAA J. 21, 1480-1483.
- Shuen, J.-S., Solomon, A.S.P., Zhang, Q.-F. & Faeth, G. M. (1985) Structure of particle-laden jets: Measurements and predictions. AIAA J. 23, 396-404.
- Shuen, J.-S., Solomon, A.S.P. & Faeth, G. M. (1986) Drop-turbulence interactions in a diffusion flame. AIAA J. 24, 101-108.
- Solomon, A.S.P., Shuen, J.-S., Zhang, Q.-F. & Faeth, G. M. (1985) Structure of nonevaporating sprays: I. Near-injector conditions and mean properties. AIAA J. 23, 1548-1555. *Ibid.* II. Drop and turbulence properties. AIAA J. 23, 1724-1730.
- Solomon, A.S.P., Shuen, J.-S., Zhang, Q.-F. & Faeth, G. M. (1985a) Measurements and predictions of the structure of evaporating sprays. J. Heat Transfer 107, 679-686.



END

DATE  
FILMED

5-88

DTIC